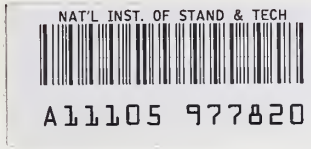



# NBS TECHNICAL NOTE 1082

U.S. DEPARTMENT OF COMMERCE / National Bureau of Standards

# A Near-Field Array of Yagi-Uda Antennas for Electromagnetic Susceptibility Testing

David A. Hill
Galen H. Koepke

The National Bureau of Standards[1] was established by an act of Congress on March 3, 1901. The Bureau's overall goal is to strengthen and advance the nation's science and technology and facilitate their effective application for public benefit. To this end, the Bureau conducts research and provides: (1) a basis for the nation's physical measurement system, (2) scientific and technological services for industry and government, (3) a technical basis for equity in trade, and (4) technical services to promote public safety. The Bureau's technical work is performed by the National Measurement Laboratory, the National Engineering Laboratory, the Institute for Computer Sciences and Technology, and the Center for Materials Science.

## *The National Measurement Laboratory*

Provides the national system of physical and chemical measurement; coordinates the system with measurement systems of other nations and furnishes essential services leading to accurate and uniform physical and chemical measurement throughout the Nation's scientific community, industry, and commerce; provides advisory and research services to other Government agencies; conducts physical and chemical research; develops, produces, and distributes Standard Reference Materials; and provides calibration services. The Laboratory consists of the following centers:

- Basic Standards[2]
- Radiation Research
- Chemical Physics
- Analytical Chemistry

## *The National Engineering Laboratory*

Provides technology and technical services to the public and private sectors to address national needs and to solve national problems; conducts research in engineering and applied science in support of these efforts; builds and maintains competence in the necessary disciplines required to carry out this research and technical service; develops engineering data and measurement capabilities; provides engineering measurement traceability services; develops test methods and proposes engineering standards and code changes; develops and proposes new engineering practices; and develops and improves mechanisms to transfer results of its research to the ultimate user. The Laboratory consists of the following centers:

- Applied Mathematics
- Electronics and Electrical Engineering[2]
- Manufacturing Engineering
- Building Technology
- Fire Research
- Chemical Engineering[2]

## *The Institute for Computer Sciences and Technology*

Conducts research and provides scientific and technical services to aid Federal agencies in the selection, acquisition, application, and use of computer technology to improve effectiveness and economy in Government operations in accordance with Public Law 89-306 (40 U.S.C. 759), relevant Executive Orders, and other directives; carries out this mission by managing the Federal Information Processing Standards Program, developing Federal ADP standards guidelines, and managing Federal participation in ADP voluntary standardization activities; provides scientific and technological advisory services and assistance to Federal agencies; and provides the technical foundation for computer-related policies of the Federal Government. The Institute consists of the following centers:

- Programming Science and Technology
- Computer Systems Engineering

## *The Center for Materials Science*

Conducts research and provides measurements, data, standards, reference materials, quantitative understanding and other technical information fundamental to the processing, structure, properties and performance of materials; addresses the scientific basis for new advanced materials technologies; plans research around cross-country scientific themes such as nondestructive evaluation and phase diagram development; oversees Bureau-wide technical programs in nuclear reactor radiation research and nondestructive evaluation; and broadly disseminates generic technical information resulting from its programs. The Center consists of the following Divisions:

- Inorganic Materials
- Fracture and Deformation[3]
- Polymers
- Metallurgy
- Reactor Radiation

[1]Headquarters and Laboratories at Gaithersburg, MD, unless otherwise noted; mailing address Gaithersburg, MD 20899.
[2]Some divisions within the center are located at Boulder, CO 80303.
[3]Located at Boulder, CO, with some elements at Gaithersburg, MD.

# A Near-Field Array of Yagi-Uda Antennas for Electromagnetic Susceptibility Testing



David A. Hill
Galen H. Koepke

Electromagnetic Fields Division
Center for Electronics and Electrical Engineering
National Engineering Laboratory
National Bureau of Standards
Boulder, Colorado 80303

U.S. DEPARTMENT OF COMMERCE, Malcolm Baldrige, Secretary

NATIONAL BUREAU OF STANDARDS, Ernest Ambler, Director

Issued July 1985

National Bureau of Standards Technical Note 1082
Natl. Bur. Stand. (U.S.), Tech Note 1082, 82 pages (July 1985)
CODEN:NBTNAE

U.S. GOVERNMENT PRINTING OFFICE
WASHINGTON: 1985

For sale by the Superintendent of Documents, U.S. Government Printing Office, Washington, DC 20402

CONTENTS

# A NEAR-FIELD ARRAY OF YAGI-UDA ANTENNAS FOR ELECTROMAGNETIC SUSCEPTIBILITY TESTING

David A. Hill and Galen H. Koepke

In electromagnetic susceptibility testing of electronic equipment, the ideal incident field is a plane wave. To approximate this condition, a seven-element array of Yagi-Uda antennas has been constructed and tested at a frequency of 500 MHz. The element weightings are determined by a near-field synthesis technique which optimizes the uniformity of the field throughout a rectangular test volume in the near field of the array. The amplitude and phase of the electric field have been measured throughout the test volume with a short dipole probe, and the agreement with the theory is excellent.

Key words: antenna array; array synthesis; dipole antenna; electromagnetic susceptibility testing; mutual coupling; near field; plane wave; Yagi-Uda antenna

## 1. Introduction

In electromagnetic susceptibility testing of electronic equipment, the ideal incident field is a plane wave. Far-field antenna ranges are generally unacceptable because they waste power outside the test volume and because the far-field distance is often inconveniently large. An ideal test facility would supply most of the power to the test volume containing the equipment under test (EUT), and the test facility dimensions should not be too much larger than the test volume so that it could be located indoors.

The compact range [1] uses a paraboloidal reflector to produce an approximately plane wave in the near field, but the compact range is most useful at frequencies above 1 GHz. At low frequencies, transverse electromagnetic (TEM) cells [2] and parallel plate transmission lines are used to produce TEM fields which are uniform over a portion of their cross section. Such transmission line structures are most effective for testing EUTs that are electrically small. There exists a frequency gap (about 50 MHz to 1 GHz) between the low frequency and high frequency methods where another method of producing a plane wave is needed.

The feasibility of using phased arrays to fill the frequency gap has been studied, and a near-field array synthesis method has been developed to compute the array element excitations [3]. The method optimizes the field quality

throughout the test volume and also constrains the element excitations to reduce the field strength outside the test volume. The synthesis method can be applied to arbitrary array elements and geometries, and in this report we apply the method to a seven-element, planar array of dipole antennas. To check the theory and to gain experience in working with near-field arrays, we constructed a seven-element array of dipoles and tested it at a frequency of 500 MHz. In an actual electromagnetic susceptibility test, we might prefer array elements with greater bandwidth, but dipoles were useful for verifying the array theory because their characteristics are well understood. Earlier experimental results have been obtained by Lynggaard [4] who built and tested a five-element array of horns.

The organization of this report is as follows. Section 2 contains the analysis and numerical results for the seven-element array. Mutual coupling between the array elements is considered in section 2.4. Section 3 describes the array construction and feed network and the method of probing the amplitude and phase of the electric field. Section 4 contains the experimental results for the electric field measurements throughout the test volume and gives some comparisons with the theoretical predictions of the electric field. Section 5 summarizes the results of this study and makes recommendations for further work.

## 2. Theory

The geometry of the seven-element planar array is shown in figure 1. The equally-spaced array elements are located at the vertices and at the center of a regular hexagon in the x-z plane. This configuration can also be viewed as a triangular arrangement of the array elements, and it is known to be very efficient in filling the planar array surface without producing grating lobes [5].

Only the driven elements are shown in figure 1, but each driven element is accompanied by a passive reflector in order to reduce the radiation in the backward (negative y) direction. Thus each array element is actually a two-element, Yagi-Uda antenna as described and analyzed in section 2.1. The excitations of the Yagi-Uda antennas are chosen to optimize the plane wave character of the field in the rectangular test volume shown in figure 1. In

section 2.2, the previously developed near-field array synthesis method [3] is applied to this array, and the optimum element excitations are determined. In section 2.3, the field distributions of the array are shown.

## 2.1 Two-Element, Yagi-Uda Antenna

Since the seven array elements are identical and mutual coupling is neglected in the initial analysis, it is sufficient to analyze a single isolated Yagi-Uda antenna. The center element of the array is shown in figure 2, and it consists of a driven dipole of half length $h_d$ and a reflector of half length $h_r$. Both dipoles are z directed. The current distributions on both the driven element $I_d(z')$ and the reflector element $I_r(z')$ are assumed to be sinusoidal:

$$I_d(z') = \frac{I_d}{\sin kh_d} \sin k(h_d - |z'|)$$

and (1)

$$I_r(z') = \frac{I_r}{\sin kh_r} \sin k(h_r - |z'|),$$

where $k = \omega\sqrt{\mu_0\varepsilon_0} = 2\pi/\lambda$, $\mu_0$ and $\varepsilon_0$ are the free space permeability and permittivity, and $\lambda$ is the free space wavelength. The time dependence exp ($j\omega t$) is suppressed. The current distributions in eq (1) are symmetrical in z' and are zero at the ends of the elements. A more precise form of the currents could be obtained from three-term theory [6,7] or the method of moments [8], but the sinusoidal assumption is adequate for dipoles of length on the order of a half wavelength. The advantage of the sinusoidal current assumption is that simple expressions are available for the near fields [9] and the self and mutual impedances [10].

The base currents of the driven and reflector elements, $I_d$ and $I_r$, can be obtained from the following circuit relations:

$$V_d = Z_d I_d + Z_{dr} I_r$$

and (2)

$$0 = Z_{dr} I_d + Z_r I_r.$$

In eq (2), $V_d$ is the voltage applied to the base of the driven element, $Z_d$ is the self impedance of the driven element, $Z_r$ is the self impedance of the reflector element, and $Z_{dr}$ is the mutual impedance between the driven and reflector elements. The voltage applied to the base of the reflector element is zero because it is passive. From the second equation in eq (2), the ratio of the reflector current to the driven current is

$$I_r/I_d = -Z_{dr}/Z_r. \tag{3}$$

The other quantity of interest is the input impedance of the driven element $Z_{in}$

$$Z_{in} \equiv \frac{V_d}{I_d} = Z_d - \frac{Z_{dr}^2}{Z_r}. \tag{4}$$

To calculate the self and mutual impedances, we use the mutual impedance expressions given by King [10]. These expressions involve sine and cosine integrals, and efficient computer codes are available for evaluating these integrals [11]. Self impedances are evaluated by computing the mutual impedance at a separation equal to the dipole radius a.

The quantities in eqs (2) through (4) have been evaluated for the following parameters: $h_d/\lambda = 0.25$, $h_r/\lambda = 0.26$, $a/\lambda = 5.29 \times 10^{-3}$, and $d/\lambda = 0.25$. The value of $a/\lambda$ was determined from the experimental parameter of a = 0.318 cm (0.125") and a frequency of 500 MHz. For the above parameters the various impedances are:

$$Z_d = 7.31 + j\ 40.6\ \Omega,$$

$$Z_r = 82.2 + j\ 67.0\ \Omega, \text{ and}$$

$$Z_{dr} = 43.2 - j\ 29.8\ \Omega. \tag{5}$$

By substituting eq (5) into eqs (3) and (4), the following values are obtained for the current ratio and the input impedance:

$$I_r/I_d = -\ 0.138 + j\ 0.476$$

and

$$Z_{in} = 81.3 + j\ 65.2\ \Omega. \tag{6}$$

Thus the input impedance is larger than the self impedance of the driven element given in eq (5). The fields of the two elements add constructively in the forward direction (positive y) and cancel in the backward direction (negative y) because the phase of $I_r/I_d$ is near 90 deg. The resultant far-field radiation patterns in the two principal planes are shown in figure 3. The E plane is the yz plane, and the H plane is the xy plane. The patterns were computed from the far-field expressions derived in appendix A. The front-to-back field ratio is 2.94 (i.e., 9.37 dB). Some calculations were done for other values of d and $h_r$, but not much improvement was observed.

In the following sections, the near fields of the Yagi-Uda antenna are required. For the sinusoidal current distribution given in eq (1), the electric field radiated by the driven element $\underline{E}^d$ is given by [9]

$$\underline{E}^d = \hat{x}\, E_x^d + \hat{y}\, E_y^d + \hat{z}\, E_z^d\ , \tag{7}$$

where

$$E_x^d = \frac{x}{\rho} E_\rho,\ E_y^d = \frac{y}{\rho} E_\rho,$$

$$E_\rho = \frac{-j\eta I_d}{4\pi \sin kh_d}\left[\frac{(z - h_d)}{\rho}\frac{\exp(-jkr_1)}{r_1}\right.$$

$$\left. + \frac{(z + h_d)}{\rho}\frac{\exp(-jkr_2)}{r_2} - \frac{2z \cos kh_d}{\rho}\frac{\exp(-jkr_0)}{r_0}\right],$$

$$E_z^d = \frac{-j\eta I_d}{4\pi \sin kh_d}\left[\frac{\exp(-jkr_1)}{r_1} + \frac{\exp(-jkr_2)}{r_2} - 2 \cos kh_d \exp(-jkr_0)/r_0\right],$$

$$r_1 = \sqrt{\rho^2 + (z - h_d)^2},\quad r_2 = \sqrt{\rho^2 + (z + h_d)^2},$$

$$r_0 = \sqrt{\rho^2 + z^2},\ \rho = \sqrt{x^2 + y^2},\ \text{and}\ \eta = \sqrt{\mu_0/\varepsilon_0}.$$

The magnetic field radiated by the driven element $\underline{H}^d$ is given by [9]

$$\underline{H}^d = \hat{x}\, H_x^d + \hat{y}\, H_y^d, \tag{8}$$

where $H_x^d = \frac{-y}{\rho} H_\phi$, $H_y^d = \frac{x}{\rho} H_\phi$, and

$$H_\phi = \frac{jI_d}{4\pi\rho \sin kh_d} [\exp(-jkr_1) + \exp(-jkr_2) - 2 \cos kh_d \exp(-jkr_0)].$$

The same expressions apply for the fields of the reflector element, $\underline{E}^r$ and $\underline{H}^r$, if we replace $I_d$ by $I_r$, $h_d$ by $h_r$, and y by y + d. The total fields of the Yagi-Uda antenna, $\underline{E}^t$ ahd $\underline{H}^t$, are simply the sums of the fields of the driven and reflector elements.

$$\underline{E}^t = \underline{E}^d + \underline{E}^r \text{ and } \underline{H}^t = \underline{H}^d + \underline{H}^r. \tag{9}$$

The fields in eqs (7), (8), and (9) are those of the center element of the array in figure 1, but the expressions are also applicable to any of the six outer elements because all elements are identical. It is only necessary to replace x by $x-x_j$ and z by $z-z_j$ where the element is centered at $(x_j,z_j)$ in the xz plane.

## 2.2 Array Element Excitations

In this section we use the previously developed near-field synthesis method [3] to determine the excitations of the array elements. The desired field is a plane wave propagating in the positive y direction:

$$\underline{E}_p = \hat{z}\, E_{pz} \text{ and } \underline{H}_p = \hat{x}\, H_{px}, \tag{10}$$

where $E_{pz} = E_0 \exp(-jky)$ and $H_{px} = \frac{E_0}{\eta} \exp(-jky)$.

The array and test volume in figure 1 have two planes of symmetry, the xy plane and the yz plane. Consequently, the excitations of the array elements possess the same symmetry as shown in figure 1, and there are only three independent excitations. $I_1$ is the base current of the driven element at the origin, $I_2$ is the base current of the four driven elements above and below the x axis, and $I_3$ is the base current of the two elements on the x axis at x = ± s. For later use in the synthesis procedure, we define a three-element column matrix:

$$[I] = \begin{bmatrix} I_1 \\ I_2 \\ I_3 \end{bmatrix} . \tag{11}$$

The values of $I_1$, $I_2$, and $I_3$ are to be chosen to approximate the plane wave given by eq (10) within the test volume shown in figure 1. If we neglect mutual coupling between the array elements, then the corresponding input voltages ($v_1$, $v_2$, and $v_3$) are proportional to the base currents:

$$\begin{bmatrix} v_1 \\ v_2 \\ v_3 \end{bmatrix} = Z_{in} \cdot \begin{bmatrix} I_1 \\ I_2 \\ I_3 \end{bmatrix}, \tag{12}$$

where $Z_{in}$ is given by eq (4). If mutual coupling is to be included, then $Z_{in}$ must be replaced by the appropriate impedance matrix as shown in section 2.4. Of course, we always include the mutual coupling between the driven element and its reflector as given by eqs (2) through (4).

The first step in the synthesis procedure [3] is to define a column matrix [P] of the desired plane-wave values on the surface S of the test volume:

$$[P] = \begin{bmatrix} \underline{P}_1 \\ \underline{P}_2 \\ \vdots \\ \underline{P}_i \\ \vdots \\ \underline{P}_M \end{bmatrix}, \tag{13}$$

where $$\underline{P}_i = (\underline{E}_{p\,tan} - \eta\, \hat{n} \times \underline{H}_p)\Big|_{\underline{r} = \underline{r}_i} .$$

The subscript tan indicates the component tangential to S, and $\hat{n}$ is a unit inward normal. The element $\underline{P}_i$ is a tangential vector evaluated at the point $\underline{r} = \underline{r}_i$ as shown in figure 4. M is the number of points considered on S. In addition we define an M x 3 rectangular matrix [T]:

$$[T] = \begin{bmatrix} \underline{T}_{11} & \underline{T}_{12} & \underline{T}_{13} \\ \underline{T}_{21} & \underline{T}_{22} & \underline{T}_{23} \\ \vdots & \vdots & \vdots \\ \underline{T}_{M1} & \underline{T}_{M2} & \underline{T}_{M3} \end{bmatrix}, \tag{14}$$

where $\underline{I}_{ij} = (\underline{E}_{tan} - n\,\hat{n} \times \underline{H})\big|_{\underline{r}=\underline{r}_i}$.

The fields in the expression for $\underline{I}_{ij}$ are evaluated for $I_j = 1$ and all other currents equal to zero. The actual expressions for the electric and magnetic fields of the Yagi-Uda elements are given in eqs (7) through (9). The reason for using the hybrid vector involving the tangential components of both the electric and magnetic fields on S is that this particular hybrid vector possesses the desired uniqueness properties when specified over a closed surface [3].

The synthesis problem amounts to determining [I] when [P] (the desired plane-wave field) and [T] (the solution to the forward problem) are known. We can write the approximate relationship between [P] and [T][I]:

$$[T][I] \simeq [P]. \tag{15}$$

Since [P] is an M x 1 column matrix of two-component (tangential) vectors and [I] is a 3 x 1 column matrix of scalars, eq (15) actually represents 2M equations in 3 unknowns. Normally, 2M is greater than 3, and eq (15) can only be solved approximately. The least squares solution to eq (15) yields the best approximation to the plane-wave field on the surface of test volume, and uniqueness guarantees that the field is also optimized throughout the test volume [3].

If the least squares solution to eq (15) yields large element excitations and large fields outside the test volume, a more useful solution is obtained when a constraint is placed on the source norm [3,12]. For the array in figure 1, it is natural to define the following diagonal weight matrix [A] for the source inner product:

$$[A] = \begin{bmatrix} a_1 & 0 & 0 \\ 0 & a_2 & 0 \\ 0 & 0 & a_3 \end{bmatrix}, \tag{16}$$

where $a_1 = 1$, $a_2 = 4$, and $a_3 = 2$.

The values of the elements $a_j$ are chosen to equal the number of array elements with base current $I_j$. The square of the source norm $||[I]||^2$ is given by

$$||[I]||^2 = [\tilde{I}]^*[A][I] = \sum_{j=1}^{3} a_j |I_j|^2. \tag{17}$$

In eq (17), * denotes complex conjugate, and the tilde denotes transpose. The constraint on the source norm is written [12]

$$||[I]||^2 \leq C, \tag{18}$$

where C is a positive constant to be chosen.

The least squares solution to eq (15) with the constraint eq (18) requires the eigenvalues $\lambda_n$ and the eigenvectors $[\phi]_n$ which satisfy

$$[\tilde{T}]^*[T][\phi]_n = \lambda_n[A][\phi]_n. \tag{19}$$

Matrix multiplication in eq (19) has the usual meaning, and the dot product is understood whenever the elements multiplied together are vectors. The matrix $[\tilde{T}]^*[T]$ is Hermitian, and efficient computer codes [11] are available for computing the eigenvalues and eigenvectors. The orthogonality relationship of the eigenvectors is:

$$[\tilde{\phi}]_i^*[A][\phi]_j = \begin{cases} 1, & i = j \\ 0, & i \neq j \end{cases}. \tag{20}$$

The constrained solution for [I] is [12]:

$$[I] = \sum_{n=1}^{3} \frac{C_n}{\lambda_n + \alpha} [\phi]_n, \tag{21}$$

where $C_n = [\tilde{\phi}]_n^*[\tilde{T}]^*[P]$.

The Lagrange multiplier $\alpha$ satisfies

$$C - \sum_{n=1}^{3} \frac{|C_n|^2}{(\lambda_n + \alpha)^2} = 0. \tag{22}$$

The left side of eq (22) is a monotically increasing function in $\alpha$ which is real and positive, and the equation is easily solved numerically for $\alpha$. If $\alpha$ is set equal to zero, then eq (21) gives the eigenvector expansion of the usual least squares solution of eq (15).

A normalized squared error $E_n$ can be defined as

$$E_n = \frac{||[F] - [P]||^2}{||[P]||^2} = \frac{\sum_{i=1}^{M} |\underline{F}_i - \underline{P}_i|^2}{\sum_{i=1}^{M} |P_i|^2}, \tag{23}$$

where $[F] = [T][I] = \begin{bmatrix} \underline{F}_1 \\ \vdots \\ \underline{F}_i \\ \vdots \\ \underline{F}_M \end{bmatrix}$.

It has been shown [12] that as C is decreased both $\alpha$ and $E_n$ increase. However, it is often the case that large decreases in the source norm $||I||$ can be achieved with only small increases in $E_n$. A useful value of C can be obtained by considering a uniform array where $I_1 = I_2 = I_3 = I_u$. In this case, C is given by

$$C = 7|I_u|^2. \tag{24}$$

The value of $I_u$ is derived in appendix B.

## 2.3 Numerical Results

A computer program was written to solve for [I] by eq (21). Because of the double symmetry, the match points were taken over only one quarter of the surface S of the test volume as shown in figure 4. The number of points in the x, y, and z directions are $M_x$, $M_y$, and $M_z$, respectively. Consequently, the spacings of the points in the x, y, and z directions are $B/(2M_x)$, $A/M_y$,

and $C/(2M_z)$, respectively. The numerical results were found to be insensitive to $M_x$, $M_y$, and $M_z$ for spacings less than or equal to $\lambda/4$. There are $M_xM_z$ points on the front and back faces ($y = y_0 \pm C/2$), $M_yM_z$ points on the side face ($x = B/2$), and $M_xM_y$ points on the top face ($z = A/2$). Thus the total number of points M is

$$M = 2M_xM_z + M_y(M_x + M_z). \tag{25}$$

The numerical results in figures 5 through 15 apply to the following array parameters: $s = \lambda$, $h_d = d = \lambda/4$, $h_r = 0.26\ \lambda$, and $a = 5.29 \times 10^{-3}\ \lambda$. In figures 5 through 11, the test volume is a 1.5 $\lambda$ cube ($A = B = C = 1.5\ \lambda$) which is centered 1.75 $\lambda$ from the array ($y_0 = 1.75\ \lambda$). Thus the front of the test volume is one wavelength from the array ($y_0 - C/2 = \lambda$). The magnitudes and phases of the synthesized currents are shown in figure 5. For this particular case, the constraint has no effect because the unconstrained currents ($\alpha = 0$) satisfy eq (18). The currents in figure 5 are normalized to the current of the uniform array $I_u$ as given in appendix B. The center current $I_1$ has the largest magnitude, and this was true for all cases which were studied.

For the synthesized currents in figure 5, the normalized squared error $E_n$ as given by eq (23) is 0.077 compared to $E_n = 0.385$ for the uniform array. This difference in the quality of both the magnitude and phase of the electric field is evident in figures 6 through 11. In all cases the plane-wave value is shown over the extent of the test volume for comparison. The decay in the field for x and z outside the test zone in figures 7 and 8 is about the same for the synthesized and uniform arrays. In the $z = 0$ plane, the electric field has only a z-component, and there are no cross-polarized components. For $z \neq 0$, there is a small cross-polarized field ($E_y$) as shown in figure 12. (Here we refer to either orthogonal component of the electric field, $E_x$ or $E_y$, as a cross-polarized component. In propagation theory, $E_y$ is more often called a longitudinal component producing a wave tilt.) In general the amplitude errors in figures 6 through 8 tend to be more significant than the phase errors in figures 9 through 11. Although not shown here, the errors in the magnetic field have similar characteristics.

There are several ways to reduce the size of the field errors: (1) increase the number of array elements, (2) decrease the size of the test volume,

(3) move the test volume farther from the array. An increase in the number of elements gives more degrees of freedom for the synthesis procedure, but increases the cost and complexity of the array. A decrease in the size of the test volume makes it easier to maintain a uniform field, but limits the size of the test object. In figures 13 through 17, we show numerical results for $y_0 = 2.75\ \lambda$. Thus the front face of the test volume is now two wavelengths from the array. All other parameters remain the same. The synthesized currents both with and without a constraint are shown in figure 13. For this case, the normalized squared error $E_n$ is 0.020 for the unconstrained synthesized array, 0.046 for the constrained synthesized array, and 0.340 for the uniform array. Thus the errors are smaller, as expected, when the test volume is farther from the array. The magnitude of the electric field is shown along the three axes in figures 14 through 16, and the errors are seen to be smaller than those in figures 6 through 8. The cross-polarized component is shown in figure 17, and it is seen to be smaller than in figure 12.

Because it is difficult to display fields throughout a volume, only the fields on the three centerlines of the cube have been shown. However, the normalized squared error $E_n$ which represents the surface field errors is a good indicator of average field errors throughout the volume.

Some cases were run for different values of the element spacing as shown in figure 1, and the best results were obtained for $s \simeq \lambda$. For smaller values of s, the array size gets smaller, and it becomes necessary to decrease the size of the test volume. For larger values of s, undesirable grating lobes begin to form. If we assume that spacings on the order of one wavelength are good for broadside arrays which are not electronically scanned, then the width of the test volume must be somewhat less than $\sqrt{N}\ \lambda$, where N is the number of elements. In other words, the width of the array must be somewhat greater than the width of the test volume.

## 2.4 Mutual Coupling

In the previous sections, the optimum values of the base currents were determined. When mutual coupling between the array elements is neglected, the input voltages are proportional to the base currents as shown in eq (12). In this section we derive more accurate expressions for the input voltages which

include the effect of mutual coupling. The results tell us when mutual coupling is important and how to account for it.

The base currents $I_j$ and input voltages $v_j$ for the seven-element array are shown in figure 18. The voltages and currents satisfy the following matrix relationship:

$$\begin{bmatrix} v_1 \\ v_2 \\ \vdots \\ v_7 \end{bmatrix} = \begin{bmatrix} Z_{11} & Z_{12} \cdots Z_{17} \\ Z_{21} & Z_{22} \\ \vdots & \\ Z_{71} & Z_{77} \end{bmatrix} \begin{bmatrix} I_1 \\ \\ \\ I_7 \end{bmatrix}. \tag{26}$$

The mutual impedances $Z_{ij}$ are defined as

$$Z_{ij} = \frac{v_i}{I_j}, \tag{27}$$

where all base currents except $I_j$ are zero. The reflector currents are assumed to satisfy the approximate relationship given in eq (3). Thus the mutual impedance in eq (27) can be written as the sum of two terms:

$$Z_{ij} = Z_{ij}{}^{d} + \left(\frac{I_r}{I_d}\right) Z_{ij}{}^{r}, \tag{28}$$

where $Z_{ij}{}^{d}$ is the mutual impedance between the $i^{th}$ and $j^{th}$ driven elements and $Z_{kj}{}^{r}$ is the mutual impedance between the $i^{th}$ driven element and the $j^{th}$ reflector. The ratio $(I_r/I_d)$ is approximately given by eq (3). A more accurate expression for $(I_r/I_d)$ can be obtained by adding seven more equations to eq (26) and solving the entire set of equations simultaneously [7], but we have found that the resultant value for $(I_r/I_d)$ varies little from that given by eq (3). The expressions for $Z_{ij}{}^{d}$ and $Z_{ij}{}^{r}$ in eq (28) are those for dipoles in echelon [10].

Because of the double symmetry of the array, many of the voltages and currents in figure 18 are equal:

$$v_2 = v_4 = v_5 = v_7, \; v_3 = v_6,$$

$$I_2 = I_4 = I_5 = I_7, \text{ and } I_3 = I_6. \tag{29}$$

Thus there are only three independent voltages ($v_1$, $v_2$, $v_3$) and currents ($I_1$, $I_2$, $I_3$) as shown in figure 1, and the matrix equation in eq (26) can be reduced to three rows:

$$\begin{bmatrix} v_1 \\ v_2 \\ v_3 \end{bmatrix} = \begin{bmatrix} Z_{11} & Z_{12} \cdots Z_{17} \\ Z_{21} & \cdots \\ Z_{31} & \cdots \quad Z_{37} \end{bmatrix} \begin{bmatrix} I_1 \\ I_2 \\ I_3 \\ I_2 \\ I_2 \\ I_3 \\ I_2 \end{bmatrix}.$$

$$= \begin{bmatrix} Z_{11} & (Z_{12} + Z_{14} + Z_{15} + Z_{17}) & (Z_{13} + Z_{16}) \\ Z_{21} & (Z_{22} + Z_{24} + Z_{25} + Z_{27}) & (Z_{23} + Z_{26}) \\ Z_{31} & (Z_{32} + Z_{34} + Z_{35} + Z_{37}) & (Z_{33} + Z_{36}) \end{bmatrix} \begin{bmatrix} I_1 \\ I_2 \\ I_3 \end{bmatrix}. \tag{30}$$

Many of mutual impedances are equal:

$$Z_{11} = Z_{22} = Z_{33},$$

$$Z_{12} = Z_{14} = Z_{15} = Z_{17} = Z_{21} = Z_{23} = Z_{32} = Z_{34},$$

$$Z_{13} = Z_{16} = Z_{27} = Z_{31},$$

and

$$Z_{26} = Z_{37} = Z_{35}. \tag{31}$$

By substituting eq (31) in eq (30), we have

$$\begin{bmatrix} v_1 \\ v_2 \\ v_3 \end{bmatrix} = \begin{bmatrix} Z_{11} & 4\,Z_{12} & 2\,Z_{13} \\ Z_{12} & (Z_{11} + Z_{13} + Z_{24} + Z_{25}) & (Z_{12} + Z_{26}) \\ Z_{13} & 2(Z_{12} + Z_{26}) & (Z_{11} + Z_{36}) \end{bmatrix} \begin{bmatrix} I_1 \\ I_2 \\ I_3 \end{bmatrix}. \tag{32}$$

$Z_{11}$ in eq (38) is equal to $Z_{in}$ in eqs (4) and (12). Thus, eq (32) reduces to eq (12) only when the mutual impedances ($Z_{12}$, $Z_{13}$, $Z_{24}$, $Z_{25}$, $Z_{26}$, and $Z_{36}$) are all zero. These mutual impedances decrease in magnitude as the interelement spacing s is increased.

Since the currents ($I_1$, $I_2$, $I_3$) are already known from eq (21), the required input voltages ($v_1$, $v_2$, $v_3$) can be obtained directly from eq (32) by matrix multiplication. The resultant input voltages are shown in figures 19 and 20 for the same parameters which were used to obtain the currents in figure 5 and the constrained currents in figure 13. The voltages are normalized to the voltage $v_u$ for a uniform array which is given by

$$v_u = I_u Z_{in}, \tag{33}$$

where $I_u$ is given by eq (B-7) and $Z_{in}$ is given by eq (4). The voltages in figures 19 and 20 which do not include mutual coupling were computed from eq (12). Thus the differences between the dashed and solid results are an indication of the importance of mutual coupling. The differences occur primarily in the phases, but this is not necessarily true for other cases. The effect of the interelement spacing s on mutual coupling has been studied, and the mutual coupling has been found to decrease as s is increased as expected. This is why the hexagonal geometry was chosen to allow a larger interelement spacing [5].

## 3. Experiment

The array as described in section 2 and shown in figures 1 and 2 was constructed, and a series of measurements was performed throughout the test volume shown in figure 1. A test frequency of 500 MHz was chosen for convenience, although the array can be adjusted for any frequency from 100 to 1000 MHz.

### 3.1 Array Construction

Each of the seven two-element Yagi-Uda antennas was constructed as shown in figure 21. The driven dipole element is fed with a dual coaxial transmission line as described in [13]. The coaxial lines were in turn fed with a

0° - 180° hybrid junction (power splitter), as shown in figure 22, to provide optimum excitation of the dipole. Each dipole antenna was then tuned for resonance at 500 MHz by adjusting the length of the telescoping arms on the dipole. The driven to reflector distance d and the reflector length $2h_r$ (figure 2) were then adjusted according to dimensions in section 2.3; $d = \lambda/4$ and $h_r = 0.26\ \lambda$, based on the physical length of the driven element ($\lambda/2$).

The masts for the seven Yagi-Uda antennas were attached to the structure shown in figure 23. This particular arrangement allowed easy positioning of all the elements for any chosen frequency (100 to 1000 MHz), with 500 MHz chosen for this experiment. The dual-coaxial lines from each antenna extended back and perpendicular from the driven element to a wall of rf absorber (figure 24). The rf source, power splitting network, and instrumentation are behind the absorber wall and outside the anechoic chamber.

The feed system (power splitting network) consisted of 13 broadband hybrid junctions, two phase shifters, and two variable attenuators. Six junctions were connected as in-phase power splitters and seven were used to feed the dual-coaxial lines from the antennas; hence these were connected to utilize the 0° and 180° ports. The system is better described in figure 25.

### 3.2 Probe

The rf probe construction duplicated the driven element of the Yagi-Uda antennas. Here the dipole length was 1/10 λ (approximately 6 cm) rather than λ/2 used for the resonant antenna. The same dual-coaxial feed system was used and these cables were carefully positioned to minimize interactions with the rf field being measured. As near as was practical, the cables were hidden behind sections of rf absorber. The signal from the probe then traveled through coax line along the floor of the anechoic chamber and out through the door to the instrumentation. Both amplitude and phase of the electric field components were measured.

### 3.3 Track

The probe moved through the test volume on a nonconductive motorized track. The motor for the track sat on the base and, through a series of belts

and pulleys, moved the probe in a horizontal linear direction. The motor also drove a precision potentiometer. The resistance of the potentiometer was then used, after careful calibration, to determine the position of the probe along the track. The details of the track may be seen in the photograph in figure 26. The direction of the track was aligned with the z axis of the array coordinates, thus all scans are along this axis. The x position can be changed by moving the cart (a feature of the anechoic chamber) along the y coordinate, perpendicular to the array. Thus by selecting an x and y position and scanning the z direction, the test volume can be mapped. The amplitude and phase measurements were taken by manually controlling the track position via a switch located outside the anechoic chamber. At every selected location, the computer was triggered to accumulate the data and store it on disk. A single scan read 60 to 80 data points. A more elaborate arrangement would have allowed the computer to control the track also; however, this system proved adequate for these measurements.

### 3.4 Instrumentation

The measurement system (fig. 24), used a vector analyzer (phase amplitude receiver), digital multimeter to read ohms and hence track position, and a computer/instrument controller. As indicated, the track was positioned manually but all the information was read with the computer. The computer read both the field parameters and the track position at every test point. The data were then saved on floppy disk for later processing.

## 4. Experimental Results and Comparisons with Theory

Four sets of element weightings were applied to the seven element array. These amplitude and phase feeding schemes were calculated using the synthesis techniques outlined in section 2. The calculations used two cubic ($A = B = C = 1.75\ \lambda$ in figure 1) test volumes at different distances from the array, each with and without mutual coupling adjustments. We identify the four sets of element weightings as feeds 1-4 described below:

Feed 1. Test volume centered at $x = 0$, $y = 1.75\ \lambda$, and $z = 0$ without corrections for mutual coupling between array elements (fig. 19).

Feed 2. Same as 1, but with corrections for mutual coupling between array elements (fig. 19).

Feed 3. Test volume centered at $x = 0$, $y = 2.75\ \lambda$, and $z = 0$ without corrections for mutual coupling between array elements (fig. 20).

Feed 4. Same as 3, but with corrections for mutual coupling between array elements (fig. 20).

The test results are shown in figures 27 to 53. In all cases, the measured quantity is shown as a function of the z coordinate, f(z). Figures 27 through 41 show both theoretical and measured values. Figures 42 to 53 are measured values only and show more detail throughout the test volumes. All figures are scans parallel to the z axis at some distance y from the array and lying in an x = constant plane. Feed 1 was probed in the $x = -0.75\ \lambda$, $x = 0$, and $x = +0.75\ \lambda$ planes, while feeds 2, 3, and 4 were probed only in the $x = 0$ plane. All amplitude and phase values are referenced to the center of the test volume; values there are 0 dB and 0 deg. The test volume boundaries are shown by the vertical columns of dots.

Figures 27 through 29, respectively, show scans in the plane $x = 0$ along the near face ($y = 1.0\ \lambda$), center ($y = 1.75\ \lambda$), and far edge ($y = 2.5\ \lambda$) of the test volume used for feed 1. All three electric field components ($E_x$, $E_y$, and $E_z$) were calculated and measured for each of these locations. The calculated curves (shown by the symbol +) are obviously not those of a perfect plane wave; rather they represent the best approximation to the plane wave as determined by the synthesis technique for an array of only seven elements. As the number of elements increases, the field becomes closer to that of a plane wave [3].

A uniform plane wave would have a constant $E_z$ with no $E_x$ or $E_y$ components; hence, $E_x$ and $E_y$ may be considered error fields for this experiment. Theory predicts an $E_y$ component at these close distances to the array and measurement confirms it. $E_y$ is strongest closest to the array ($y = 1.0\ \lambda$) and decreases as the distance increases. $E_x$ is predicted to be zero; the measurement shows that it is small, but not zero (10 to 20 dB or more below $E_y$). These data may indicate the effectiveness of the rf probe in being able to

resolve the field components or other measurement errors. Hence, little or no emphasis should be placed on interpretation of the $E_x$ data.

The $E_x$ and $E_y$ components are low enough as to have an insignificant effect on typical EM susceptibility measurements. So the remaining figures (30 to 53) detail only the z-directed electric field $E_z$. The figures are paired to show amplitude and phase under the same conditions; i.e., figures 30 and 31 show amplitude and phase for feed 1 in the x = 0 plane at y = 1.0 λ, 1.75 λ, and 2.5 λ, figures 32 and 33 show the same for the x = -0.75 λ plane, and figures 34 and 35 are for the x = +0.75 λ plane. The amplitude data, as presented, can be interpreted as follows. Each grid line directly above any given pair (calculated and measured) of curves for a particular y value corresponds to 0 dB. For example, figure 30 shows three pairs of curves, one each for y = 1.0 λ, y = 1.75 λ, and y = 2.5 λ. The center value for y = 1.75 λ is 0 dB as this is the reference point. The center value for y = 2.5 λ is near 0 dB for the measured and about -0.7 dB for the calculated value. The values for y = 1.0 λ at the center are about -3 to -4 dB. Again, these values are measured from the grid line directly above the curves, with 10 dB between grid lines. It is interesting to note that the field amplitude does not fall off as 1/r as one proceeds away from the array, but rather increases initially and then decreases more slowly than 1/r. This trend is shown in more detail for the theoretical results in figures 6 and 14. Feed 2 results are shown in figures 36 and 37 for the x = 0 plane.

Feed 3 refers to the more distant test volume, and figures 38 and 39 show data for the x = 0 plane at the near face (y = 2.0 λ), center (y = 2.75 λ), and the far boundary (y = 3.5 λ) of the test volume. The final pair of graphs with both theoretical and measured values compared (figs. 40 and 41) detail feed 4 for the same locations as feed 3.

The agreement shown between experiment and theory in figures 27 to 41 is quite good. There is one set of data (figs. 32 and 33), howver, where an apparent error in positioning the probe caused a shift in the experimental data for y = 1.0 λ. Feeds 2 and 4 were used to account for mutual coupling between the elements, but mutual coupling effects are so small that little improvement is seen in figures 36, 37, 40, and 41. Mutual coupling would be more important if the elements were more closely spaced.

In general the measurement agrees well enough with theory that the remaining measurement data for additional locations are presented alone. Figures 42 and 53 repeat the same locations as shown in figures 27 to 41 with additional traces added to show every 1/4 wavelength in y for each chosen x plane. Again, the amplitude and phase values are referenced to the center of the test volume, the amplitude traces have a 0 dB line directly above each one, and the corresponding phase for each amplitude trace is on the following figure. This density of traces is shown to indicate the field uniformity along the y dimension in addition to the z scan. The amplitude curves can be visually grouped to show a third dimension and give the viewer a feel for the field intensity anywhere in the constant x planes.

## 5. Conclusions and Recommendations

A general near-field array synthesis technique [3] has been applied to a seven-element array of Yagi-Uda antennas in order to optimize the field uniformity throughout a rectangular test volume. The array was constructed and tested in an anechoic chamber at a frequency of 500 MHz to verify the theory and to gain experience in controlling the amplitude and phase of the array elements. The agreement between the measurements and theory was excellent for both the amplitude and phase of the electric field. The effect of mutual coupling between the array elements was sufficiently small that the feed corrections to account for mutual coupling produced a negligible change in the measured fields.

There are a number of logical extensions to this work. The magnetic field could be probed throughout the test volume with a small loop probe. The Yagi-Uda array was chosen for convenience of analysis and construction in validating the theory. However, to make the phased array useful for electromagnetic susceptibility testing, we need to be able to scan the frequency over a large bandwidth, perhaps one or two octaves. This probably can be achieved by computing frequency-dependent weightings for the array elements, but dipoles might not be the most useful elements because of their frequency-dependent input impedance. To achieve very wide bandwidths on the order of a decade, wide-band elements would probably be required. In order to avoid having to rotate the test object, the angle of arrival of the plane wave could be scanned electronically, and angular scanning would require a larger number

of elements. Also, the appropriate geometry for angular scanning would require further study.

## 6. Acknowledgements

The authors are grateful to Dr. M. T. Ma for technical discussions during the course of this work and to W. D. Bensema, E. J. Vanzura, and A. E. Wainwright for assistance in the construction and evaluation of the array. We also thank C. K. S. Miller for his continued interest and support.

## 7. References

[1] Johnson, R. C.; Ecker, H. A.; Moore, R. A. Compact range techniques and measurements. IEEE Trans. Antennas Propag. AP-17: 568-575; 1969.

[2] Crawford, M. L. Generation of standard EM fields using TEM transmission cells. IEEE Trans. Electromagn. Compat. EMC-16: 189-195; 1974.

[3] Hill, D. A. Theory of near-field phased arrays for electromagnetic susceptibility testing. Nat. Bur. Stand. (U.S.) Tech. Note 1072; 1984.

[4] Lynggaard, S. K. Plane wave synthesis for antenna measurements. Technical University of Denmark (in Danish), M.S. Thesis; 1982.

[5] Sharp. E. D. A triangular arrangement of planar-array elements that reduces the number needed. IEEE Trans. Antennas Propag. AP-9: 126-129; 1961.

[6] King, R. W. P.; Wu, T. T. Currents, charges, and near fields of cylindrical antennas. Radio Sci. 69D: 429-446; 1965.

[7] Ma, M. T. Theory and application of antenna arrays. New York: John Wiley & Sons; 1974.

[8] Harrington, R. F. Field computation by moment methods. New York: Macmillan; 1968.

[9] Jordan, E. C.; Balmain, K. G. Electromagnetic waves and radiating systems. Englewood Cliffs: Prentice Hall; 1968.

[10] King, H. E. Mutual impedance of unequal length antennas in echelon. IEEE Trans. Antennas Propag. AP-5: 306-312; 1957.

[11] Boisvert, R.; Howe, S.; Kahaner, D.; Knapp-Cordes, J.; Knapp-Cordes, M. Guide to available mathematical software. Center for Applied Mathematics, Nat. Bur. Stand. (U.S.); 1981.

[12] Mautz, J. R.; Harrington, R. F. Computational methods for antenna pattern synthesis. IEEE Trans. Antennas Propag. AP-23: 507-512; 1975.

[13] Kraus, J. D. Antennas. New York: McGraw-Hill; 1950, Sec. 14-24.

## Appendix A. Far-Field Pattern of a Two-Element, Yagi-Uda Antenna

In the far field, the Yagi-Uda antenna of figure 1 radiates only a theta component of electric field. In spherical coordinates $(r, \theta, \phi)$, the far-field of the driven element $E_\theta^d$ is given by [9]

$$E_\theta^d = \frac{j\eta I_d \exp(-jkr)}{2\pi r \sin kh_d} \left[\frac{\cos(kh_d \cos\theta) - \cos kh_d}{\sin\theta}\right]. \tag{A-1}$$

The far-field of the reflector element $E_\theta^r$ is given by

$$E_\theta^r = \frac{j\eta I_d \exp(-jkr_r)}{2\pi r \sin kh_r} \left[\frac{\cos(kh_r \cos\theta) - \cos kh_r}{\sin\theta}\right], \tag{A-2}$$

where $r_r = r + d \sin\theta \sin\phi$. The total far-field $E_\theta^t$ can be written

$$E_\theta^t = E_\theta^d + E_\theta^r = \frac{j\eta I_d \exp(-jkr)}{2\pi r} P(\theta,\phi) \tag{A-3}$$

where

$$P(\theta,\phi) = \frac{1}{\sin\theta}\left\{\frac{\cos(kh_d\cos\theta) - \cos kh_d}{\sin kh_d}\right.$$

$$\left. + \frac{I_r}{I_d}\frac{[\cos(kh_r\cos\theta) - \cos kh_r]\exp(-jkd \sin\theta \sin\phi)}{\sin kh_r}\right\}.$$

The total magnetic field $H_\phi^t$ is given by

$$H_\phi^t = E_\theta^t/\eta. \tag{A-4}$$

The pattern in the E plane (yz plane) is obtained from $P(\theta, \pi/2)$, and the pattern in the H plane (xy plane) is obtained from $P(\pi/2, \phi)$. For the case plotted in figure 3 where $d = \lambda/4$ and the phase $(I_r/I_d)$ is near $\pi/2$, the maximum of $|P|$ occurs at $\theta = \phi = \pi/2$.

## Appendix B. Uniform Array

In order to determine the actual value of the base current for uniform excitation $I_u$, we first consider the equivalent smoothed current density $\underline{J}_s$. From the previous results [3], $\underline{J}_s$ is

$$\underline{J}_s = 2\,\hat{y} \times \underline{H}_p\big|_{y=0} = -\frac{2\,E_0}{\eta}\,\hat{z}. \tag{B-1}$$

The effective dipole moment of each element $\underline{p}$ should then equal the sheet current times the area of a hexagonal cell, $\sqrt{3}\,s^2/2$:

$$\underline{p} = -\frac{\sqrt{3}\,s^2\,E_0}{\eta}\,\hat{z}. \tag{B-2}$$

The effective dipole moment of the driven element $\underline{p}_d$ is given by

$$\underline{p}_d = \hat{z} \int_{-h_d}^{h_d} I_d(z')\,dz', \tag{B-3}$$

where

$$I_d(z') = I_u \frac{\sin k(h_d - |z|)}{\sin kh_d}.$$

The integration in eq (B-3) can be performed to yield

$$\underline{p}_d = I_u \frac{2(1 - \cos kh_d)}{k \sin kh_d}\,\hat{z}. \tag{B-4}$$

Similarly, the effective dipole moment of the reflector element $\underline{p}_r$ is

$$\underline{p}_r = I_r \frac{2(1 - \cos kh_r)}{k \sin kh_r}\,\hat{z}. \tag{B-5}$$

where $I_r = -I_u\,Z_{dr}/Z_r$. Since the reflector parameters are chosen to yield an in-phase contribution in the forward direction, the total effective dipole moment $\underline{p}_t$ is

$$\underline{p}_t = \hat{z}\,\frac{2\,I_u}{k}\left[\frac{(1 - \cos kh_d)}{\sin kh_d} + \left|\frac{Z_{dr}}{Z_r}\right| \frac{(1 - \cos kh_r)}{\sin kh_r}\right]. \tag{B-6}$$

$I_u$ is determined by equating $\underline{p_t}$ in eq (B-6) with $\underline{p}$ in eq (B-2):

$$I_u = \frac{-E_0 k s^2 \sqrt{3}}{2n} \left[ \frac{(1 - \cos kh_d)}{\sin kh_d} + \left| \frac{Z_{dr}}{Z_r} \right| \frac{(1 - \cos kh_r)}{\sin kh_r} \right]^{-1}. \qquad \text{(B-7)}$$

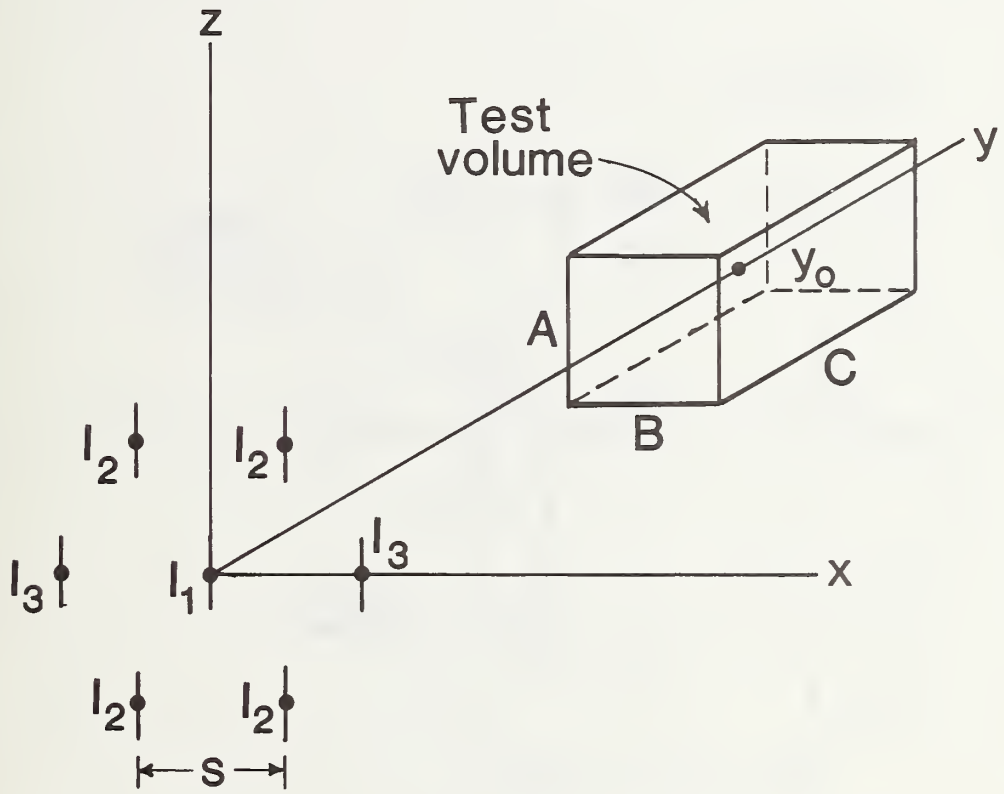


Figure 1. Seven-element (equally spaced) array in the xz plane. The rectangular test volume (A x B x C) is centered on the y-axis at $y = y_0$. Because of symmetry, there are only three independent excitations ($I_1$, $I_2$, $I_3$).

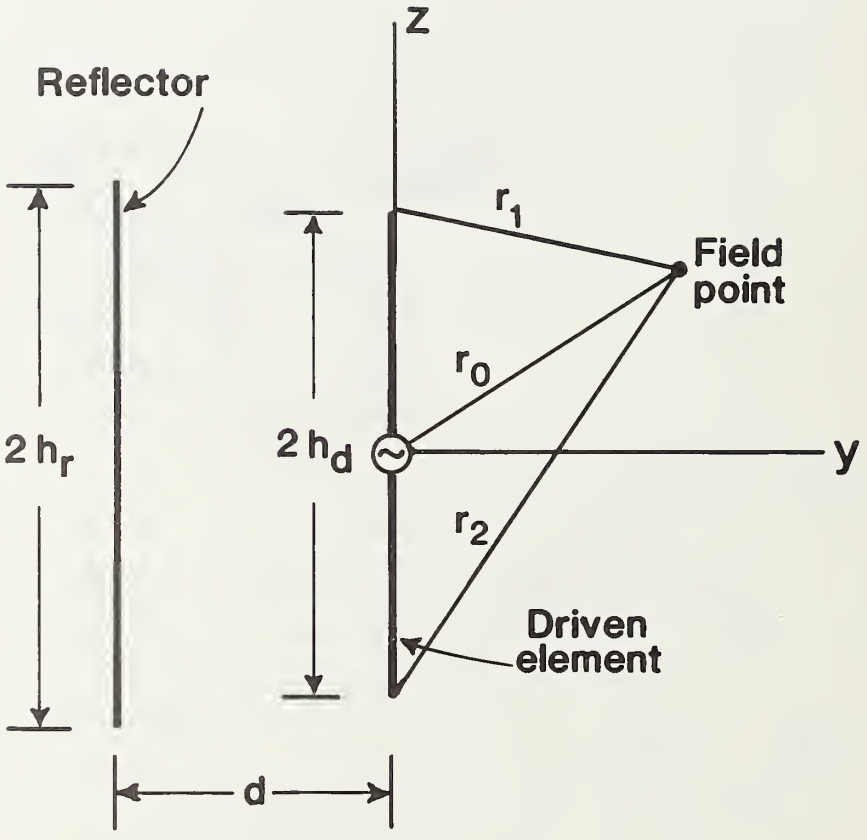


Figure 2. Two-element, Yagi-Uda antenna. Both the driven and reflector elements are cylindrical dipoles of radius a.

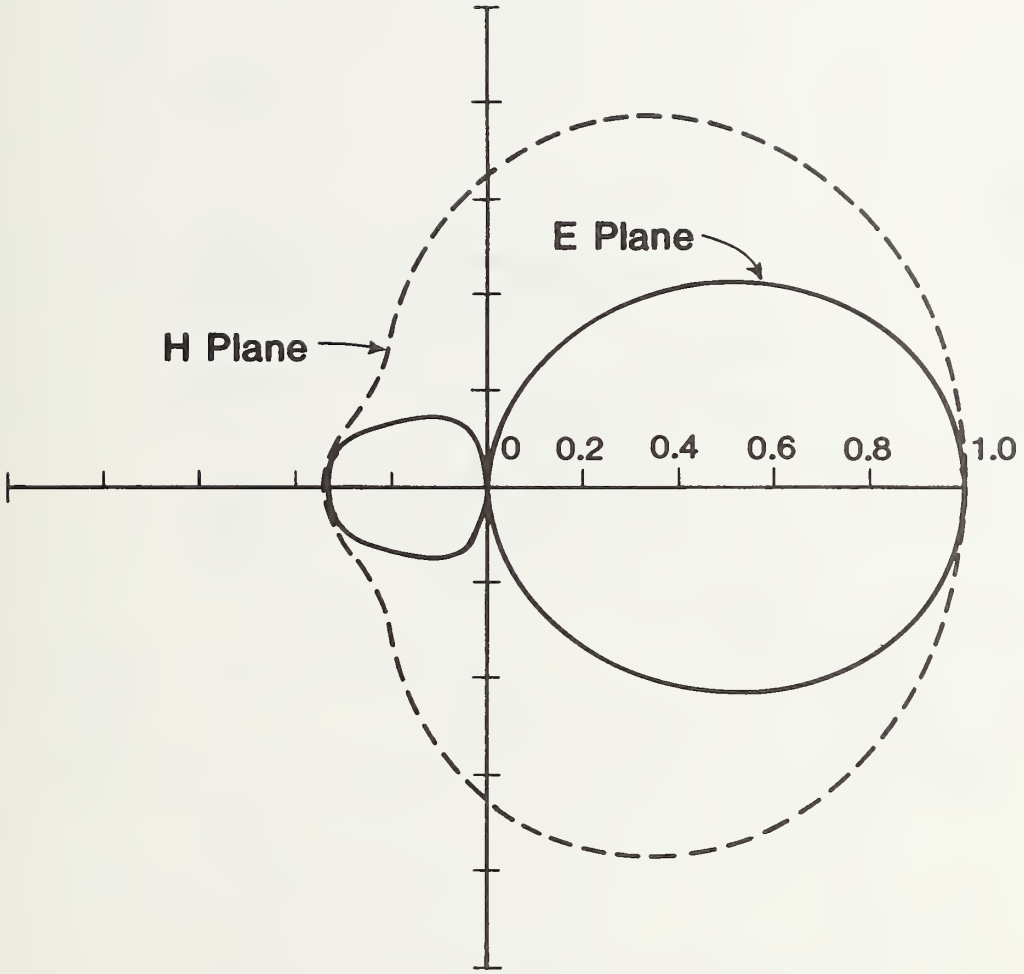


Figure 3. Normalized far-field pattern of a two-element, Yagi-Uda antenna antenna in the two principal planes. Parameters: $h_d/\lambda = 0.25$, $h_r/\lambda = 0.26$, $d/\lambda = 0.25$, and $a/\lambda = 5.29 \times 10^{-3}$.

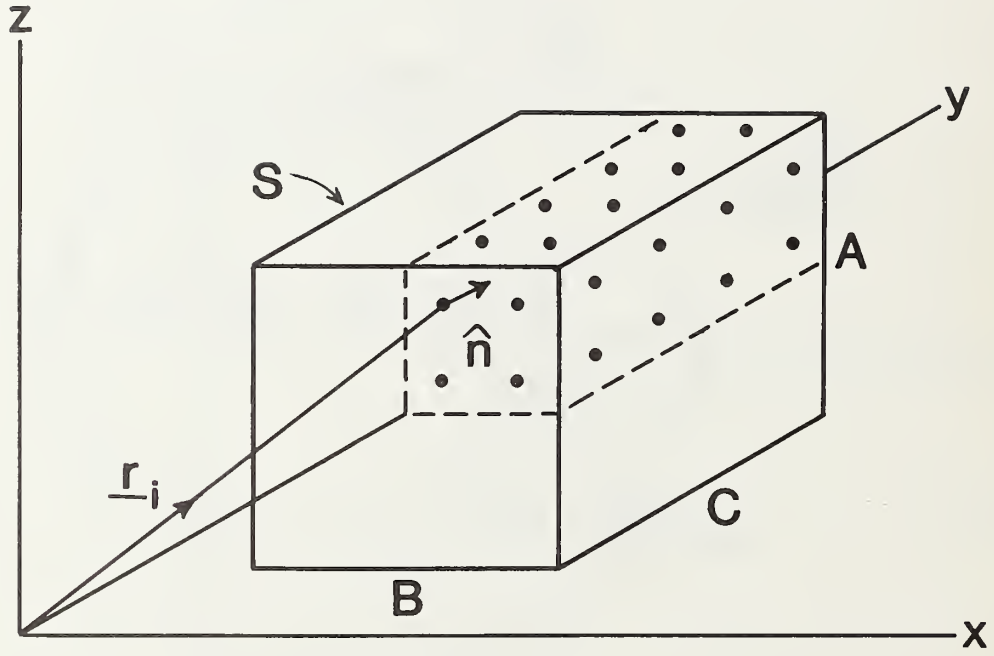


Figure 4. Closed surface S of test volume with two planes of symmetry. The match points are located at $\underline{r}_i$, and n is the unit inward normal. For this case, $M_x = M_z = 2$ and $M_y = 4$.

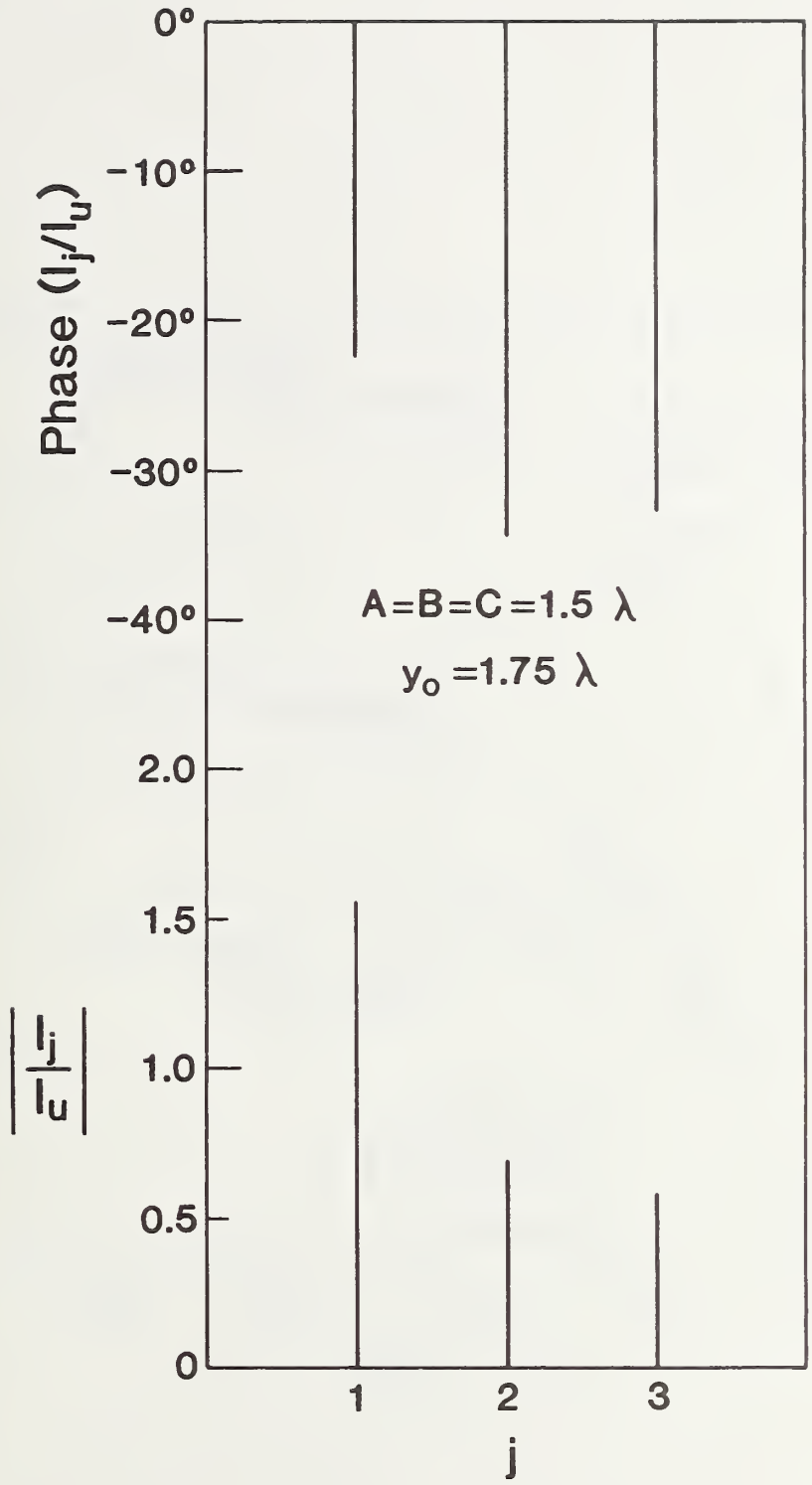


Figure 5. Magnitude and phase of the synthesized currents. For this case the constraint has no effect.

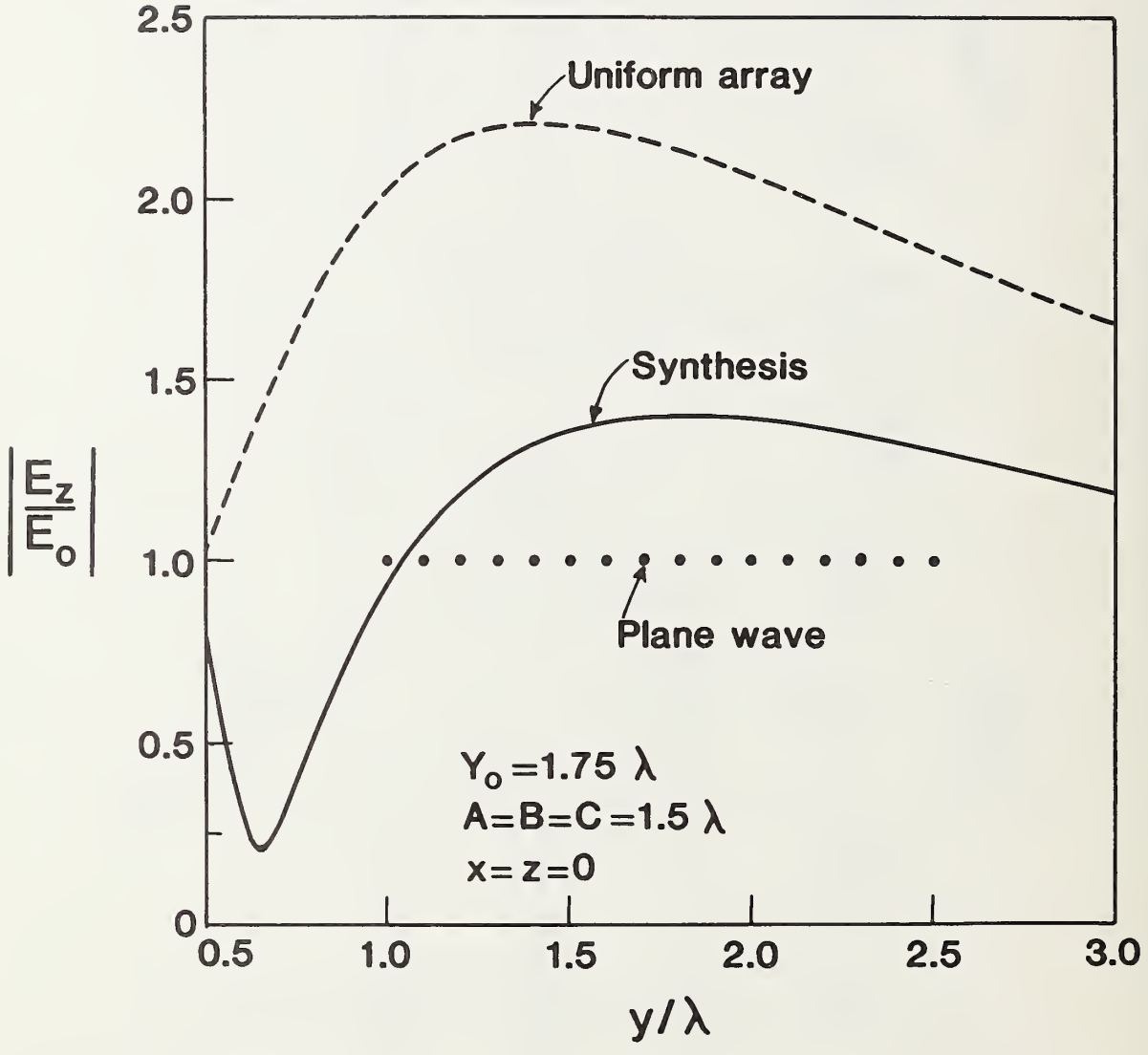


Figure 6. Normalized magnitude of the electric field for a synthesized array and a uniform array. The perfect plane wave is shown for comparison.

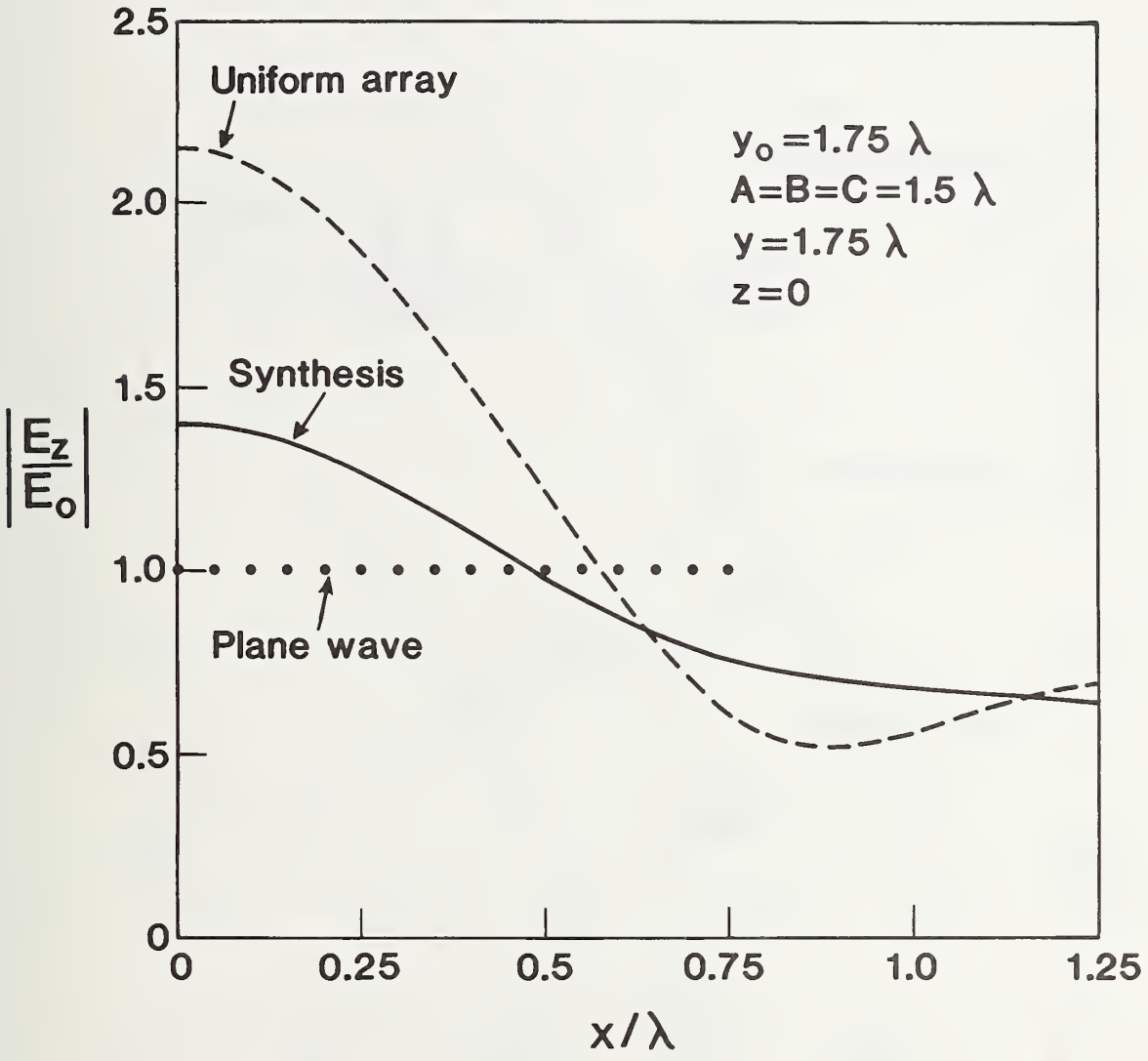


Figure 7. Normalized magnitude of the electric field for a synthesized array and a uniform array. The perfect plane wave is shown for comparison.

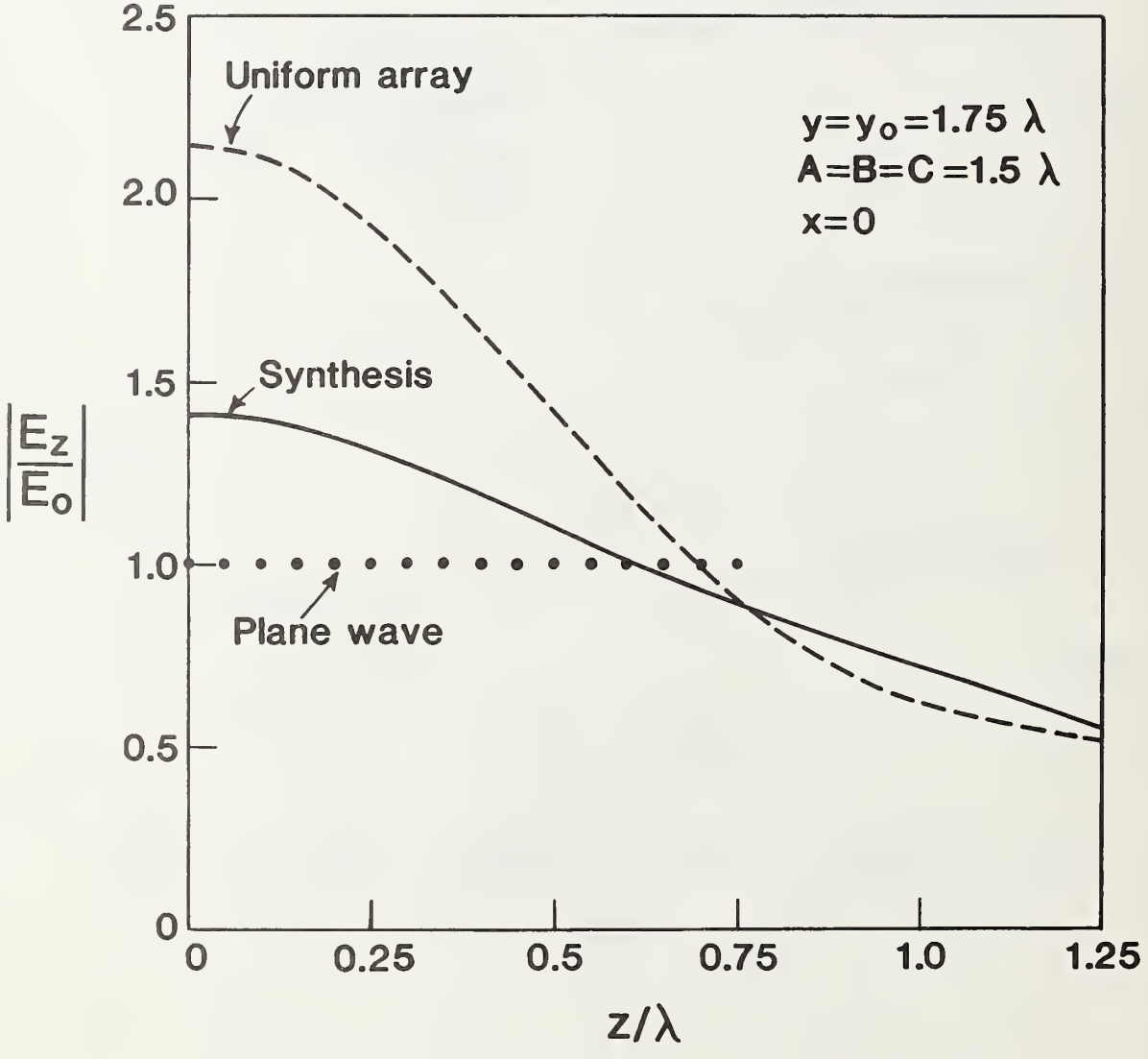


Figure 8. Normalized magnitude of the electric field for a synthesized array and a uniform array. The perfect plane wave is shown for comparison.

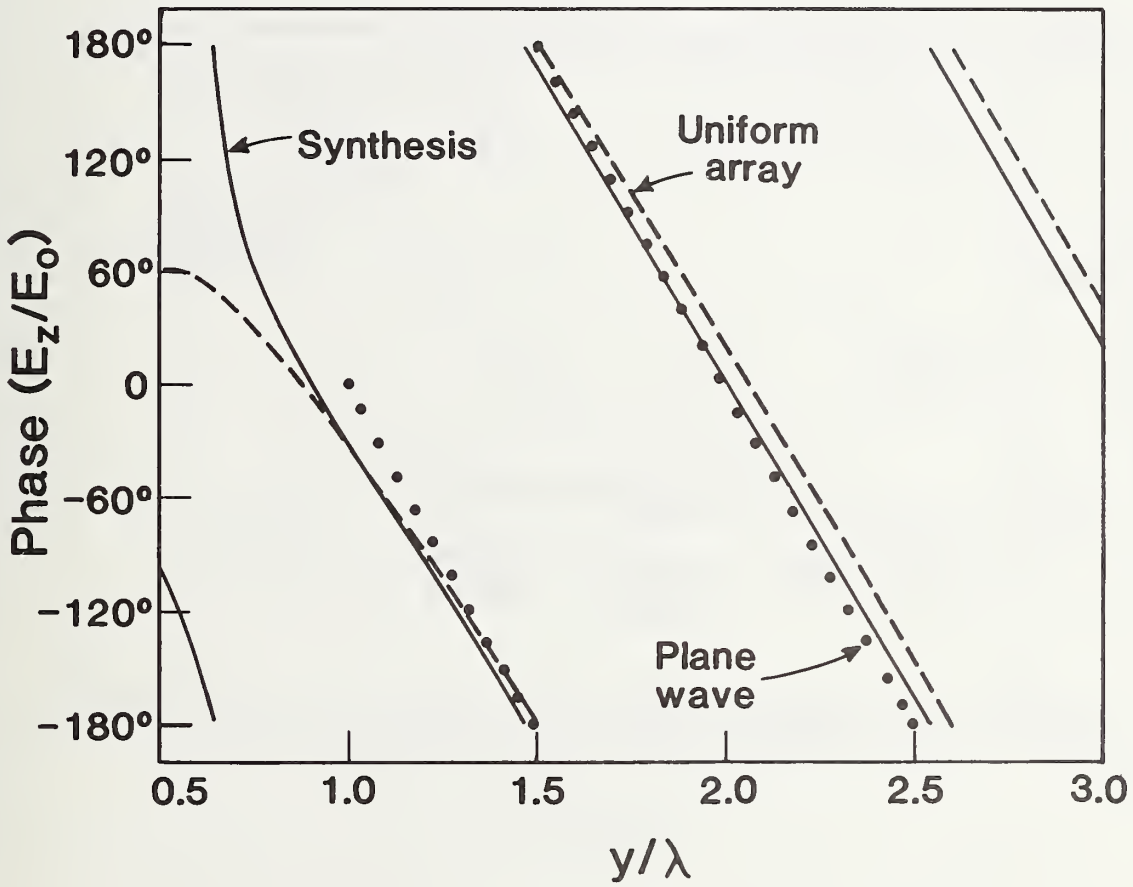


Figure 9. Phase of the electric field for a synthesized array and a uniform array. The perfect plane wave is shown for comparison. Parameters: A = B = C = 0, $y_o$ = 1.75λ, and x = z = 0.

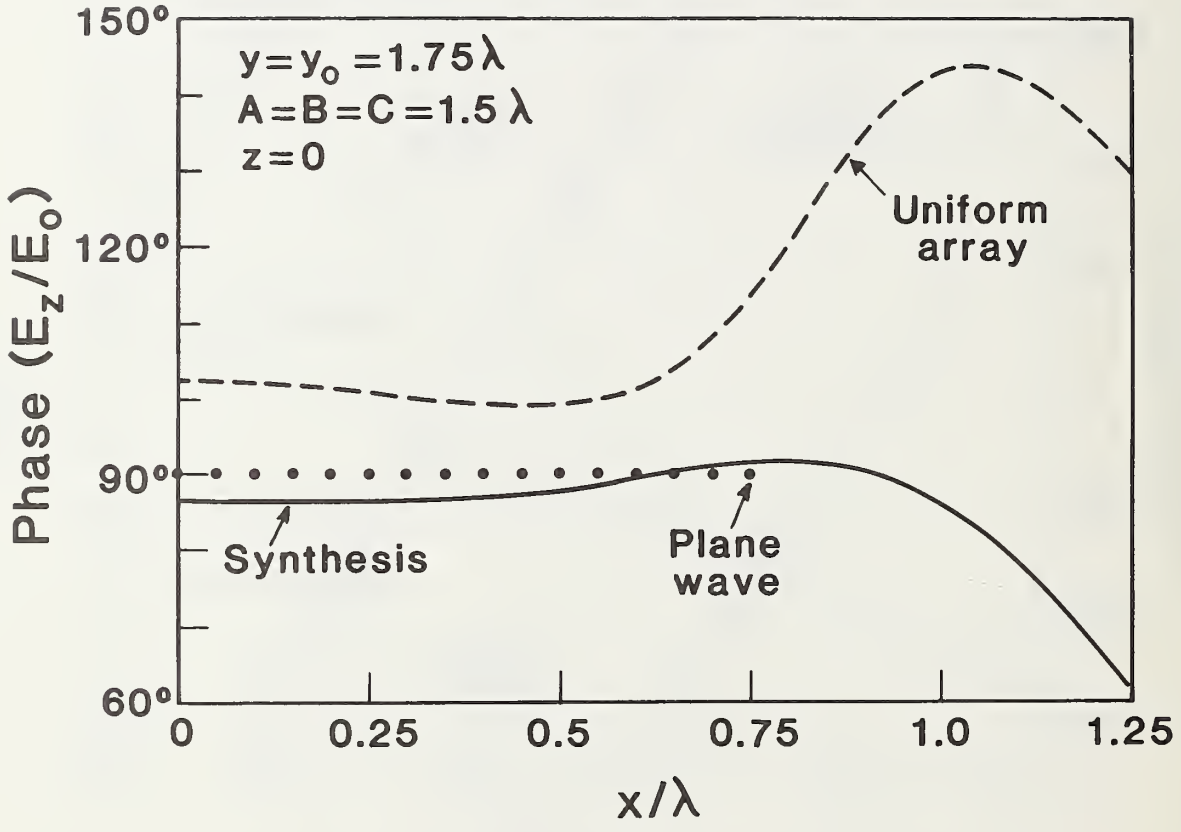


Figure 10. Phase of the electric field for a synthesized array and a uniform array. The perfect plane wave is shown for comparison.

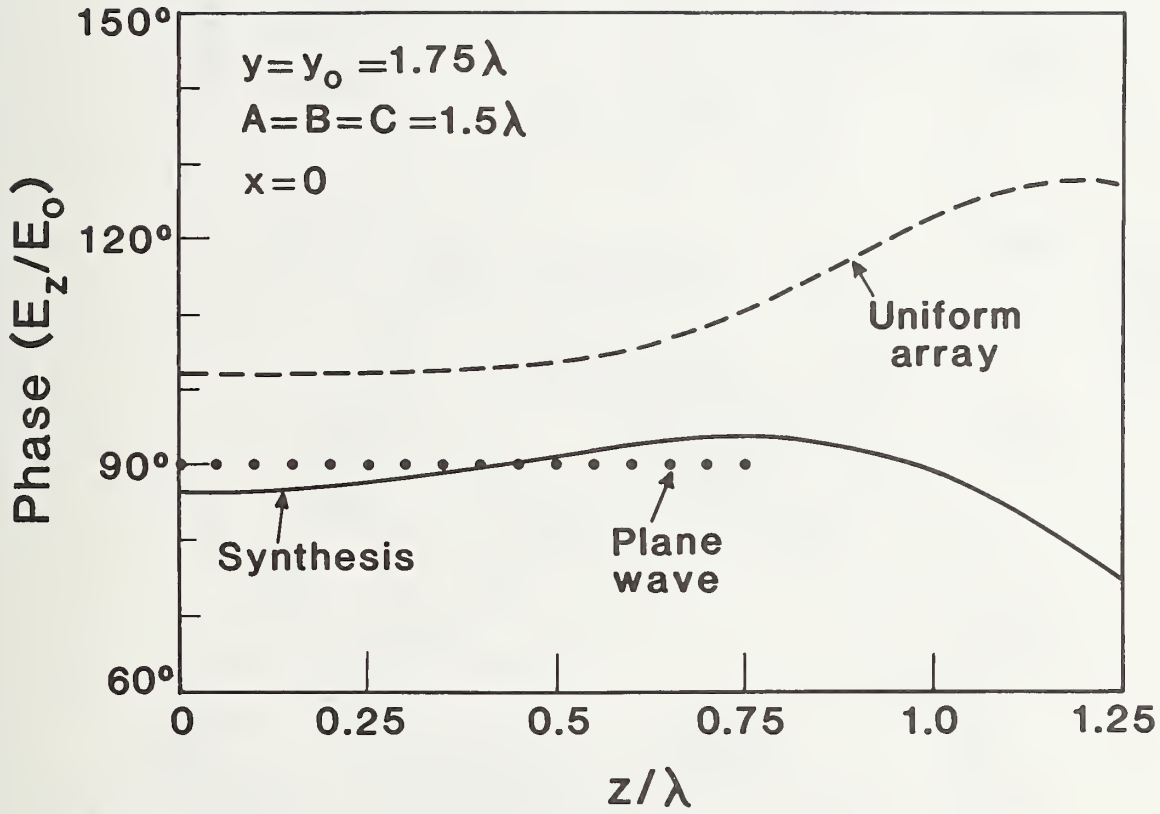


Figure 11. Phase of the electric field for a synthesized array and a uniform array. The perfect plane wave is shown for comparison.

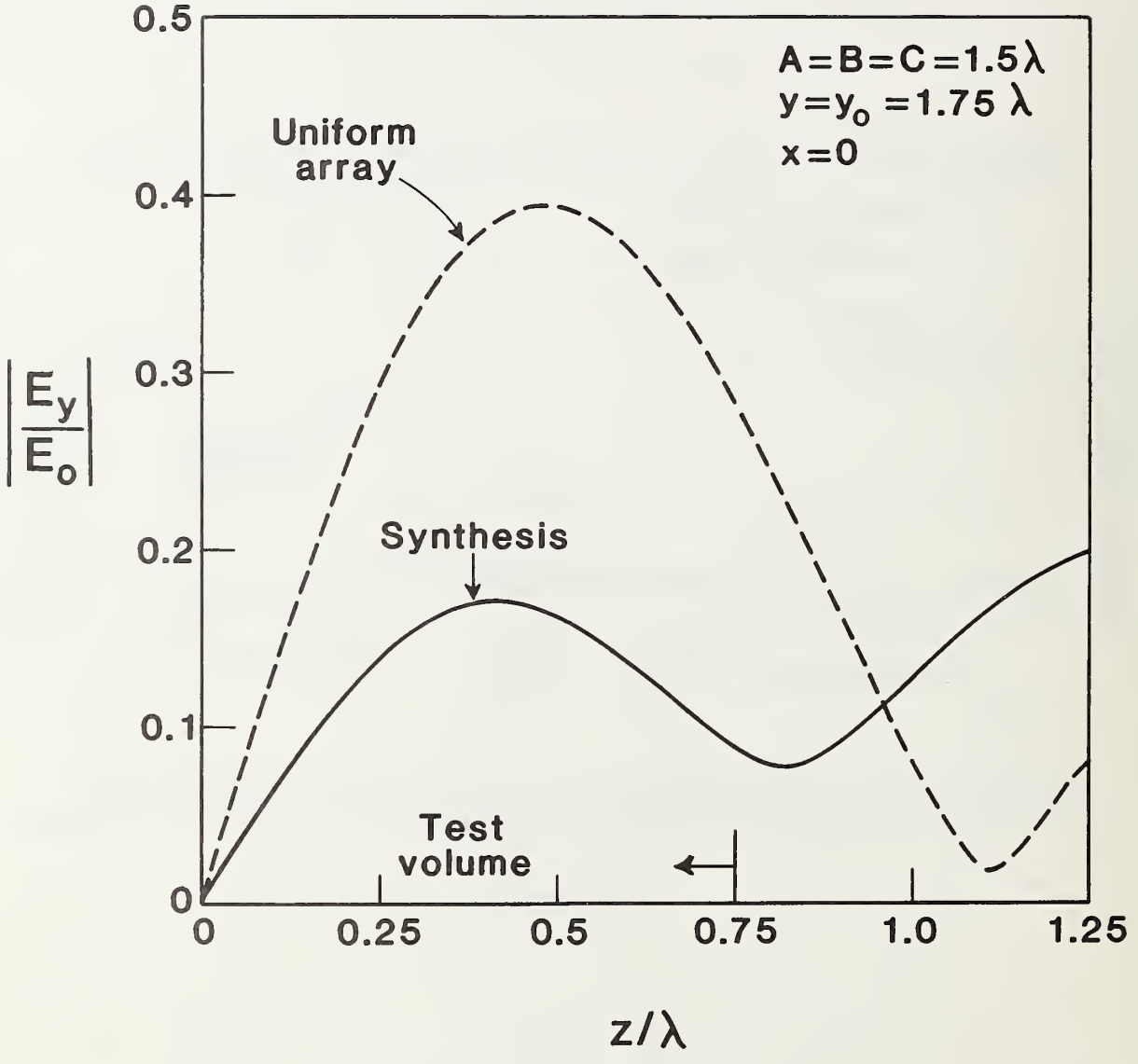


Figure 12. Normalized cross-polarized component of electric field for a synthesized array and a uniform array.

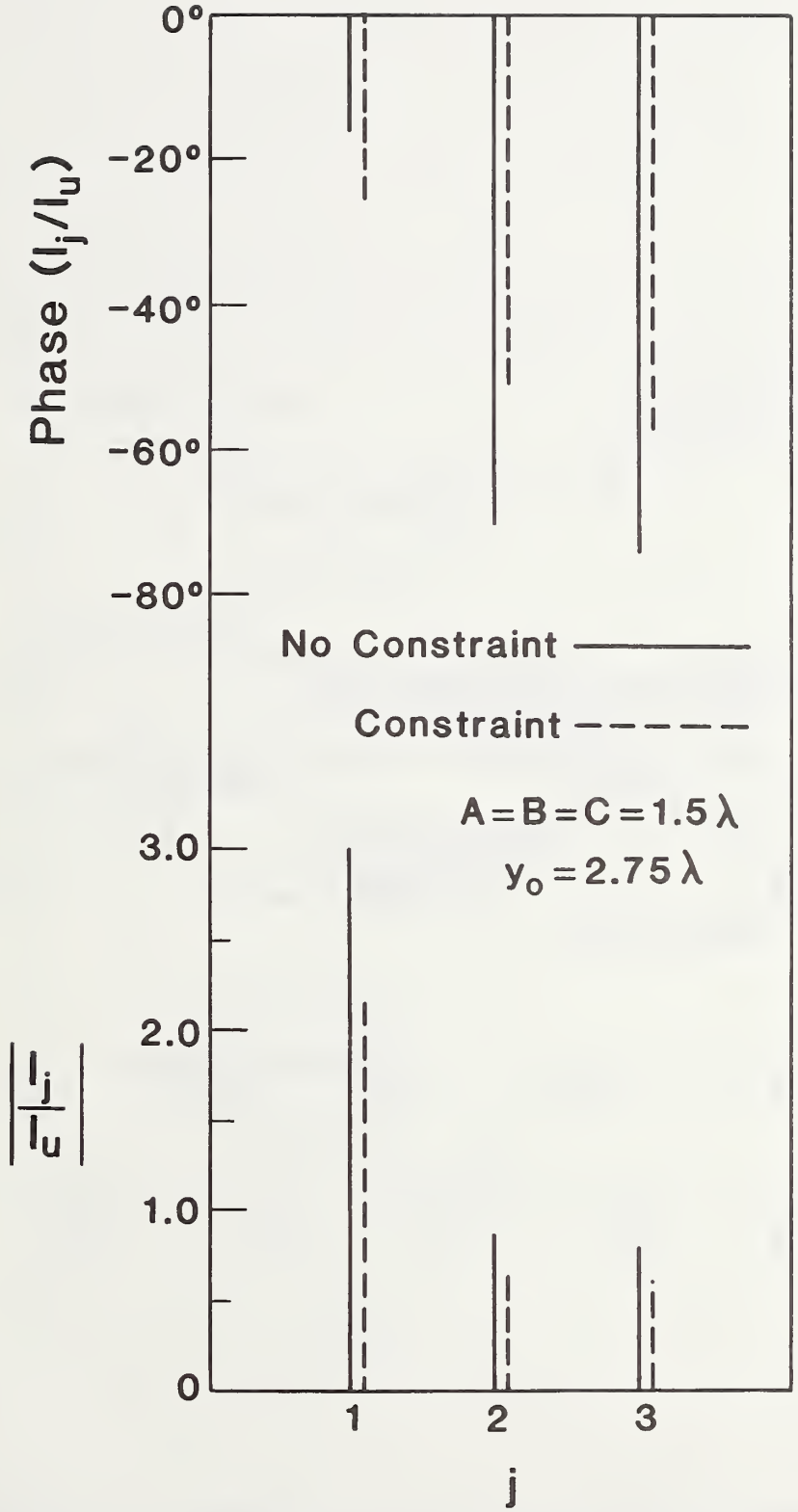


Figure 13. Magnitude and phase of the synthesized currents with and without a constraint.

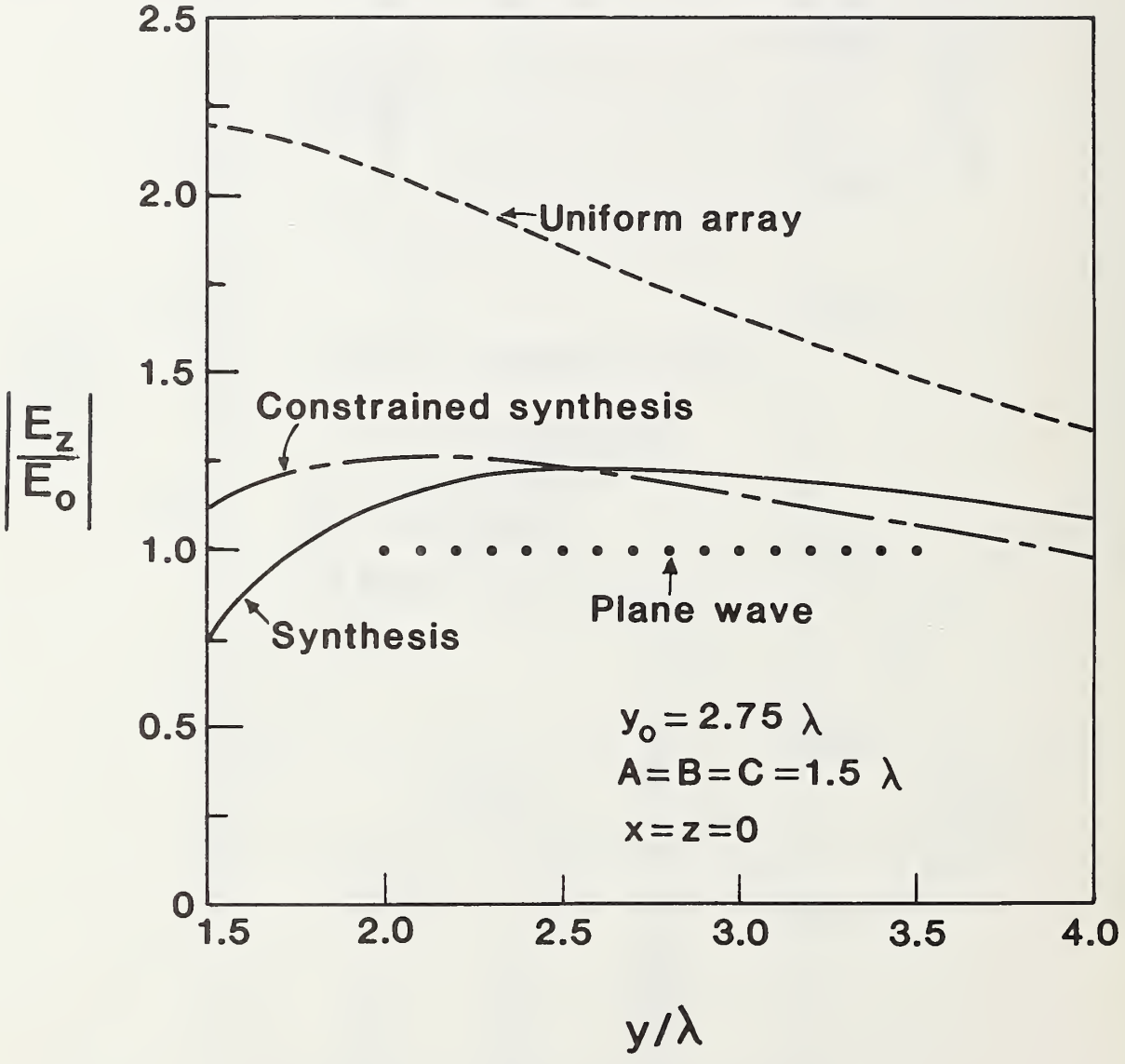


Figure 14. Normalized magnitude of the electric field for a synthesized array, a constrained synthesized array, and a uniform array. The perfect plane wave is shown for comparison.

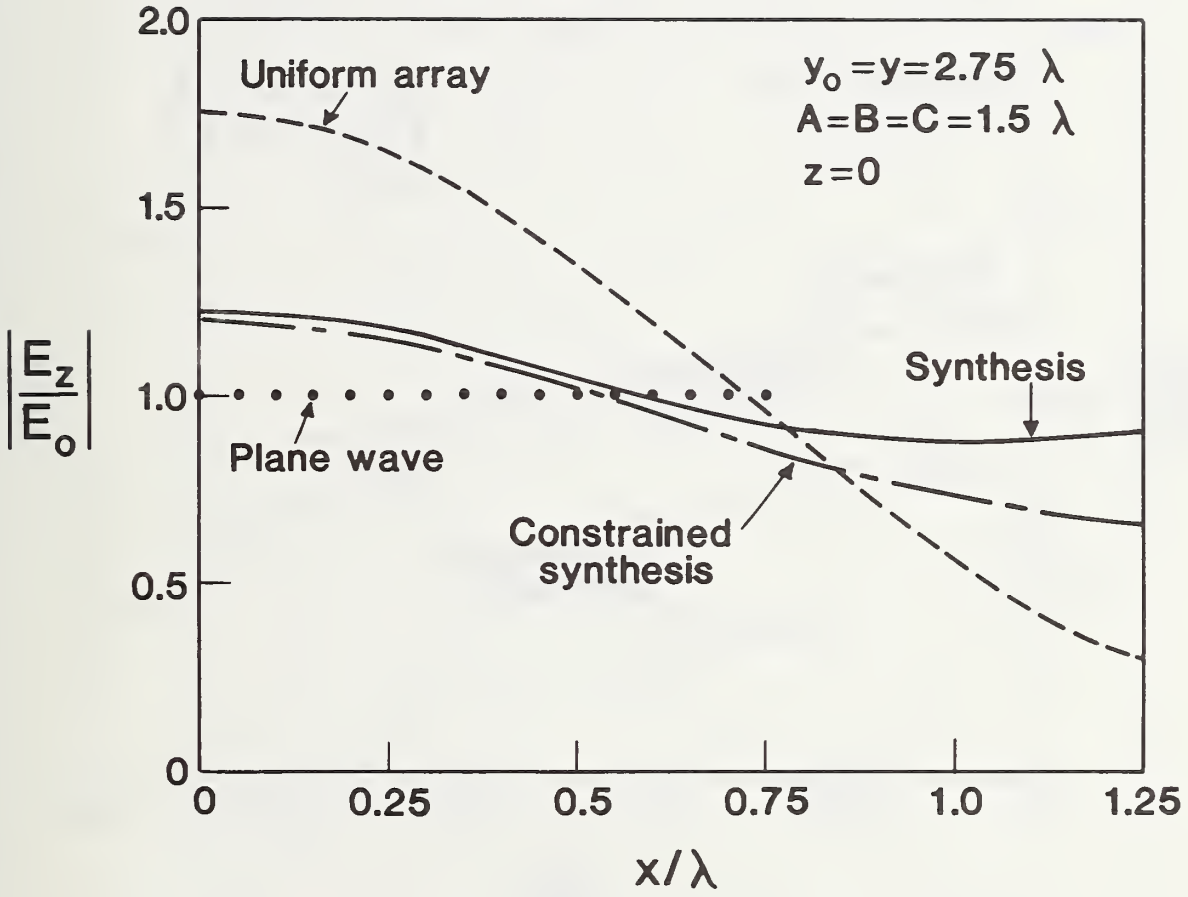


Figure 15. Normalized magnitude of the electric field for a synthesized array, a constrained synthesized array, and a uniform array. The perfect plane wave is shown for comparison.

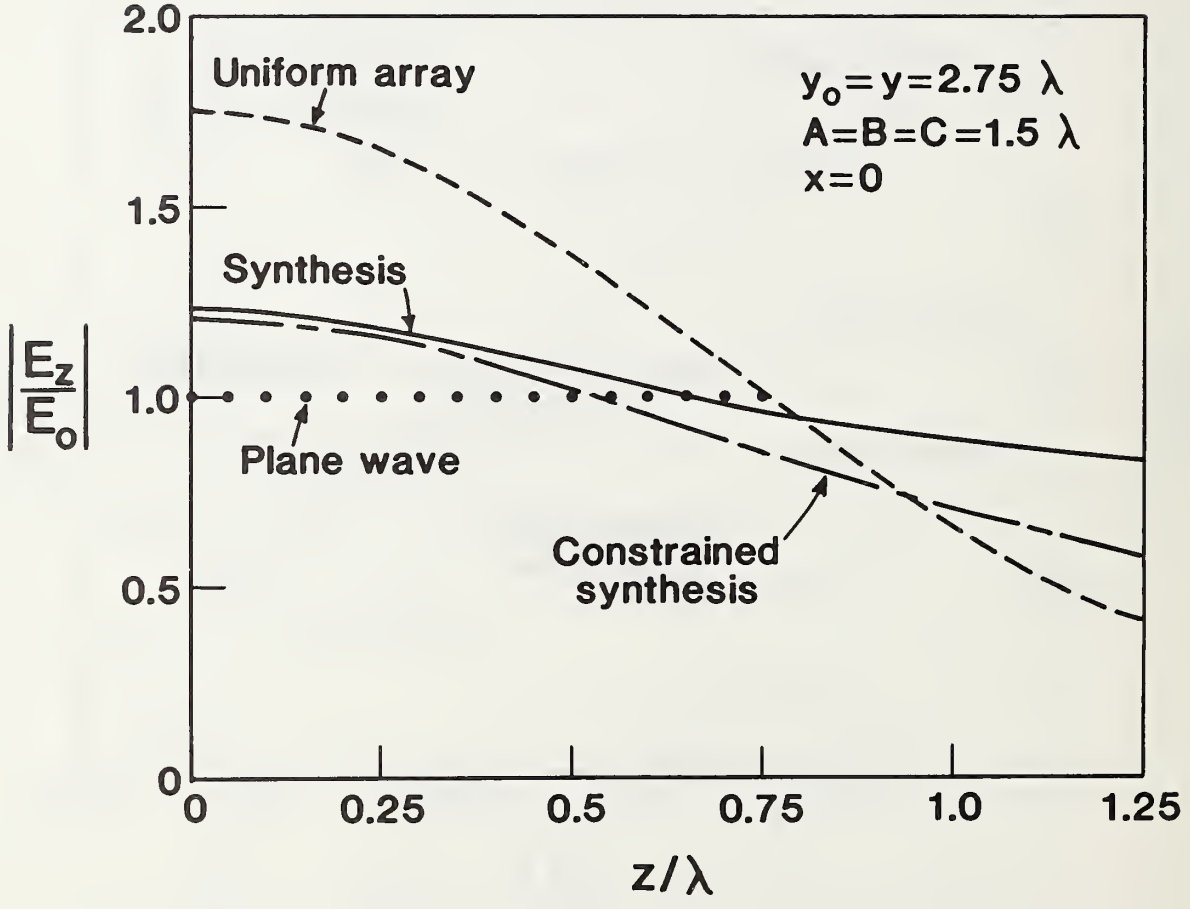


Figure 16. Normalized magnitude of the electric field for a synthesized array, a constrained synthesized array, and a uniform array. The perfect plane wave is shown for comparison.

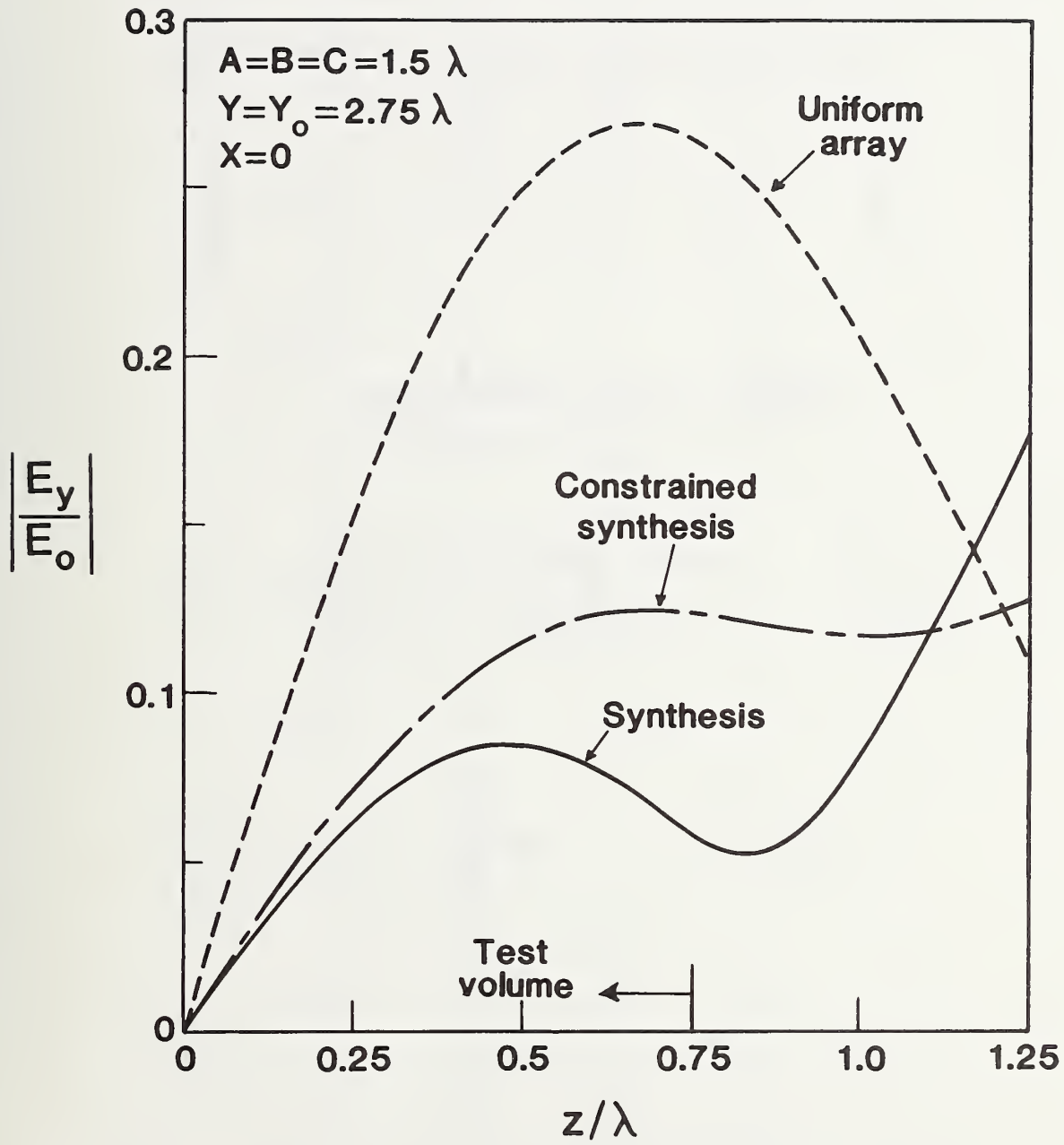


Figure 17. Normalized cross-polarized electric field for a synthesized array, a constrained synthesized array, and a uniform array.

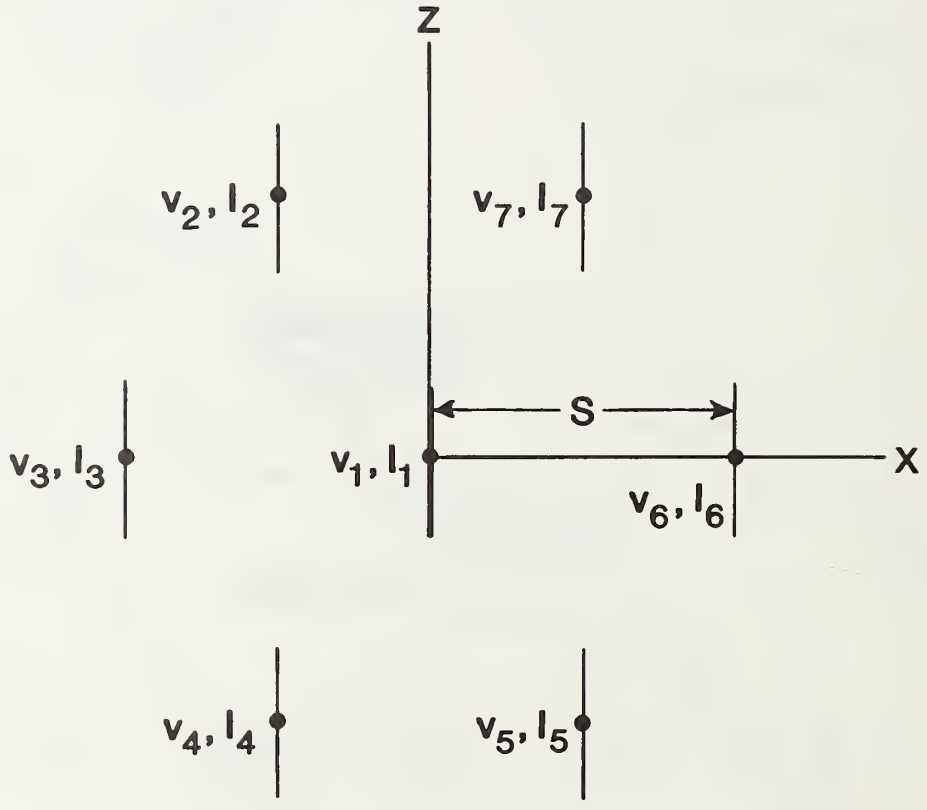


Figure 18. Voltages and currents for the seven-element array.

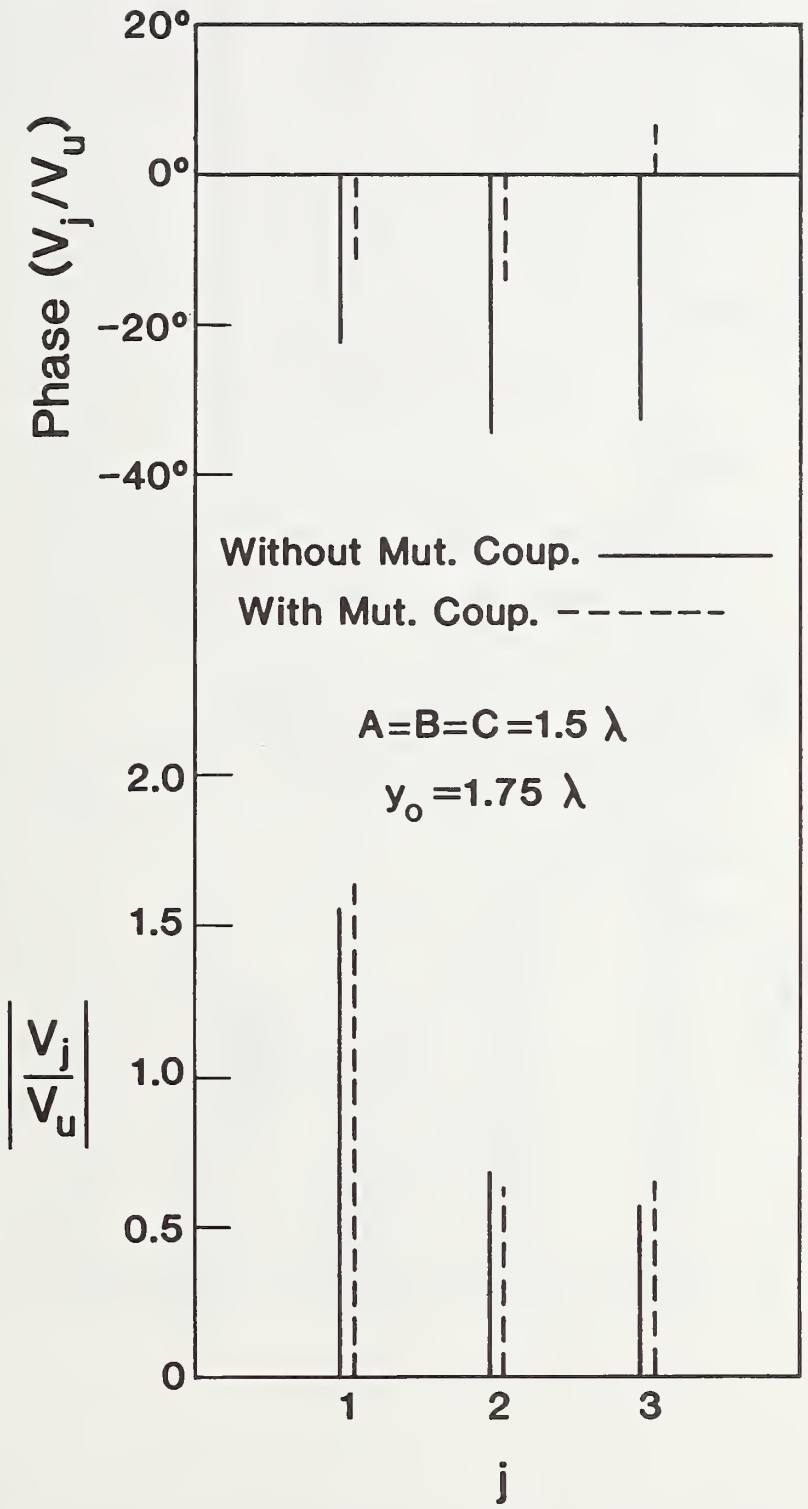


Figure 19. Magnitude and phase of the voltages with and without mutual coupling. These voltages correspond to the currents in figure 5.

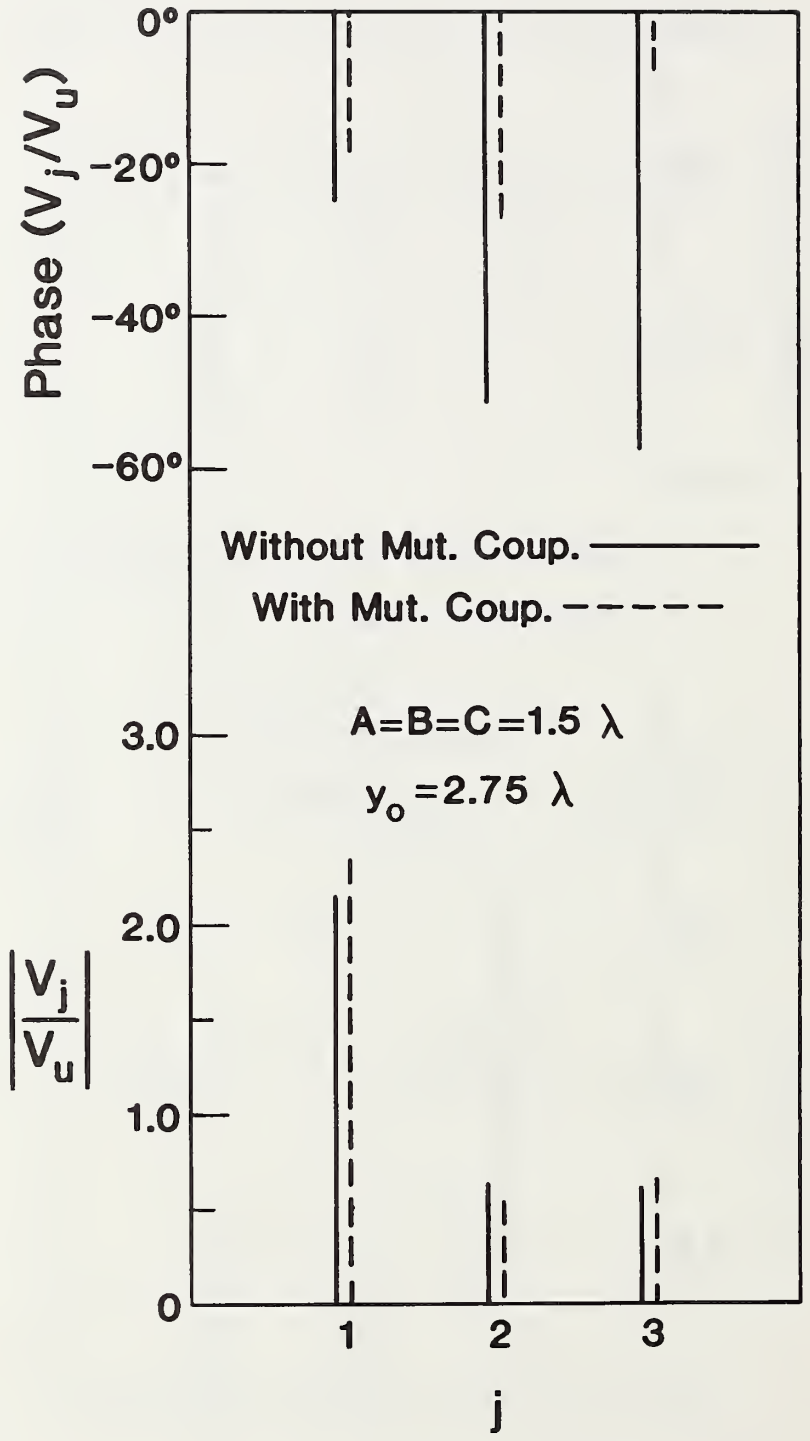


Figure 20. Magnitude and phase of the voltages with and without mutual coupling. These voltages correspond to the currents in figure 13.

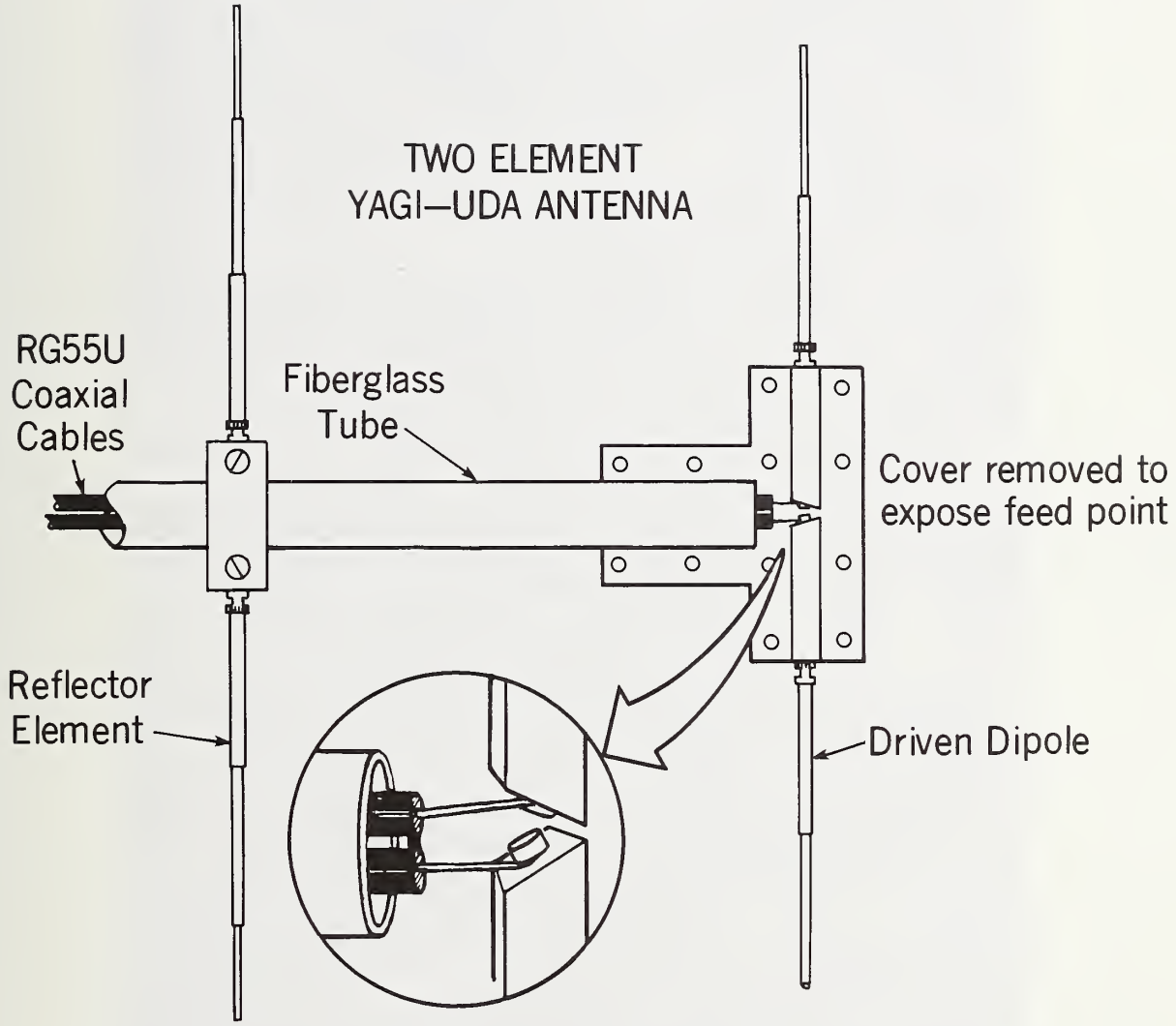


Figure 21. Construction of two-element, Yagi-Uda antenna.

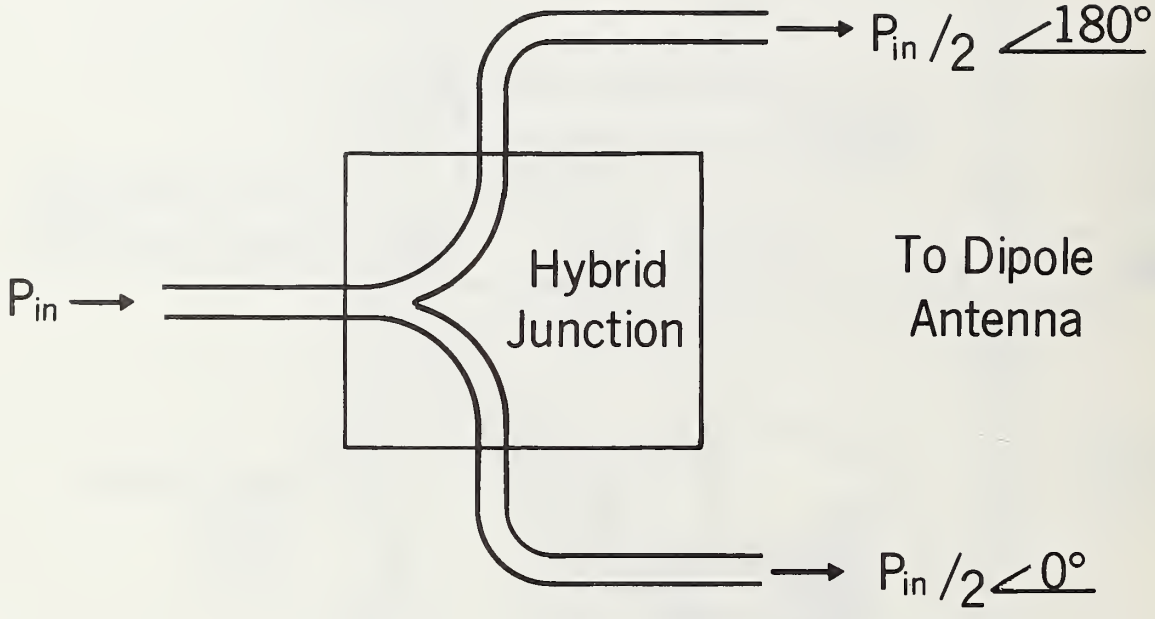


Figure 22. Dipole feed using dual coaxial lines and 0° - 180° hybrid junction.

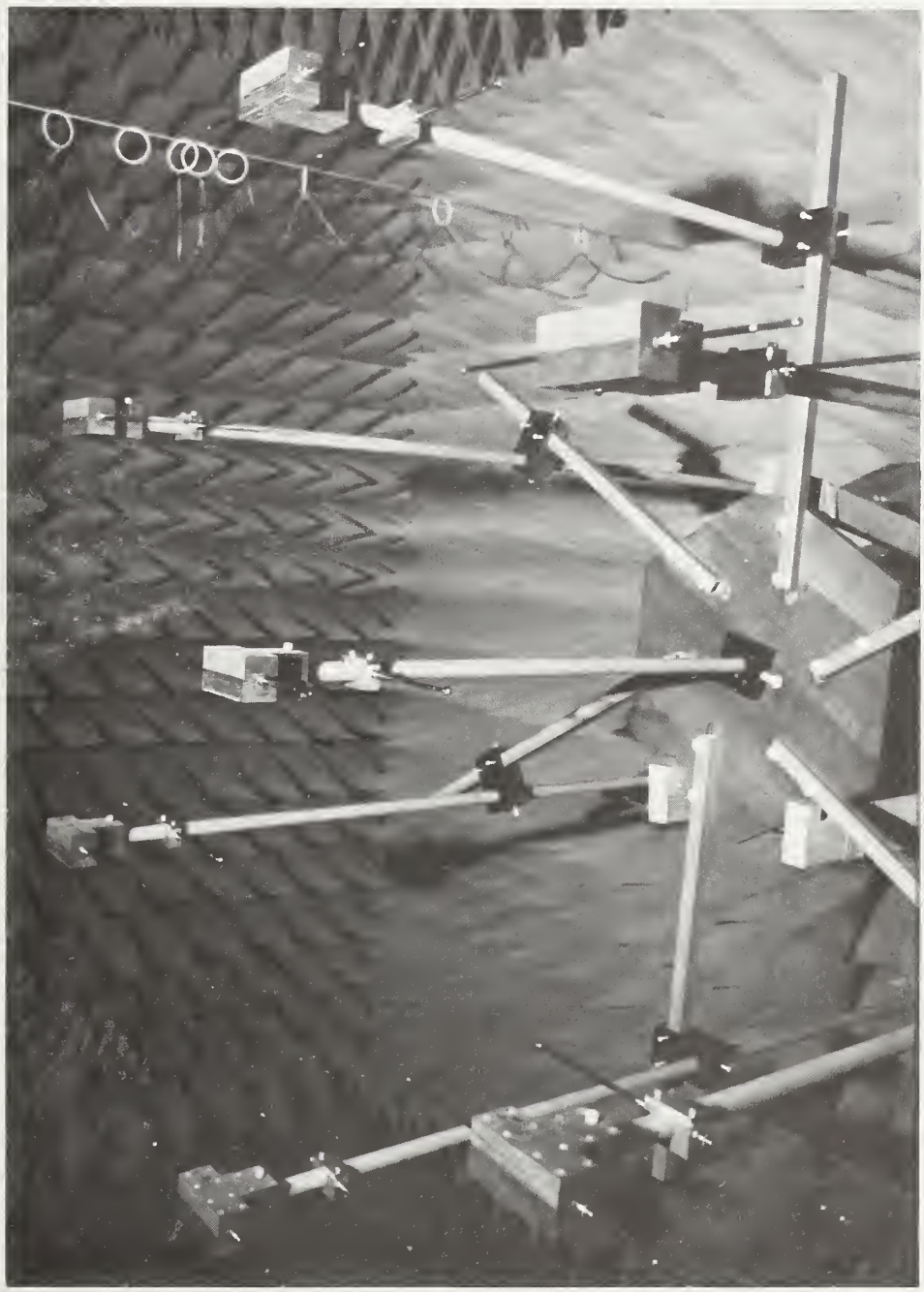

Figure 23. Seven-element array and support structure.

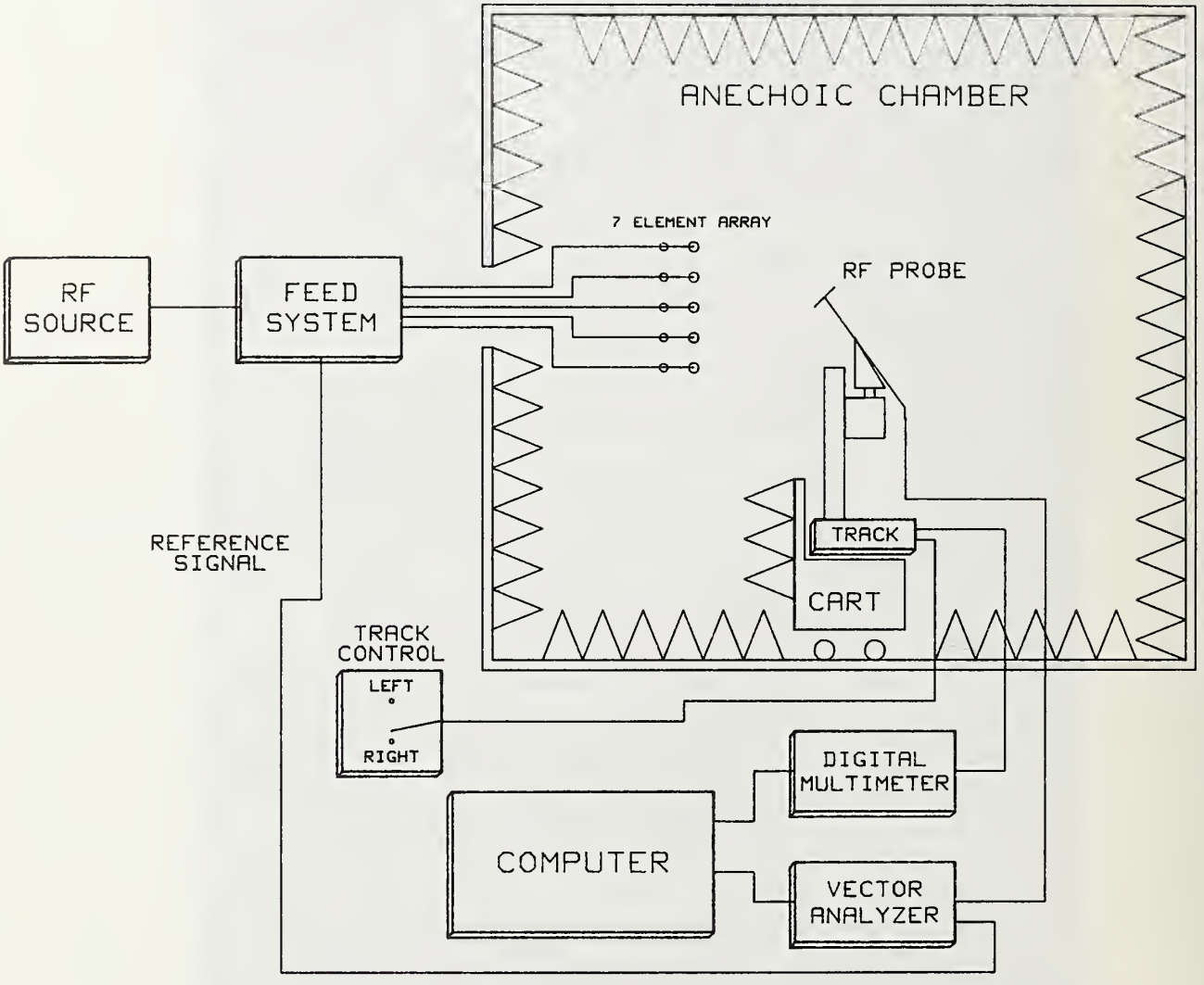


Figure 24. Measurement system.

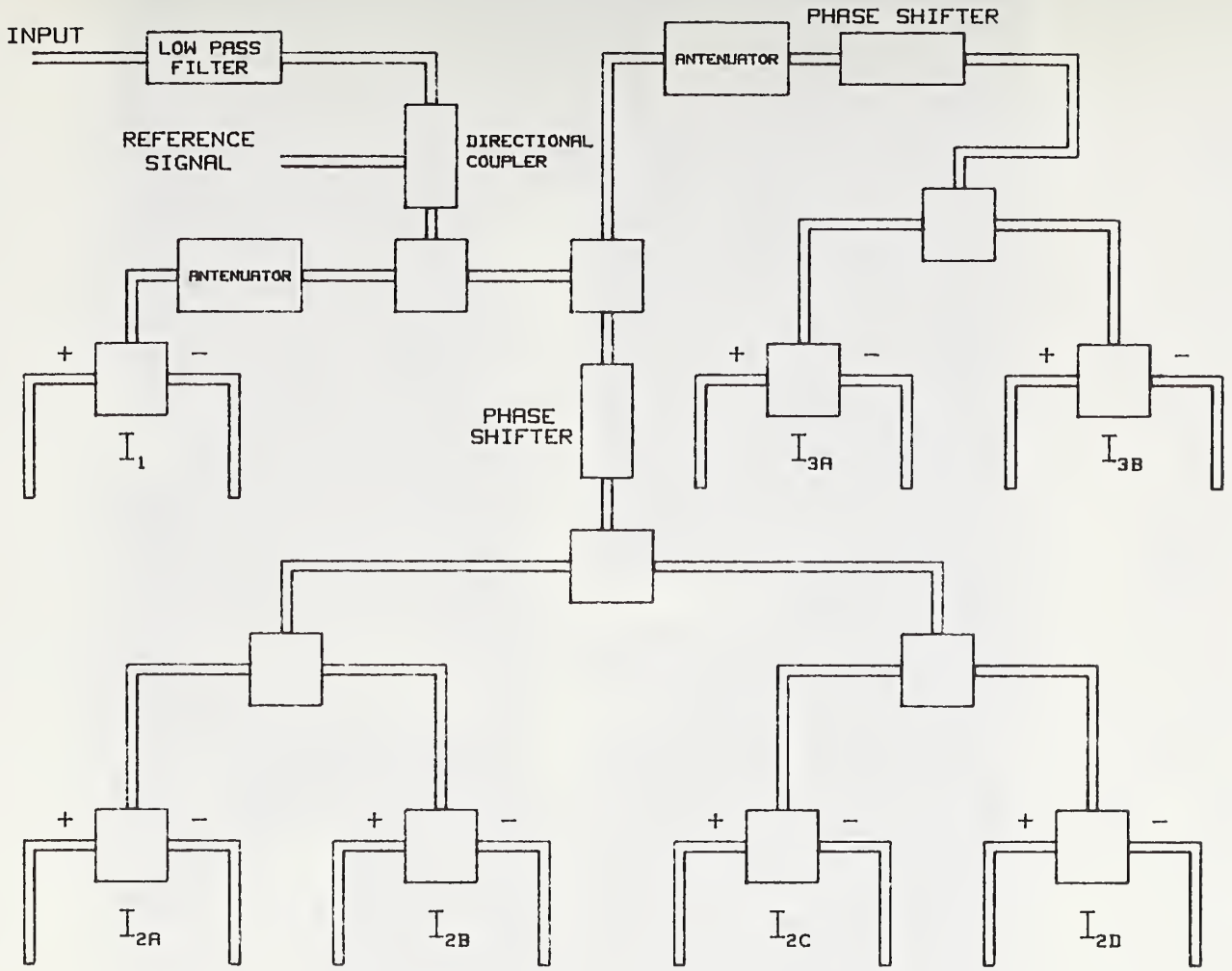


Figure 25. Array feed system.

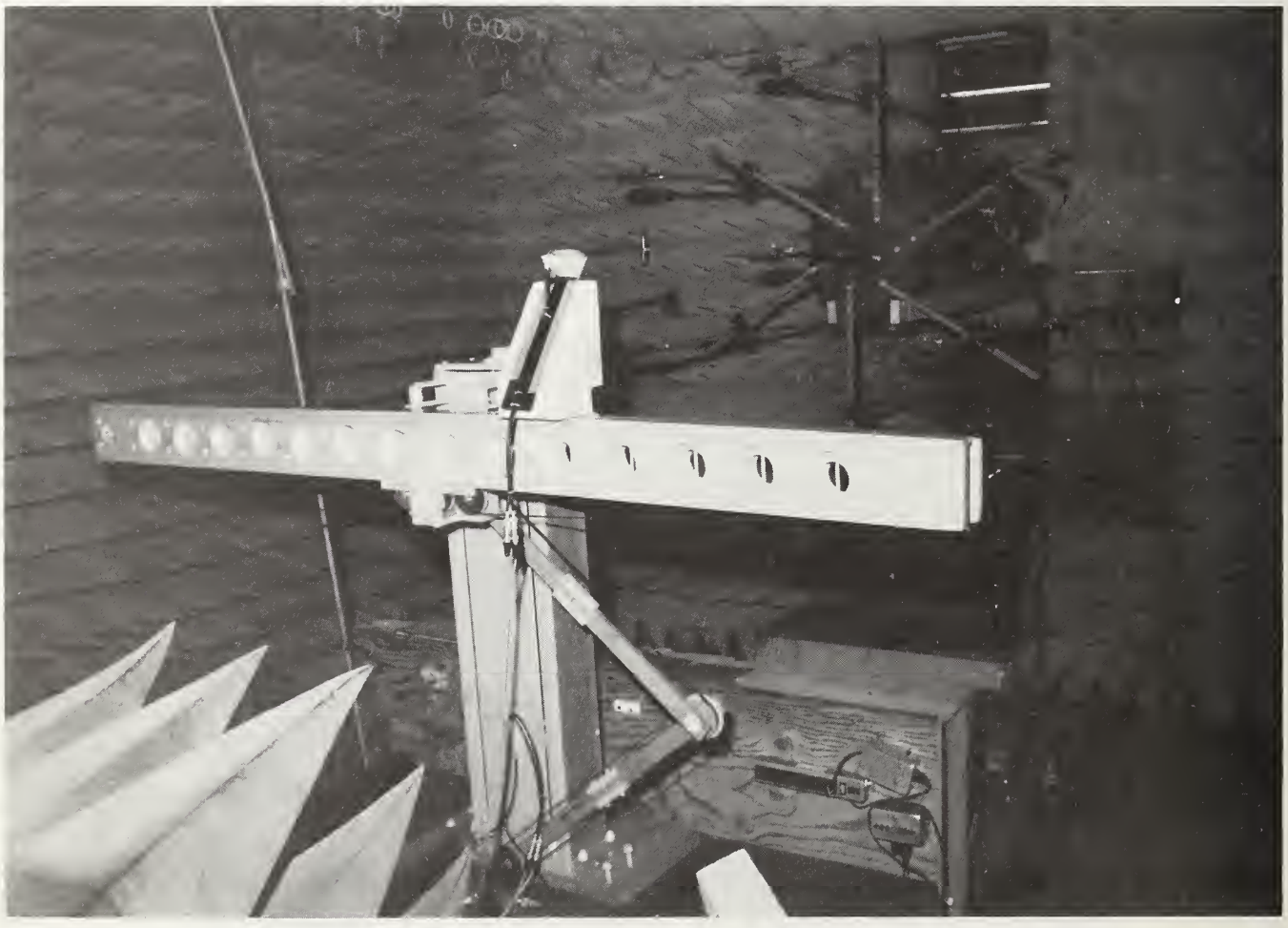

Figure 26. Experiment hardware: probe positioner (track mechanism) and seven-element array.

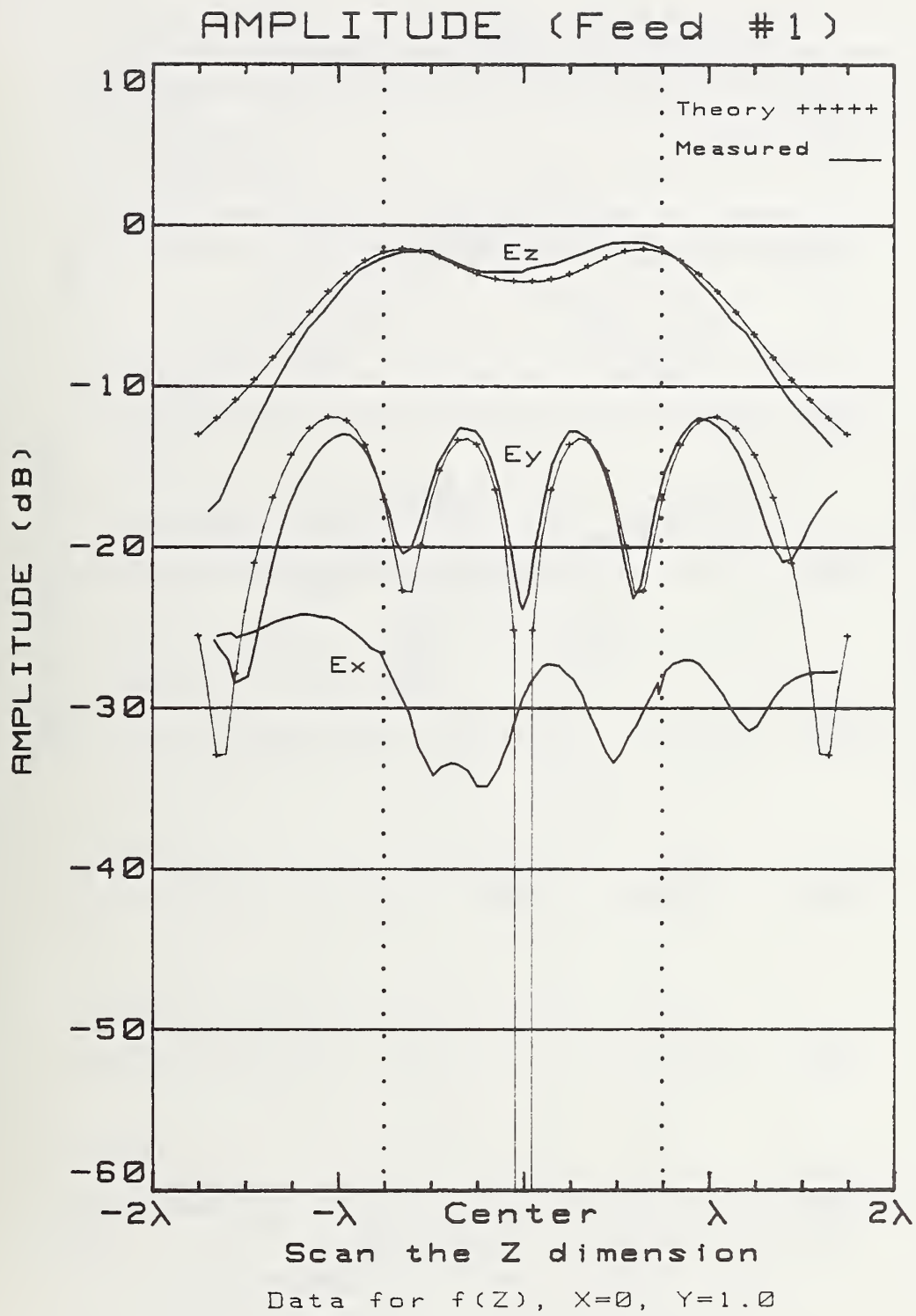


Figure 27. Theoretical and measured electric field amplitude at the center surface of the test volume (y = λ).

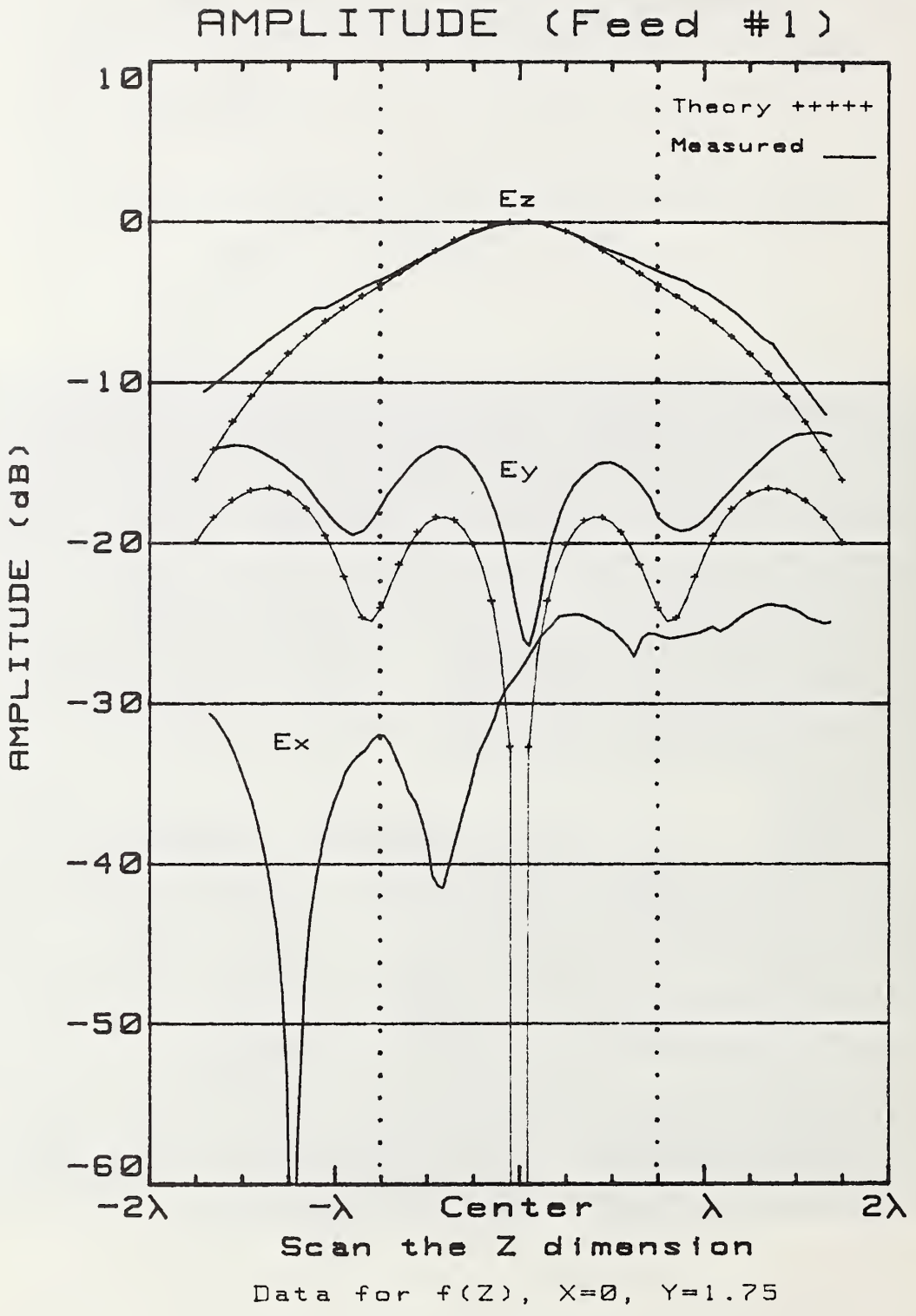


Figure 28. Theoretical and measured electric field amplitude at the far surface of the test volume (y = 1.75 λ).

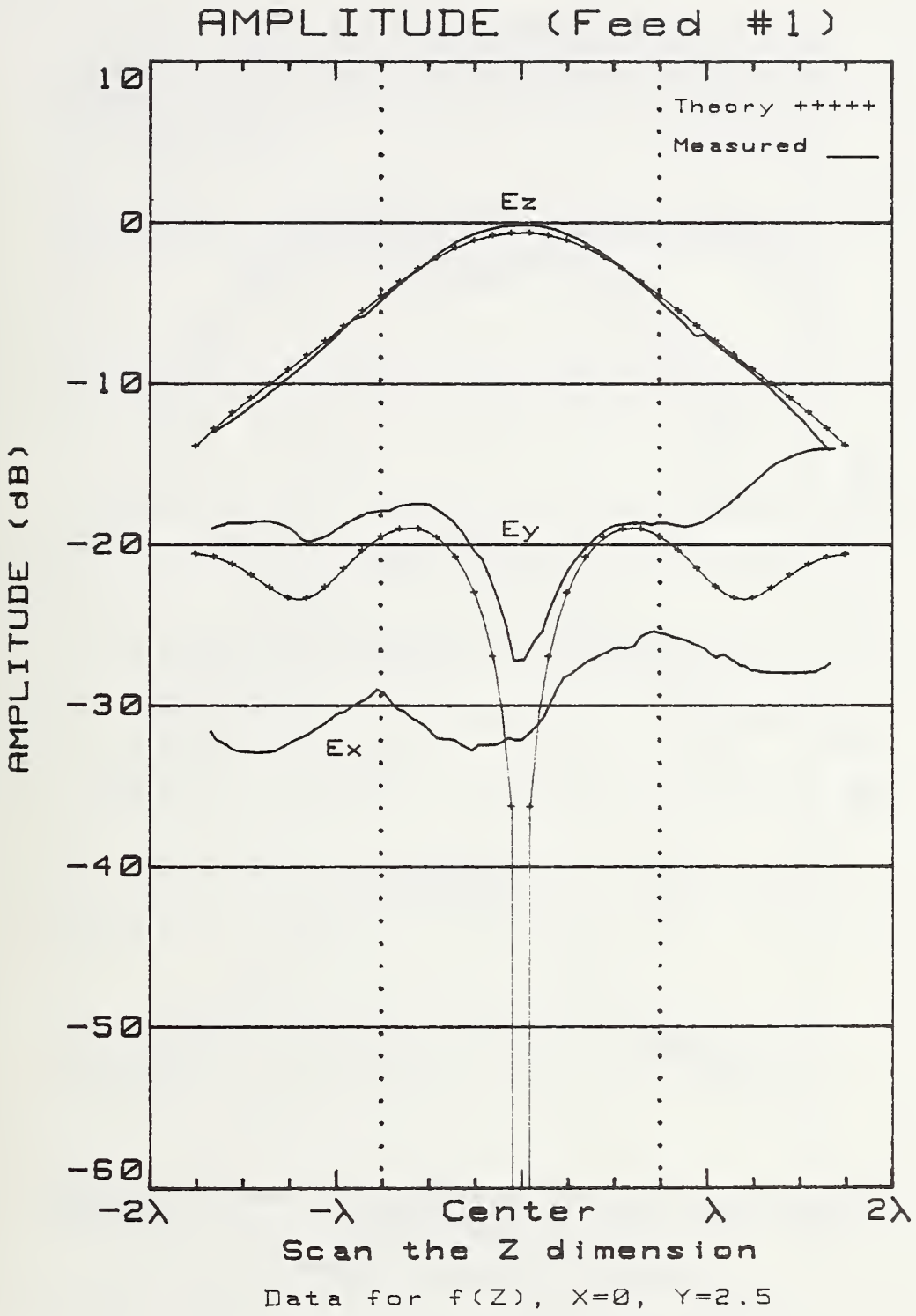


Figure 29. Theoretical and measured electric field amplitude at the near surface of the test volume (y = 2.5 λ).

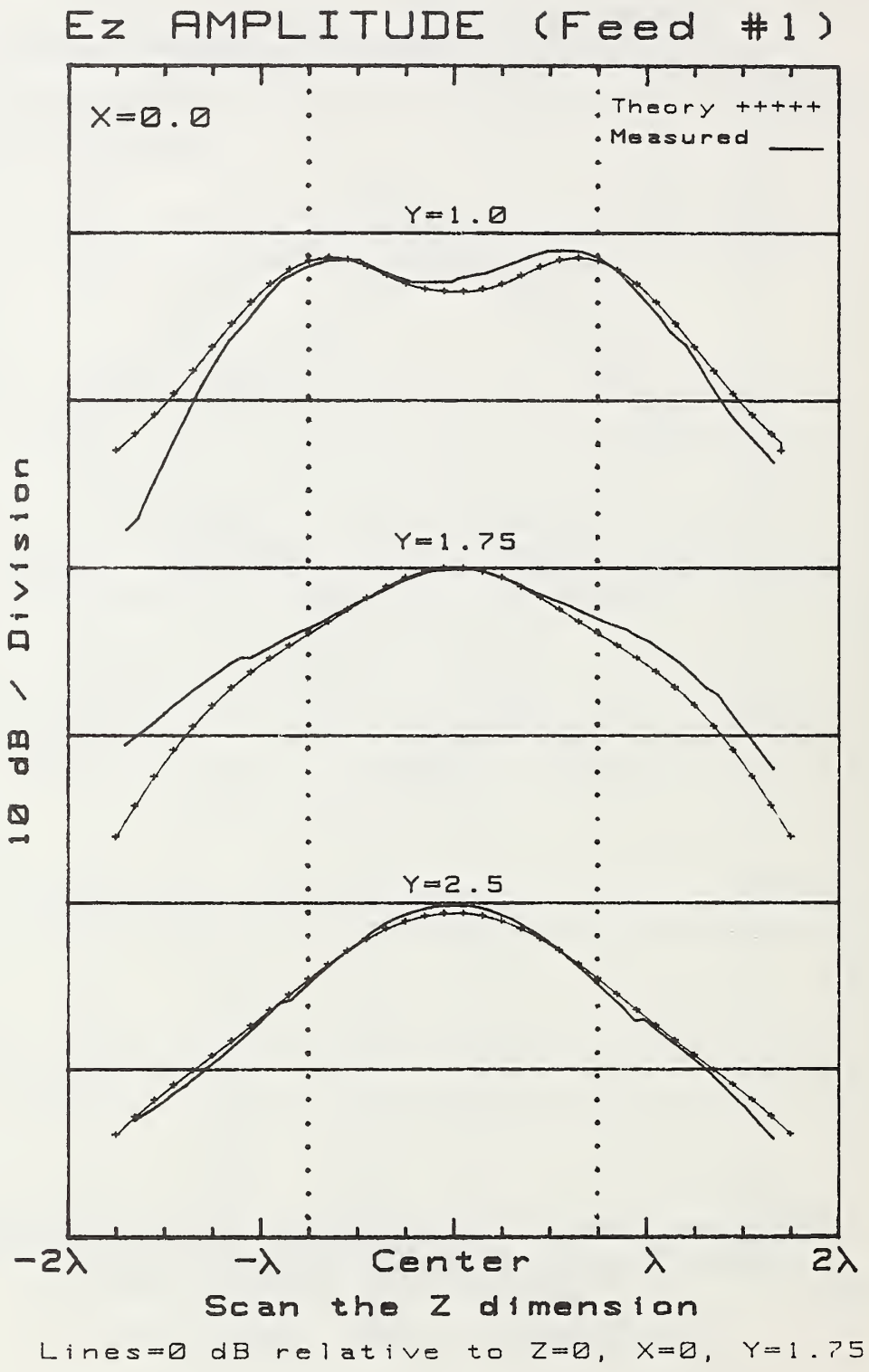


Figure 30. Theoretical and measured amplitude of $E_z$ at three distances from the array.

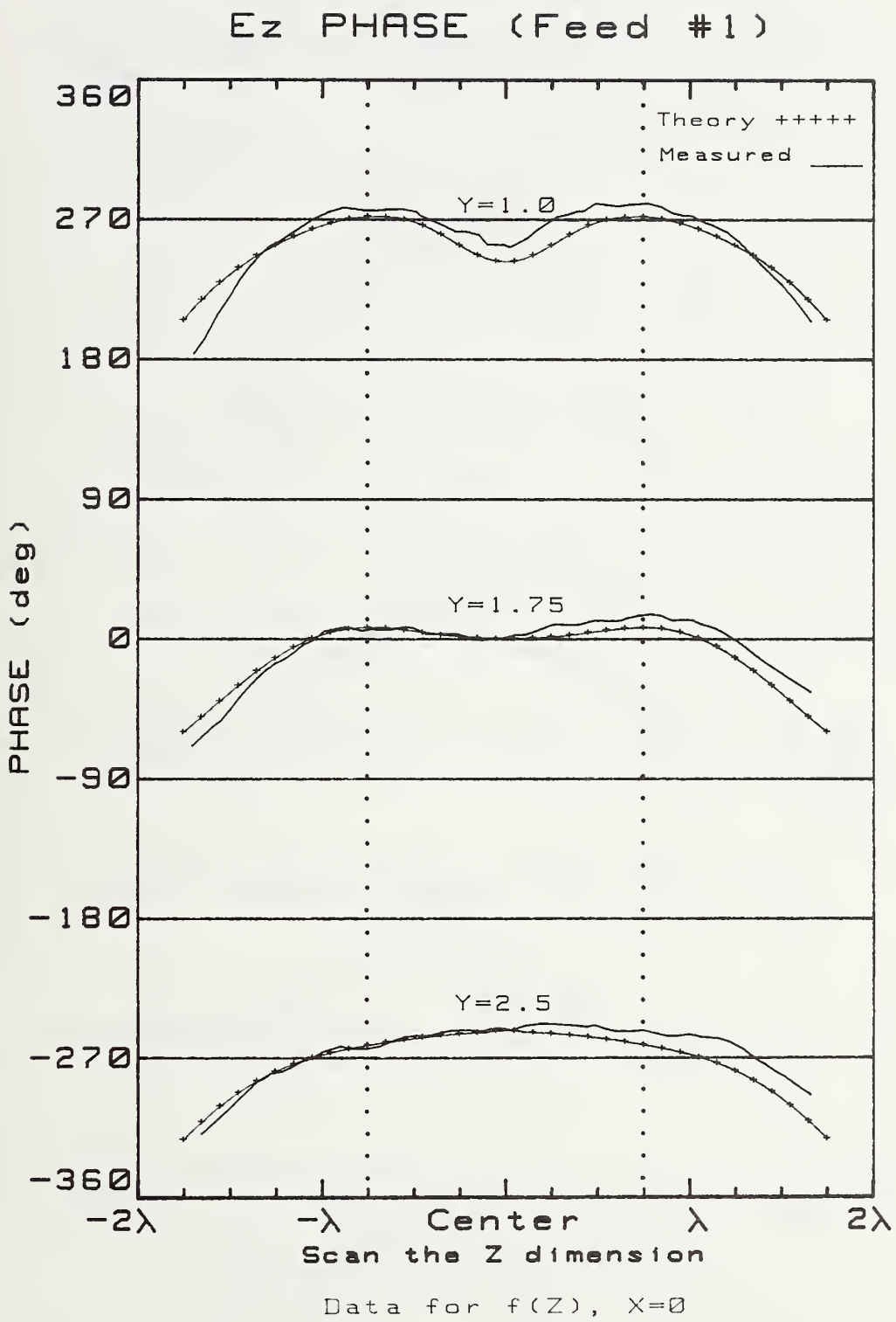


Figure 31. Theoretical and measured phase of $E_z$ at three distances from the array.

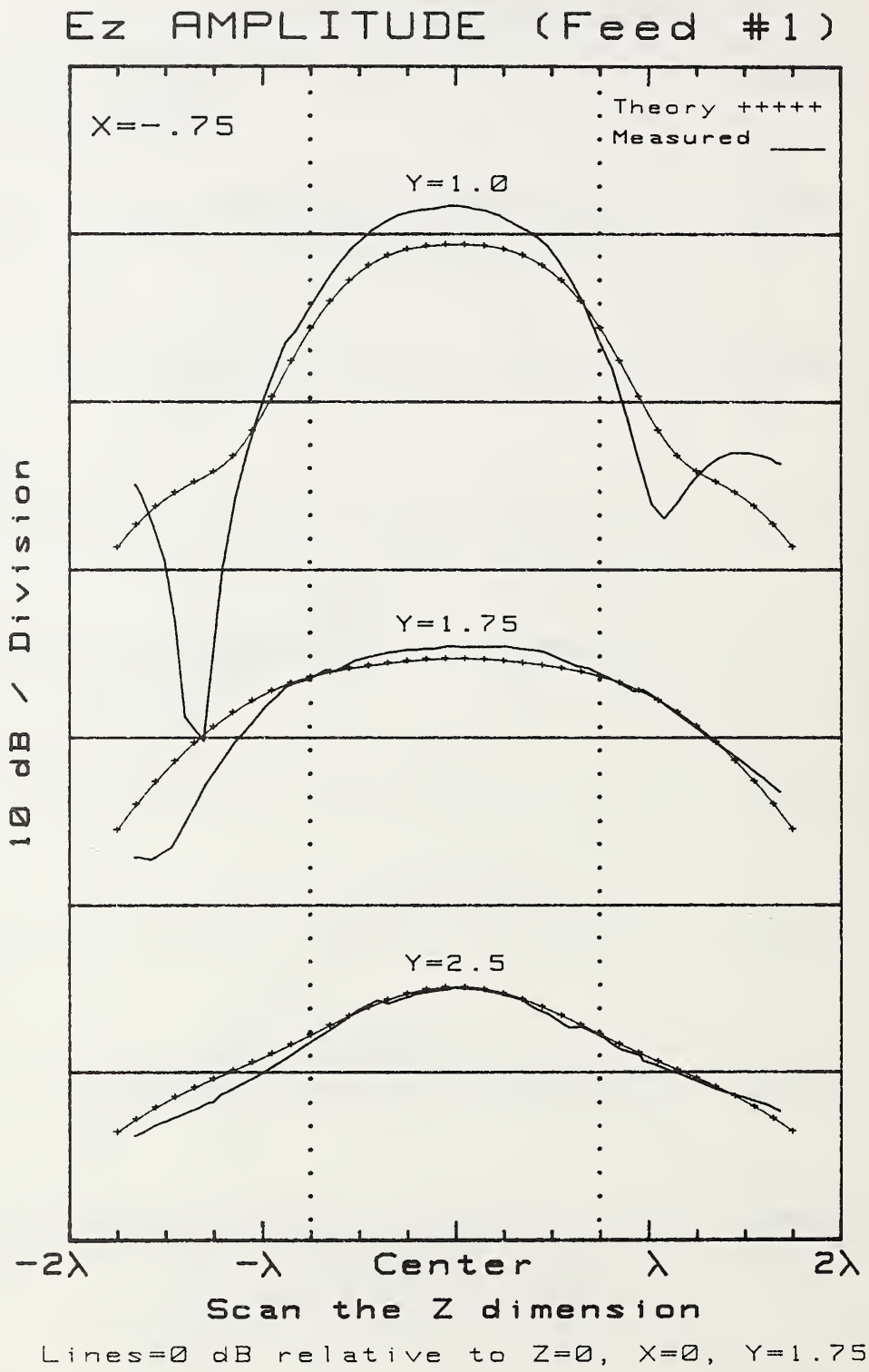


Figure 32. Theoretical and measured amplitude of $E_z$ at three distances from the array for x = 0.75 λ.

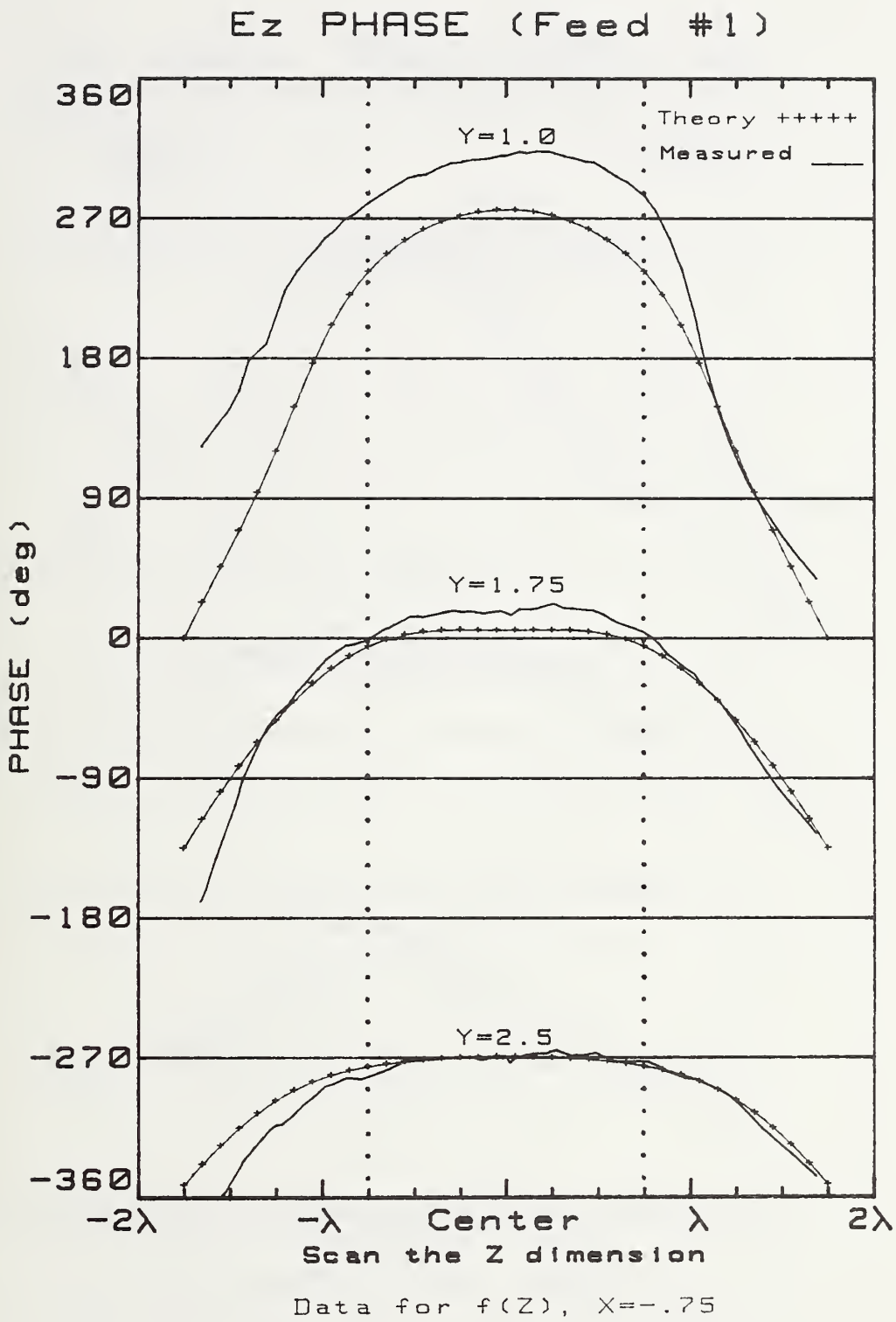


Figure 33. Theoretical and measured phase of $E_z$ at three distances from the array for x = -0.75 λ.

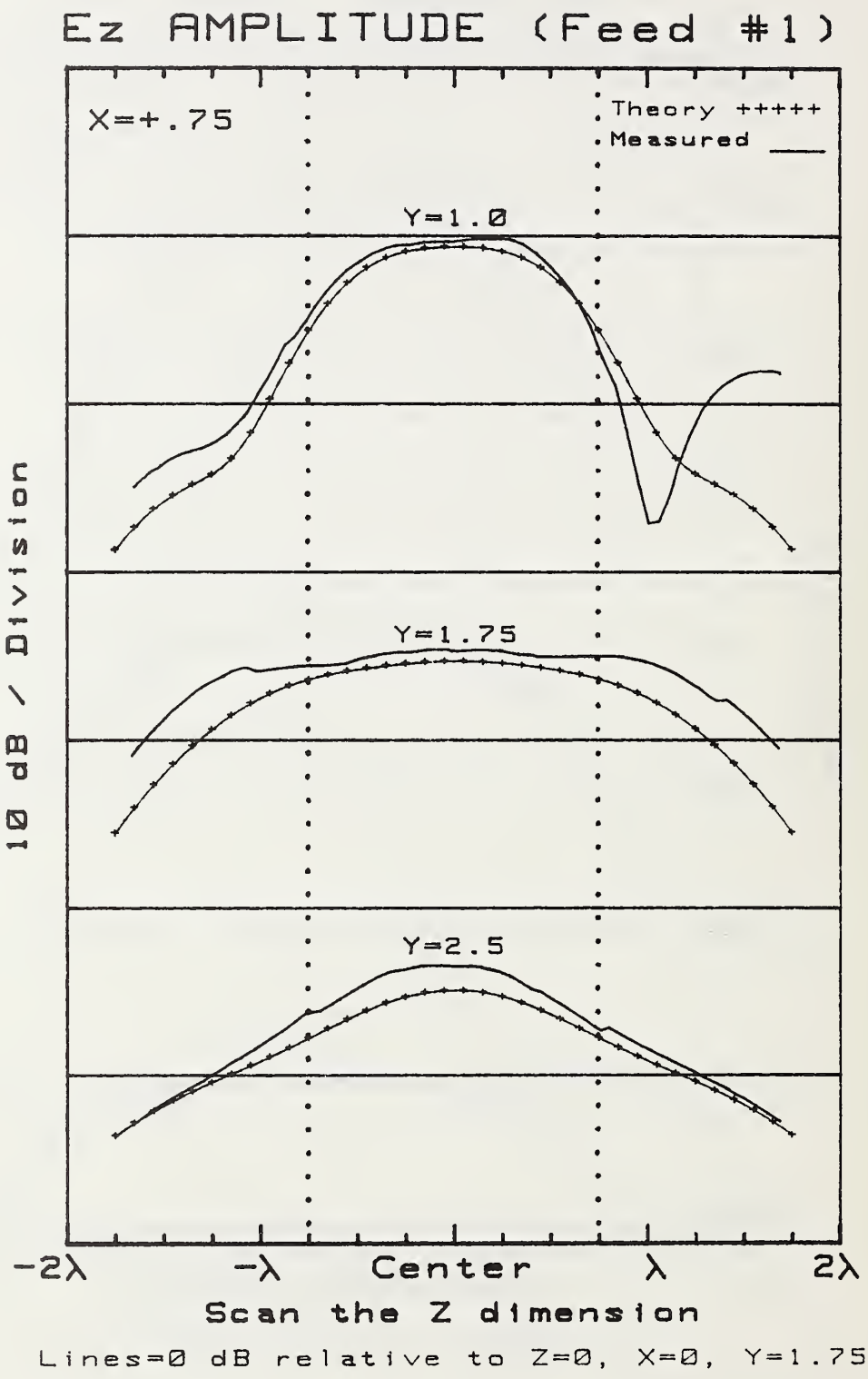


Figure 34. Theoretical and measured amplitude of $E_z$ at three distances from the array for x = 0.75 λ.

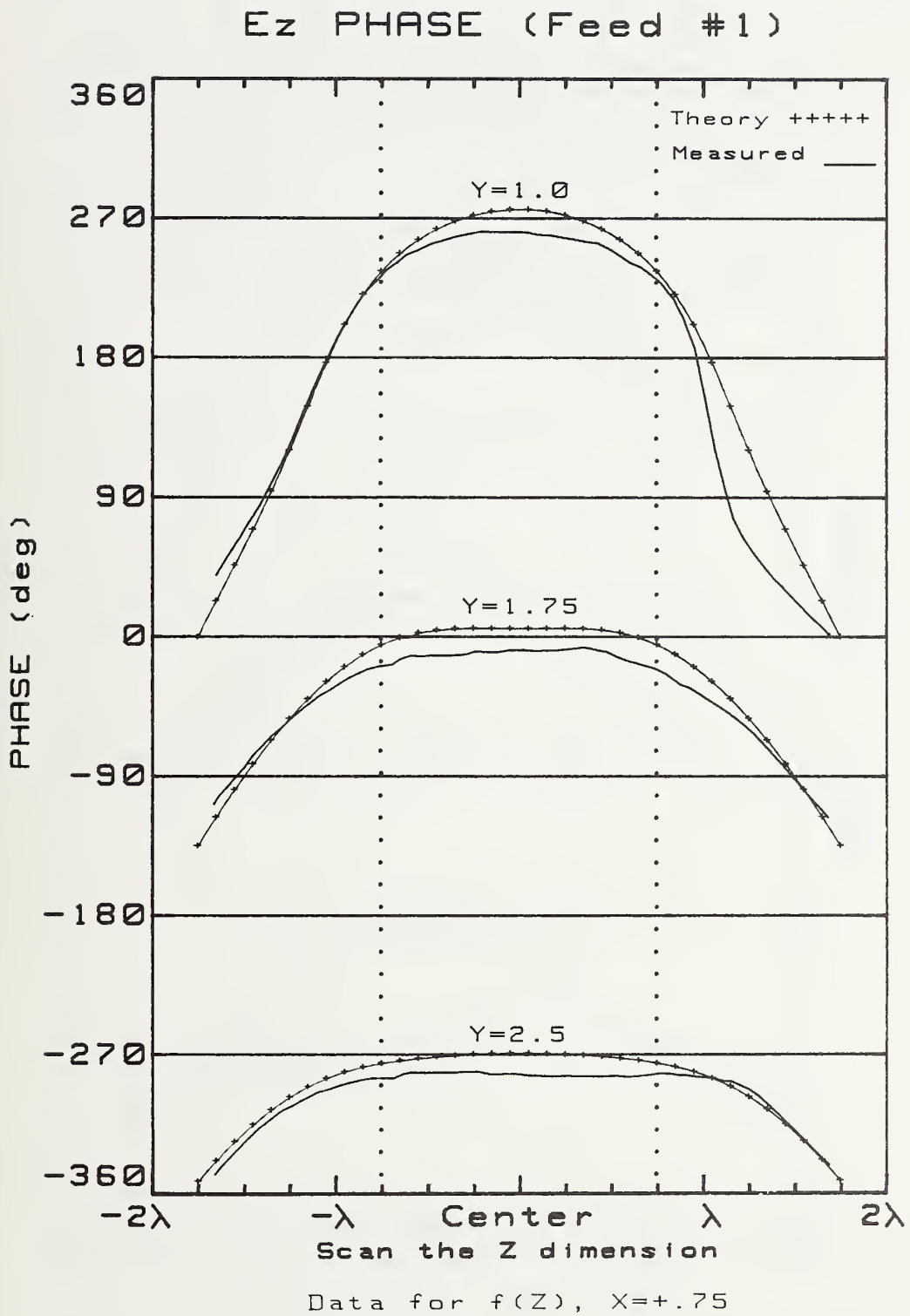


Figure 35. Theoretical and measured phase of $E_z$ at three distances from the array for x = 0.75 λ.

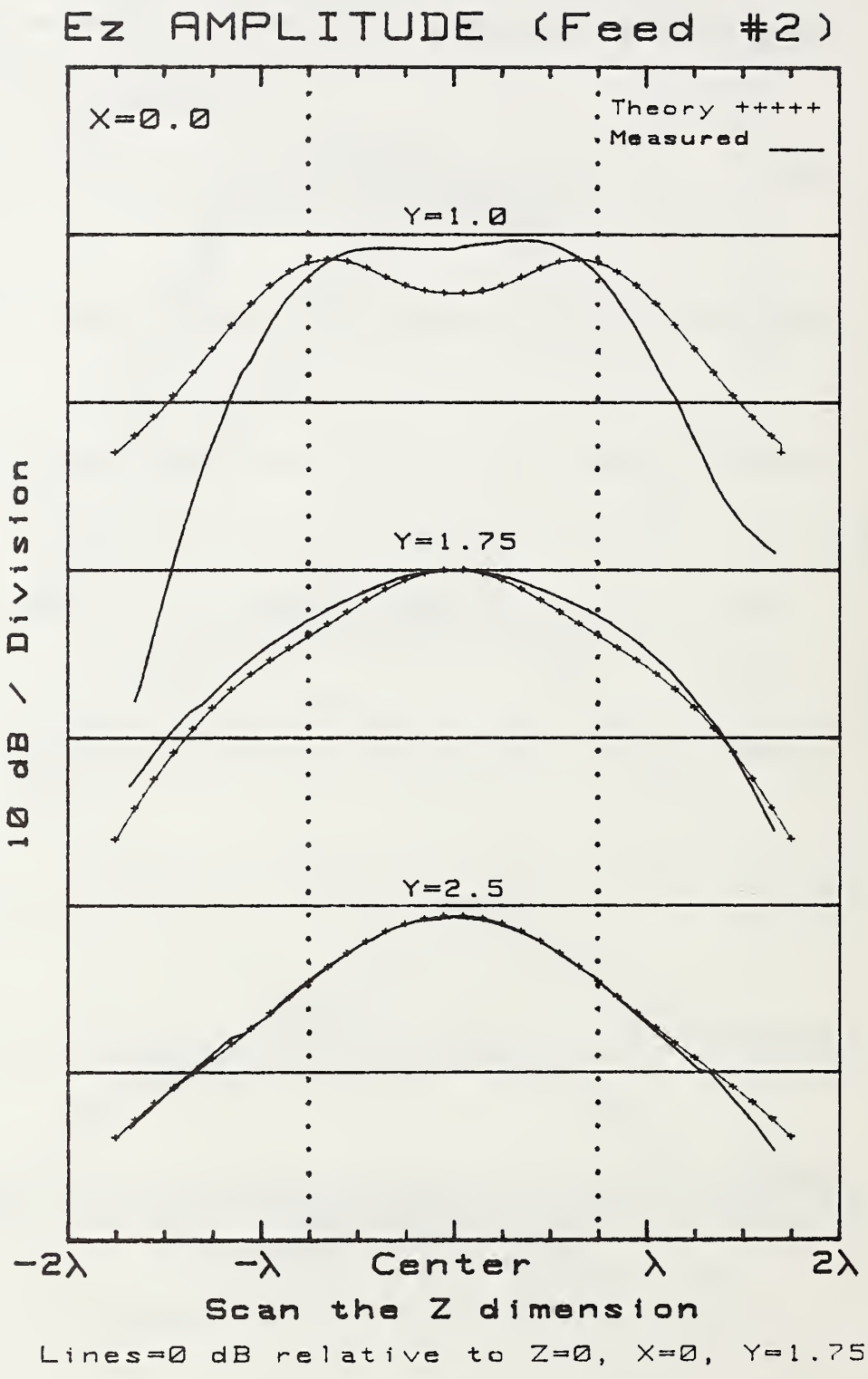


Figure 36. Theoretical and measured amplitude of $E_z$ at three distances from the array. Mutual coupling effects are included in the feed.

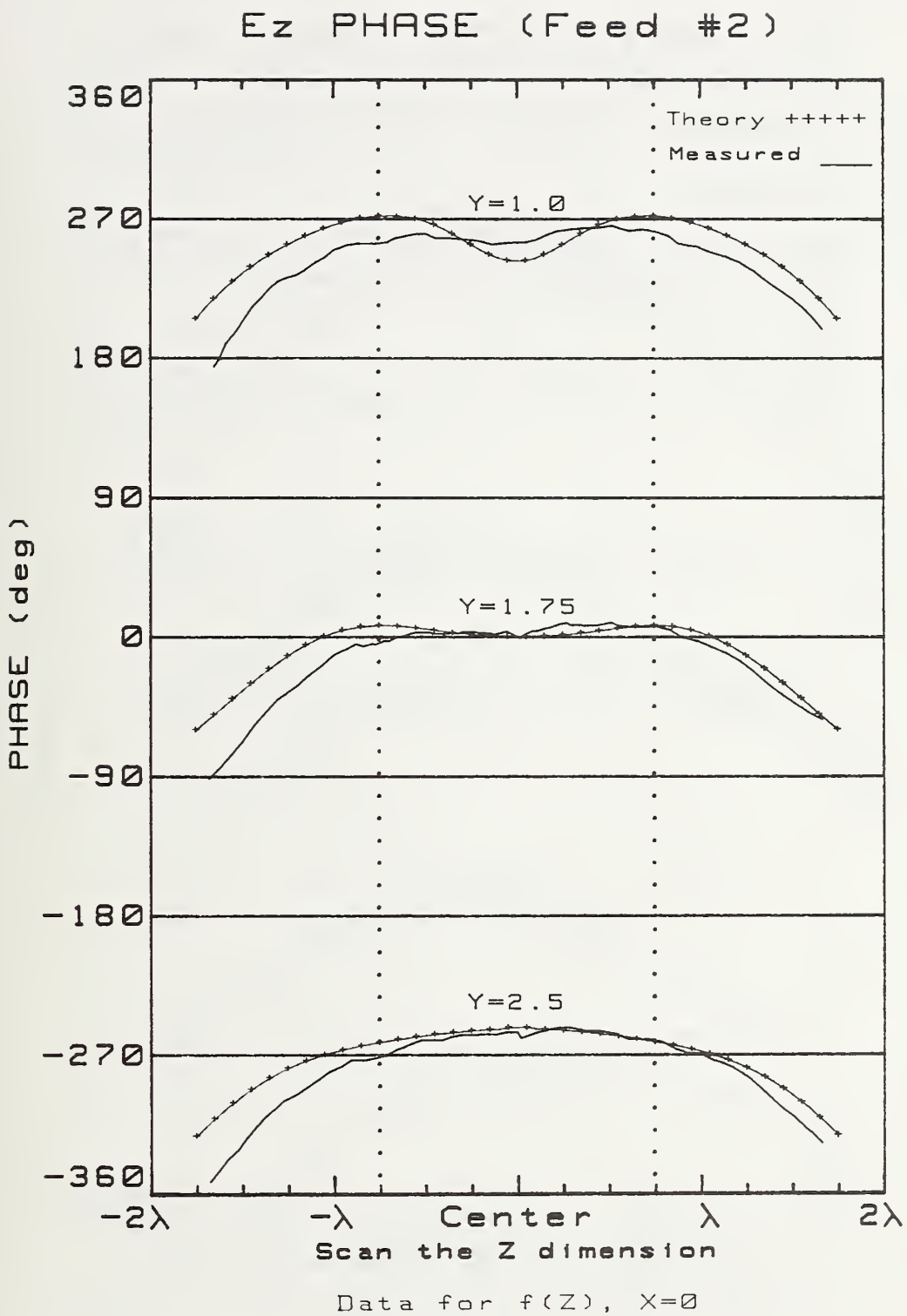


Figure 37. Theoretical and measured phase of $E_z$ at three distances from the array. Mutual coupling effects are included in the feed.

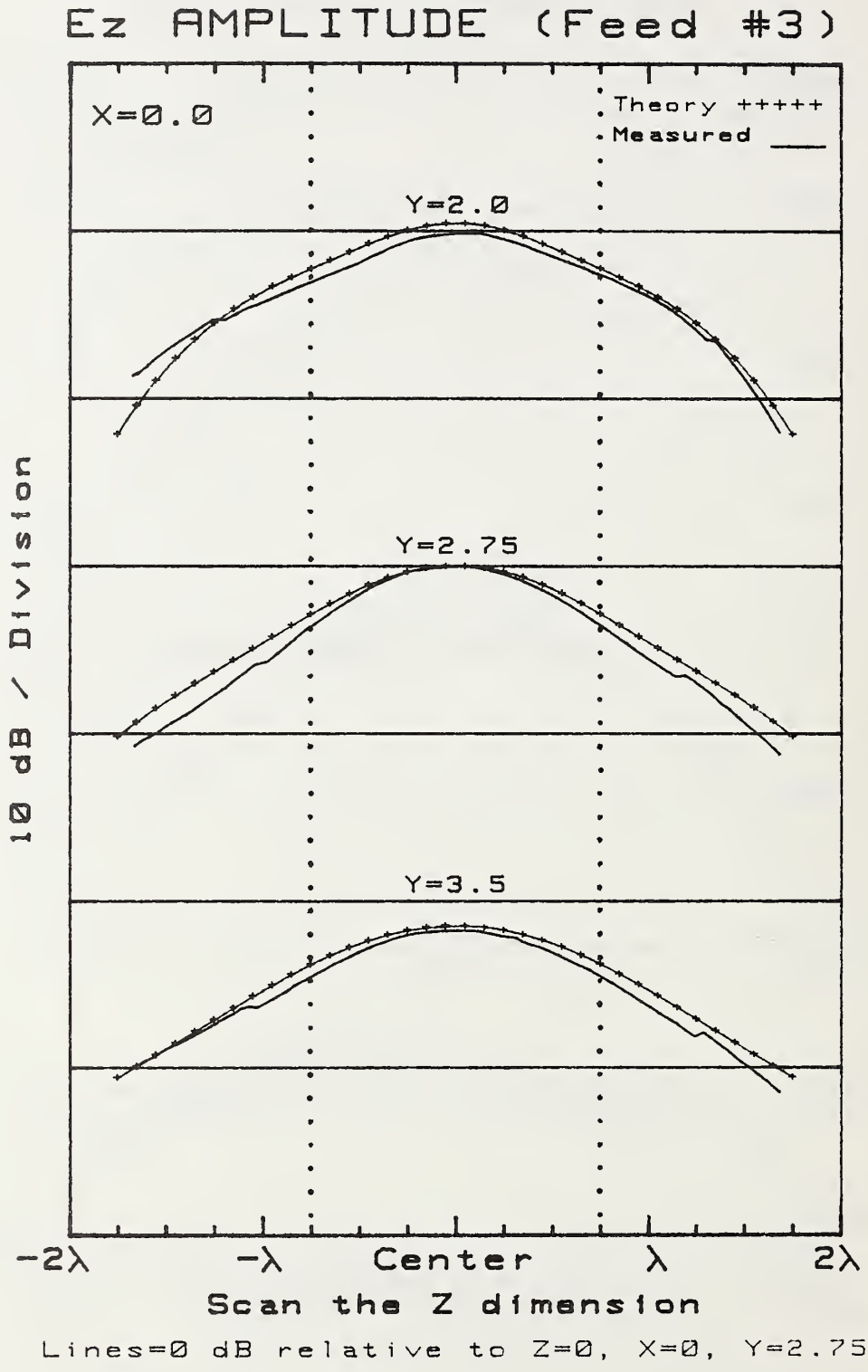


Figure 38. Theoretical and measured amplitude of $E_z$ at the boundaries (y = 2.0 λ, 3.5 λ) and the center (y = 2.75λ) of the more distant test volume.

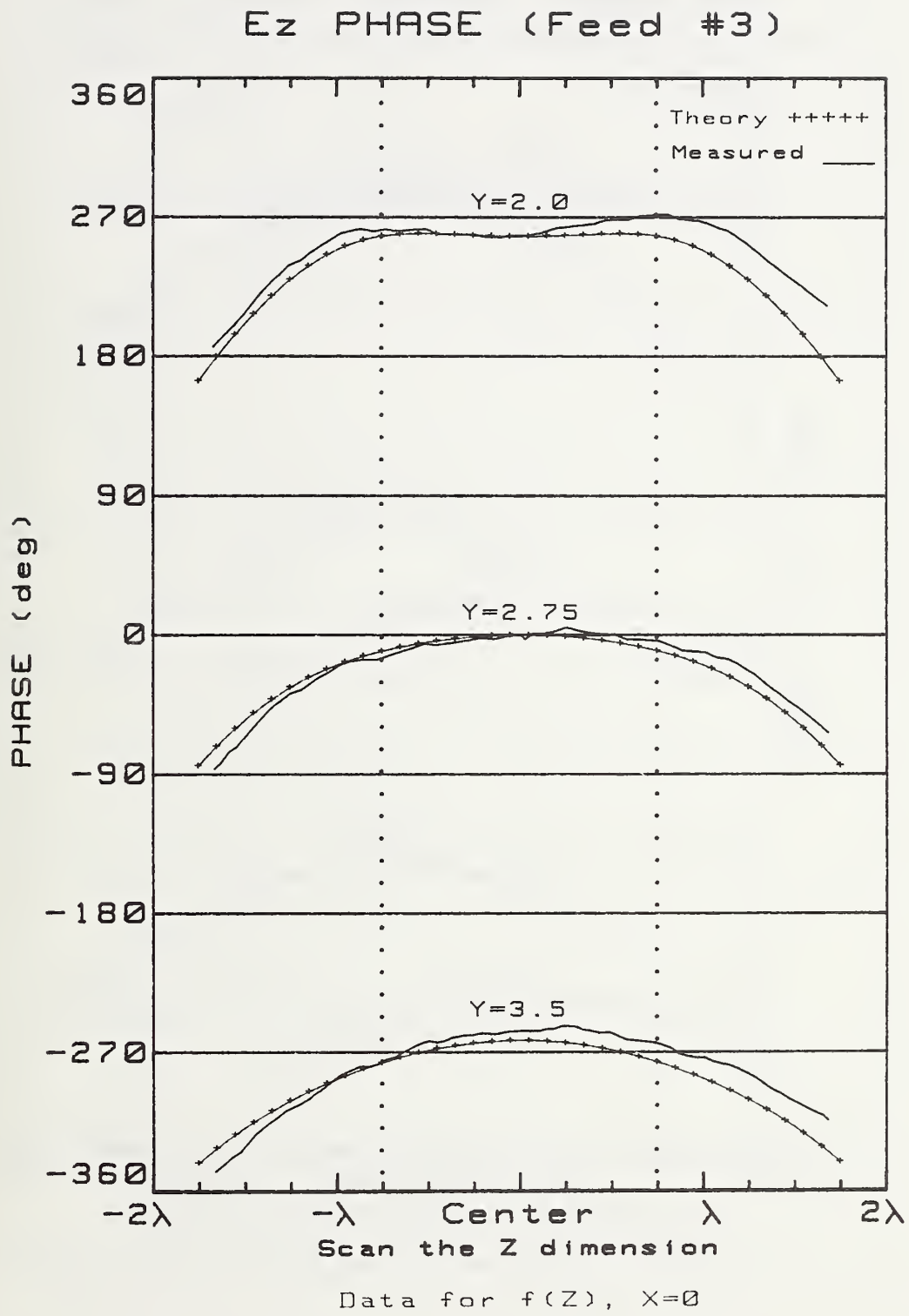


Figure 39. Theoretical and measured phase of $E_z$ at the boundaries (y = 2.0 λ, 3.5 λ) and the center of the more distant test volume.

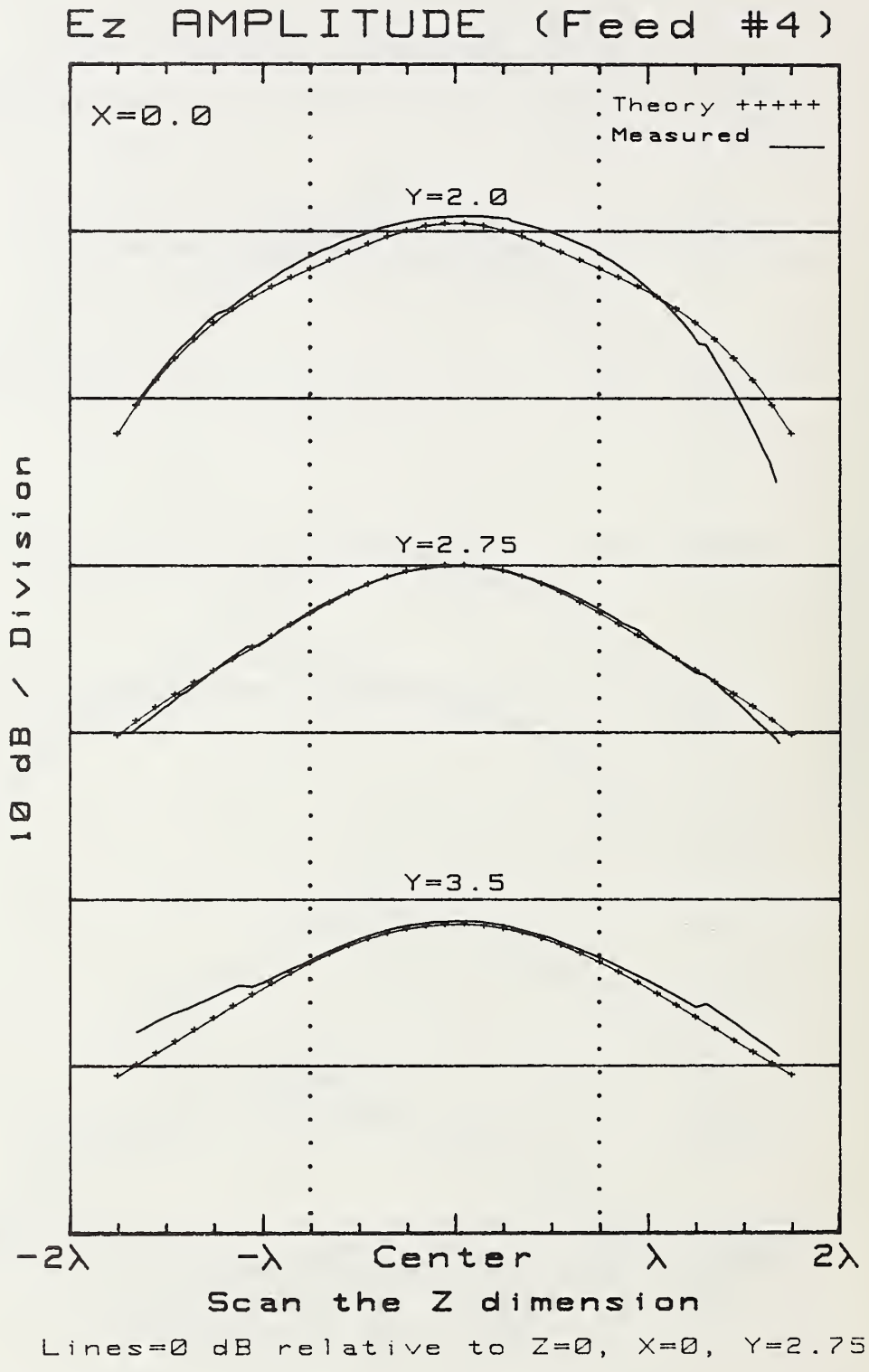


Figure 40. Theoretical and measured amplitude of $E_z$ at the boundaries and the center of the more distant test volume. Mutual coupling effects are included in the feed.

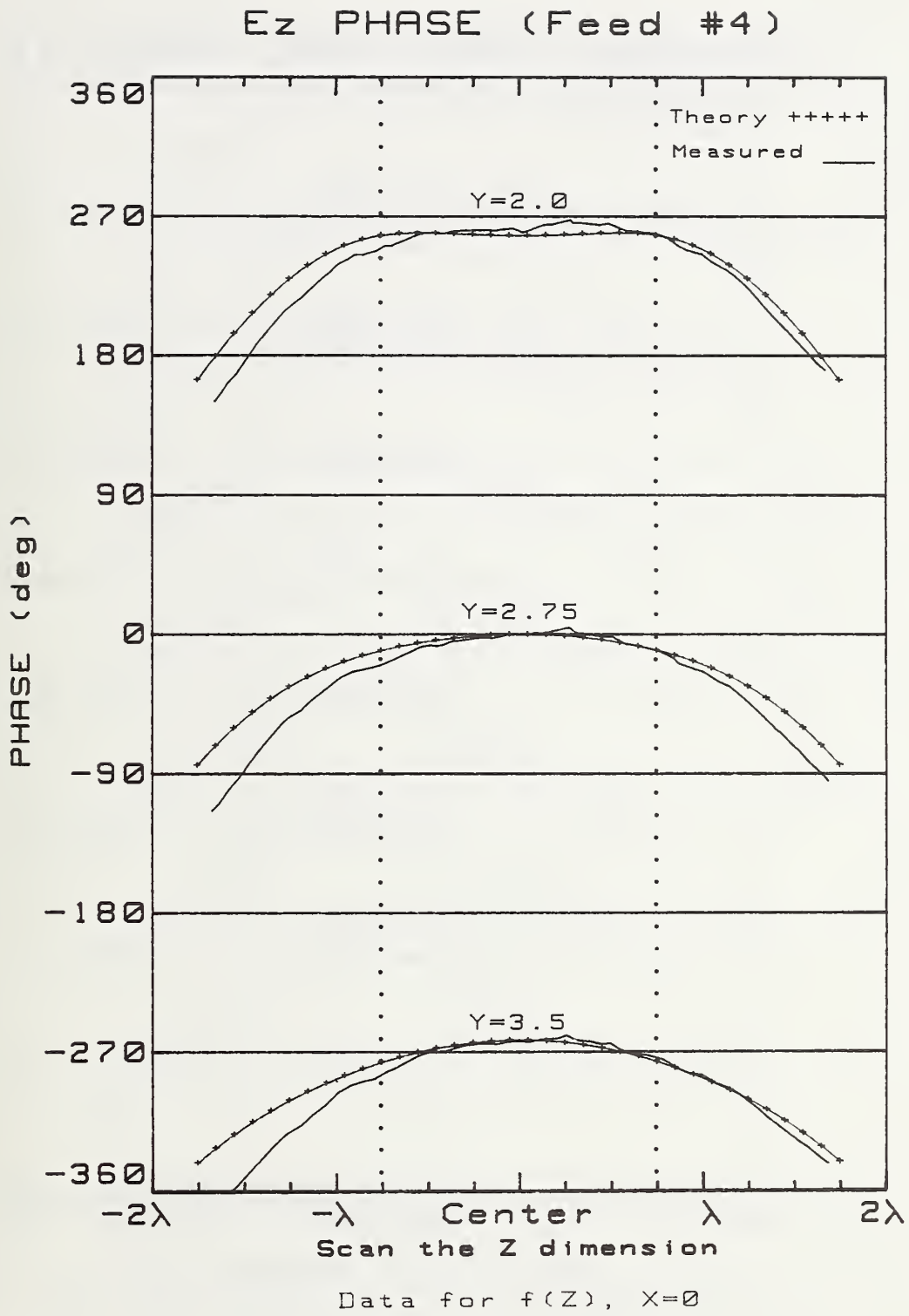


Figure 41. Theoretical and measured phase of $E_z$ at the boundaries and the center of the more distant test volume. Mutual coupling effects are included in the feed.

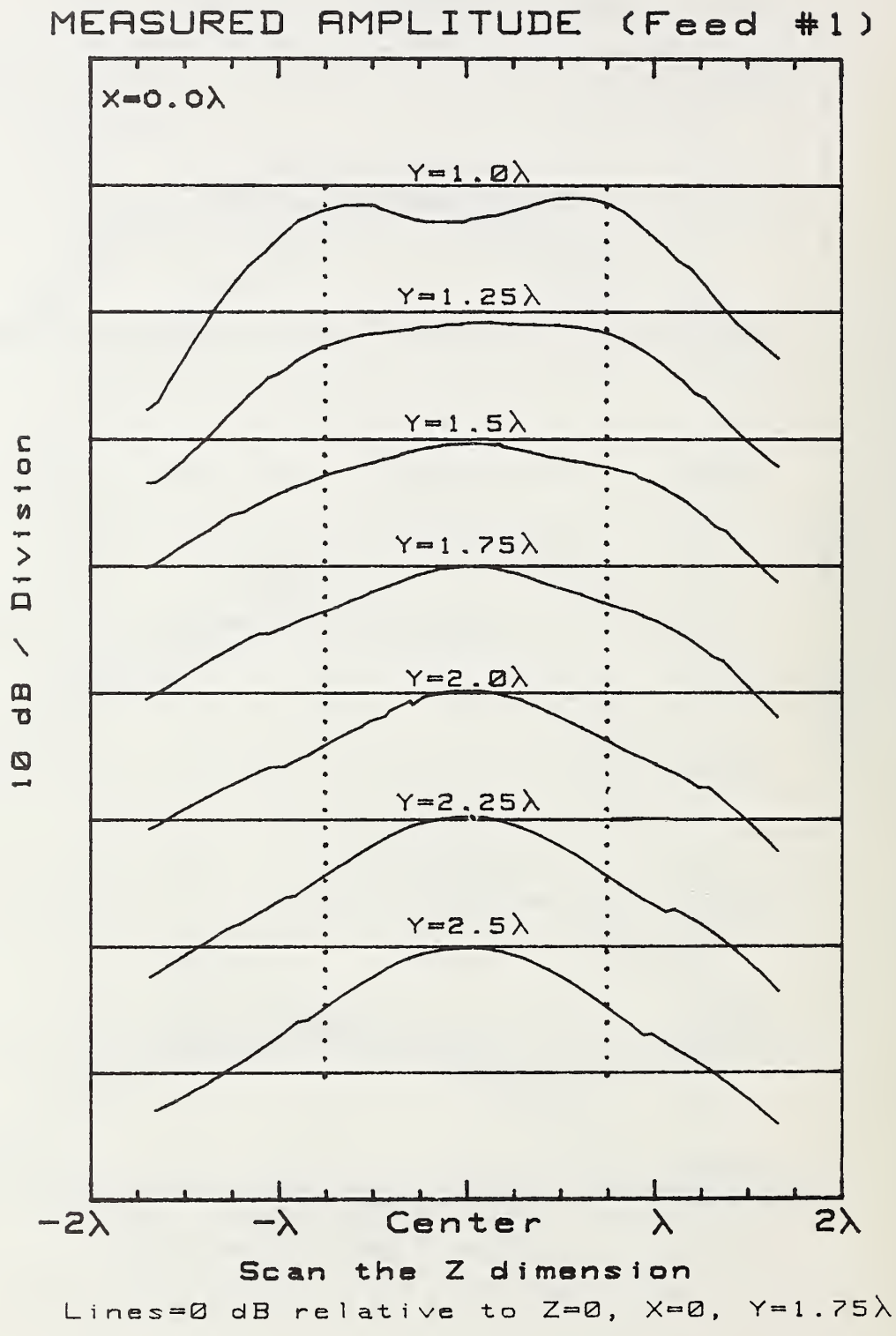


Figure 42. Measured amplitude of $E_z$ at λ/4 spacings throughout the test volume.

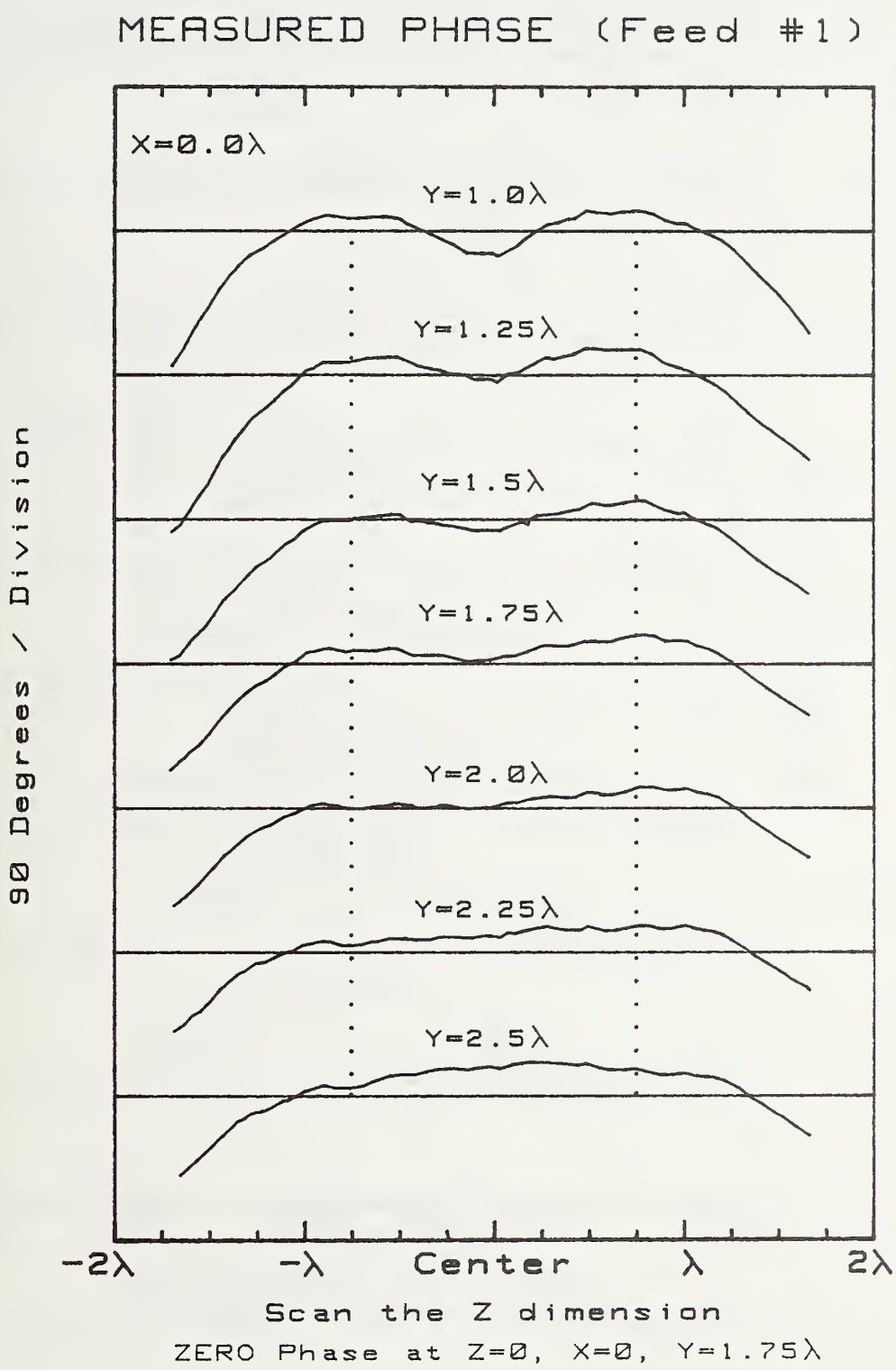


Figure 43. Measured phase of $E_z$ at λ/4 spacings throughout the test volume.

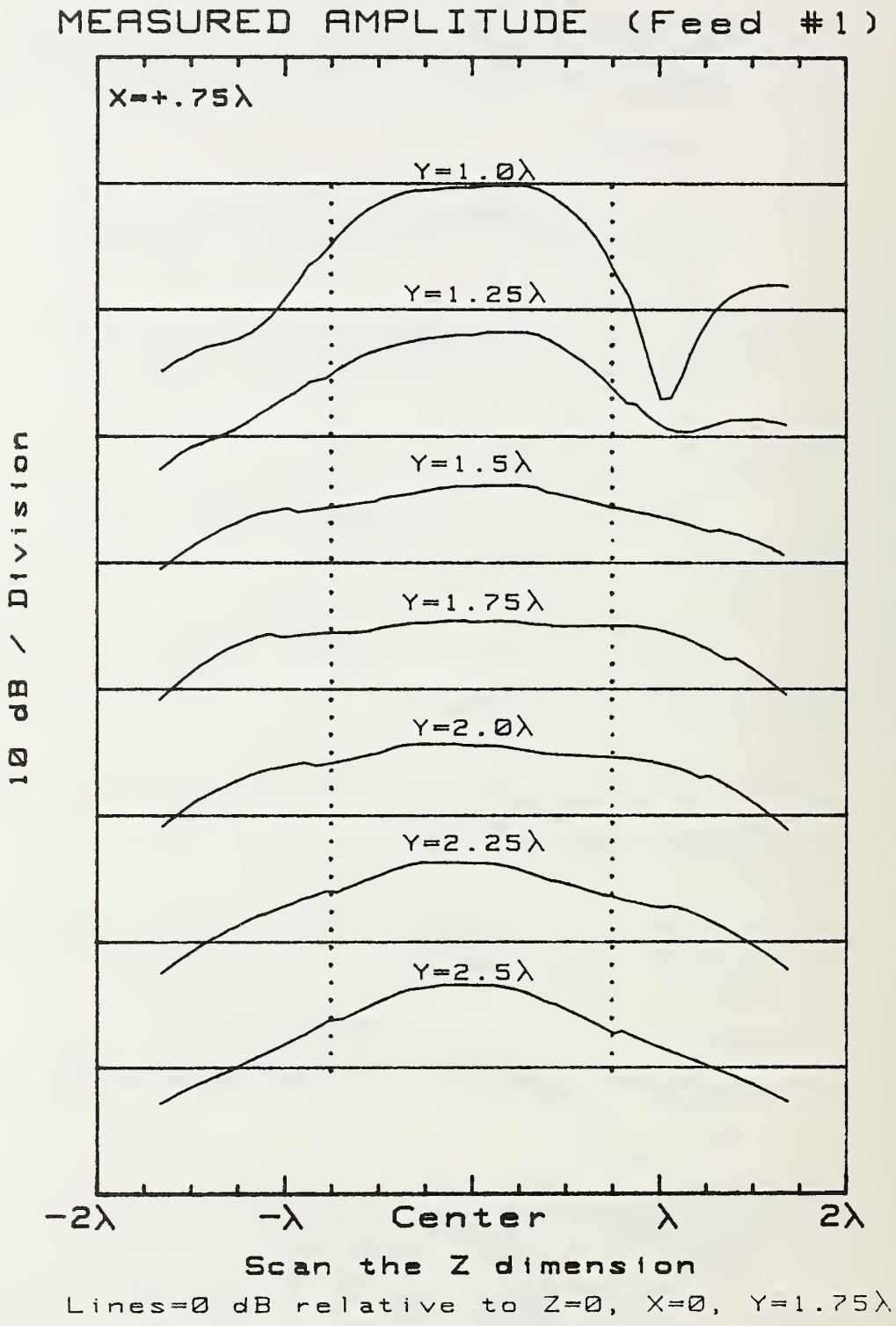


Figure 44. Measured amplitude of $E_z$ at λ/4 spacings throughout the test volume for x = 0.75 λ.

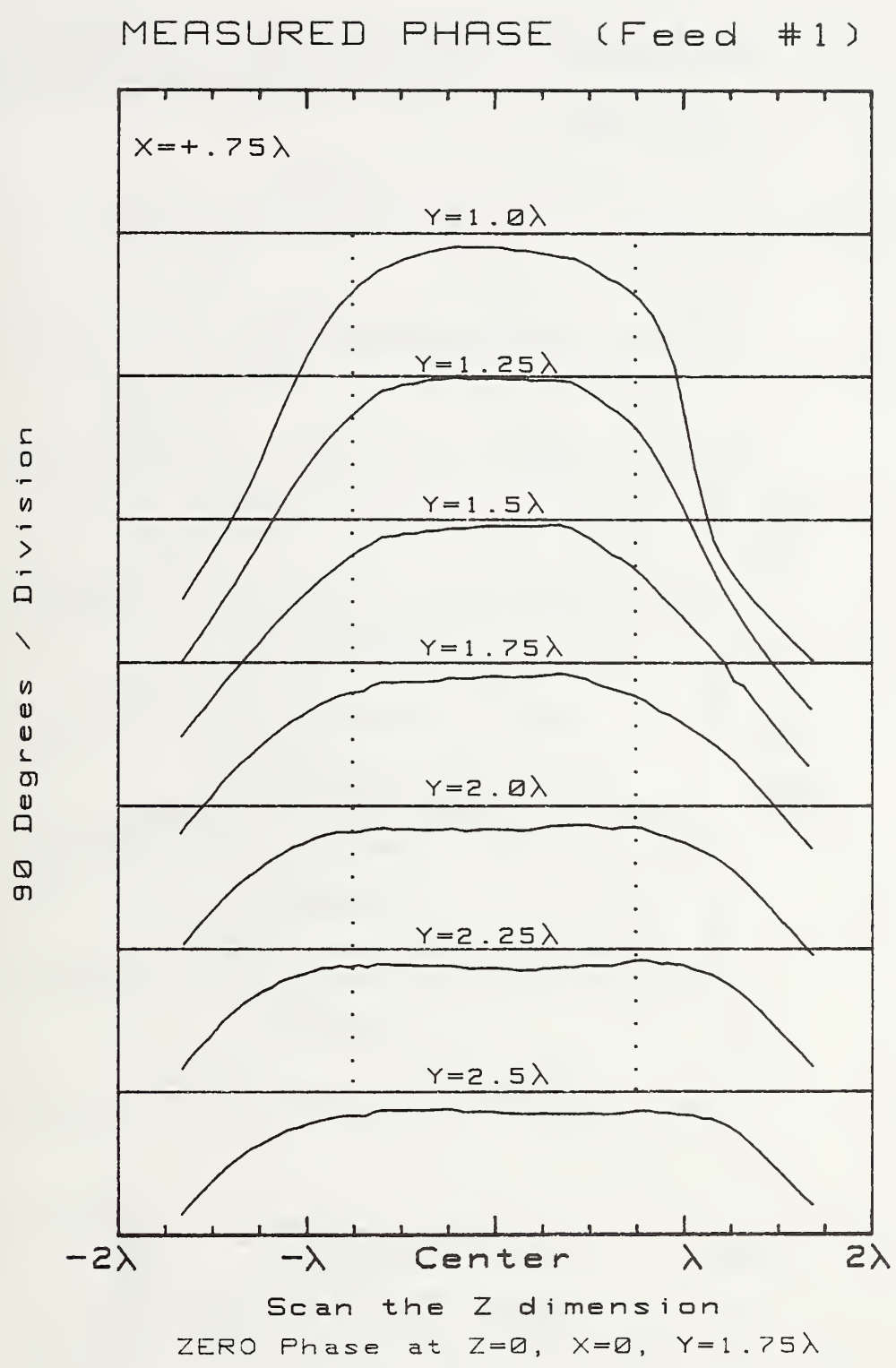


Figure 45. Measured phase of $E_z$ at λ/4 spacings throughout the test volume for x = 0.75 λ.

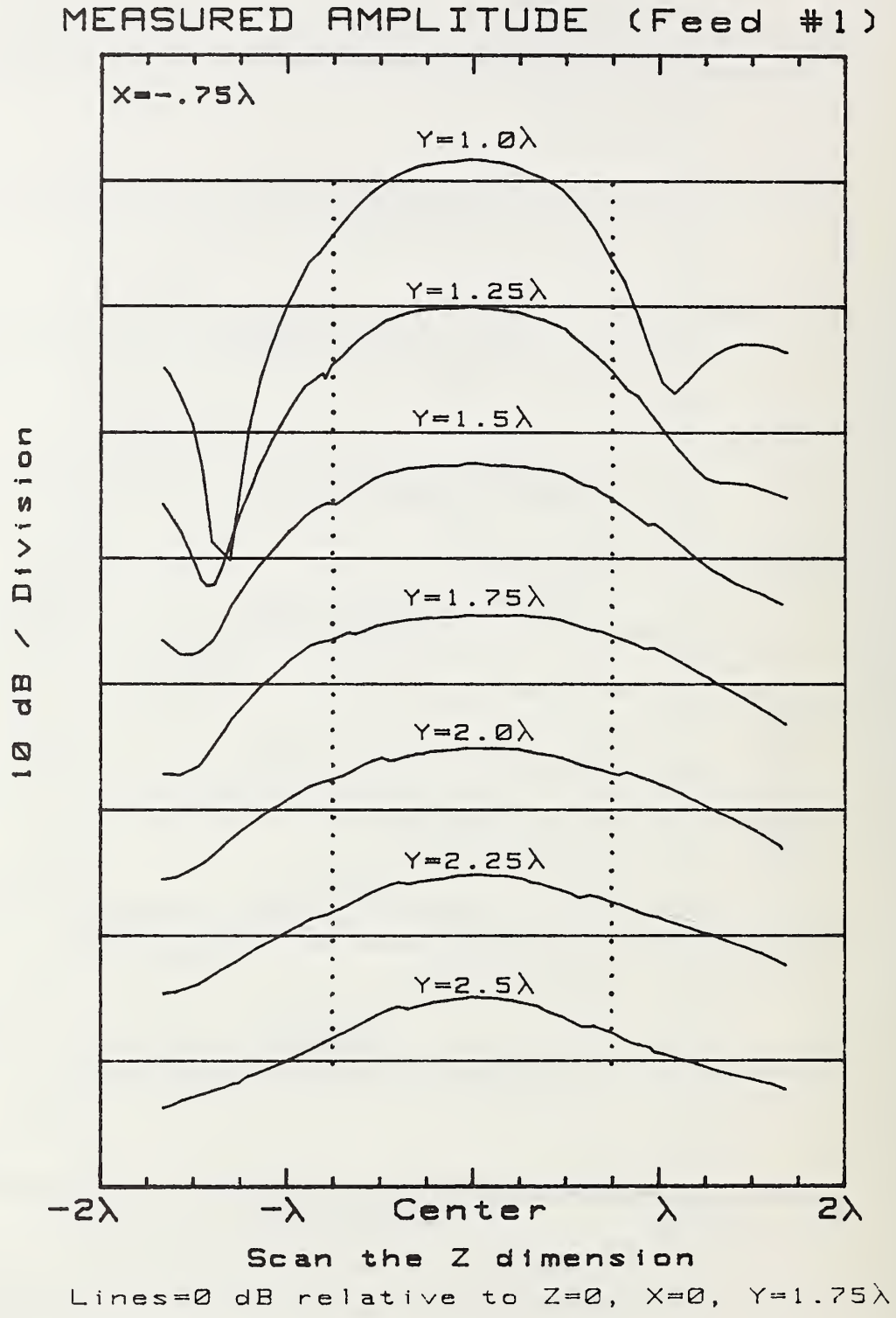


Figure 46. Measured amplitude of $E_z$ at λ/4 spacings throughout the test volume for x = -0.75 λ.

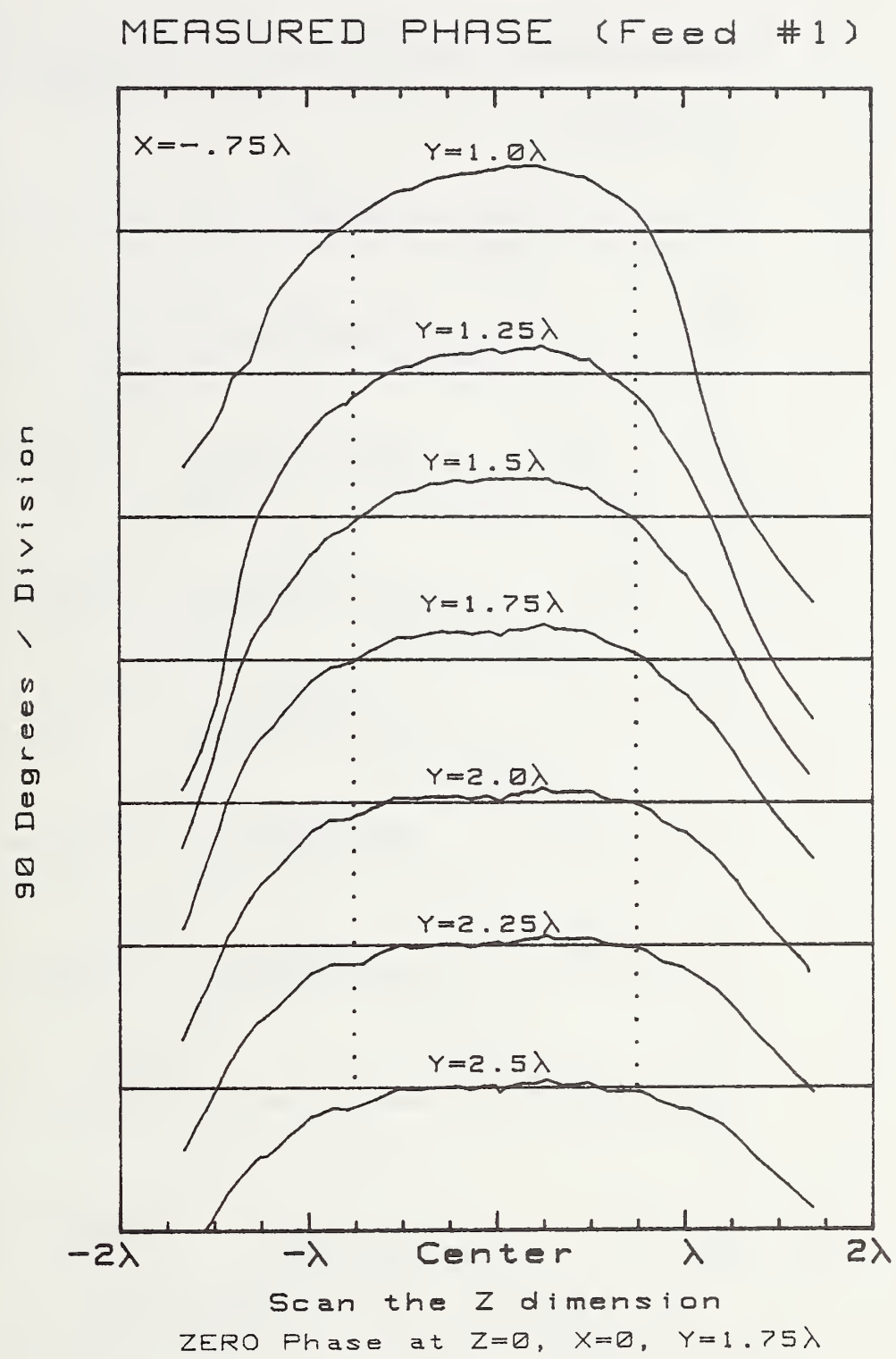


Figure 47. Measured phase of $E_z$ at λ/4 spacings throughout the test volume for x = -0.75 λ.

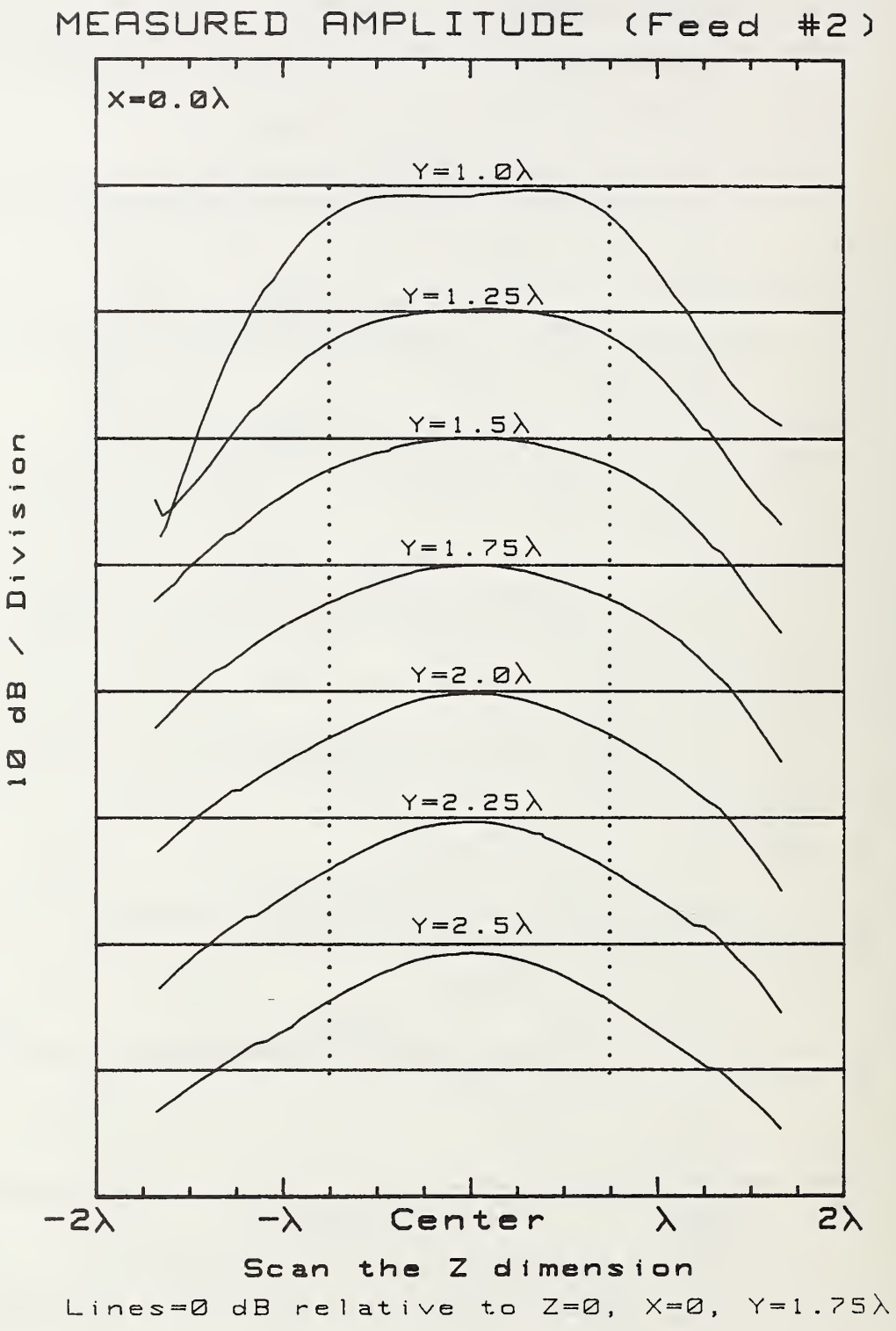


Figure 48. Measured amplitude of $E_z$ at λ/4 spacings throughout the test volume. Mutual coupling effects are included in the feed.

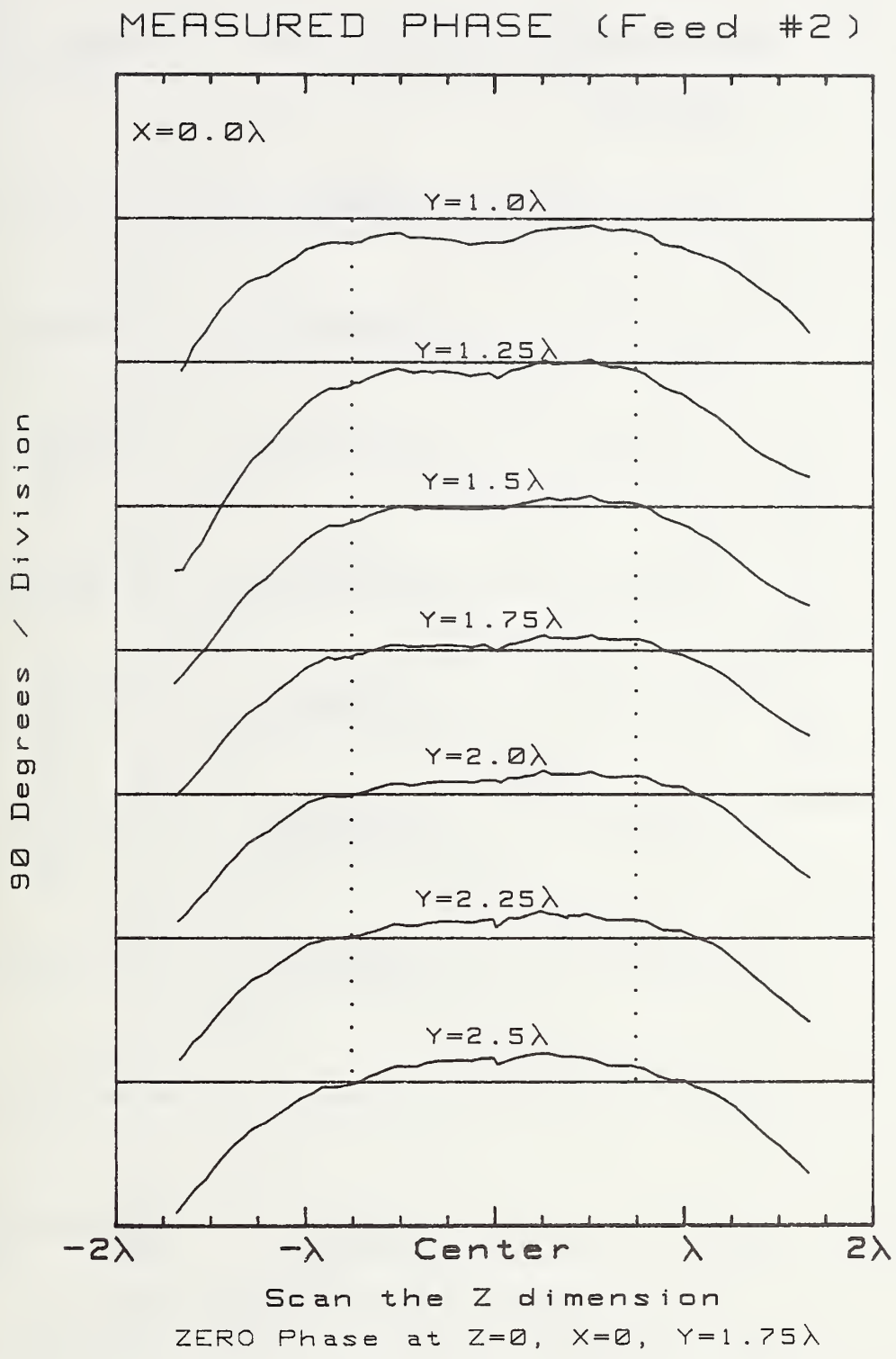


Figure 49. Measured phase of $E_z$ at λ/4 spacings throughout the test volume. Mutual coupling effects are included in the feed.

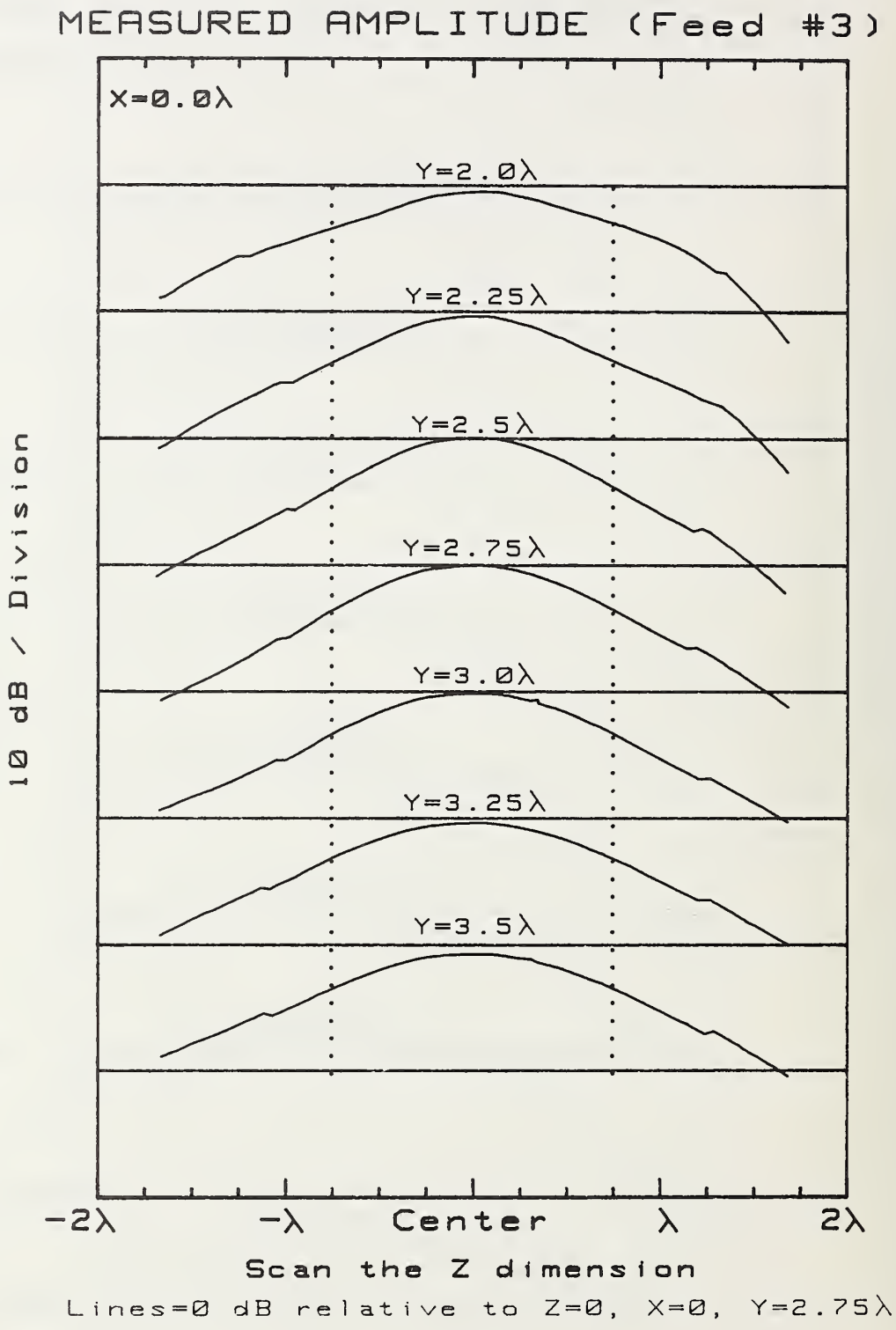


Figure 50. Measured amplitude of $E_z$ at λ/4 spacings throughout the more distant test volume (2.0 λ < y < 3.5 λ).

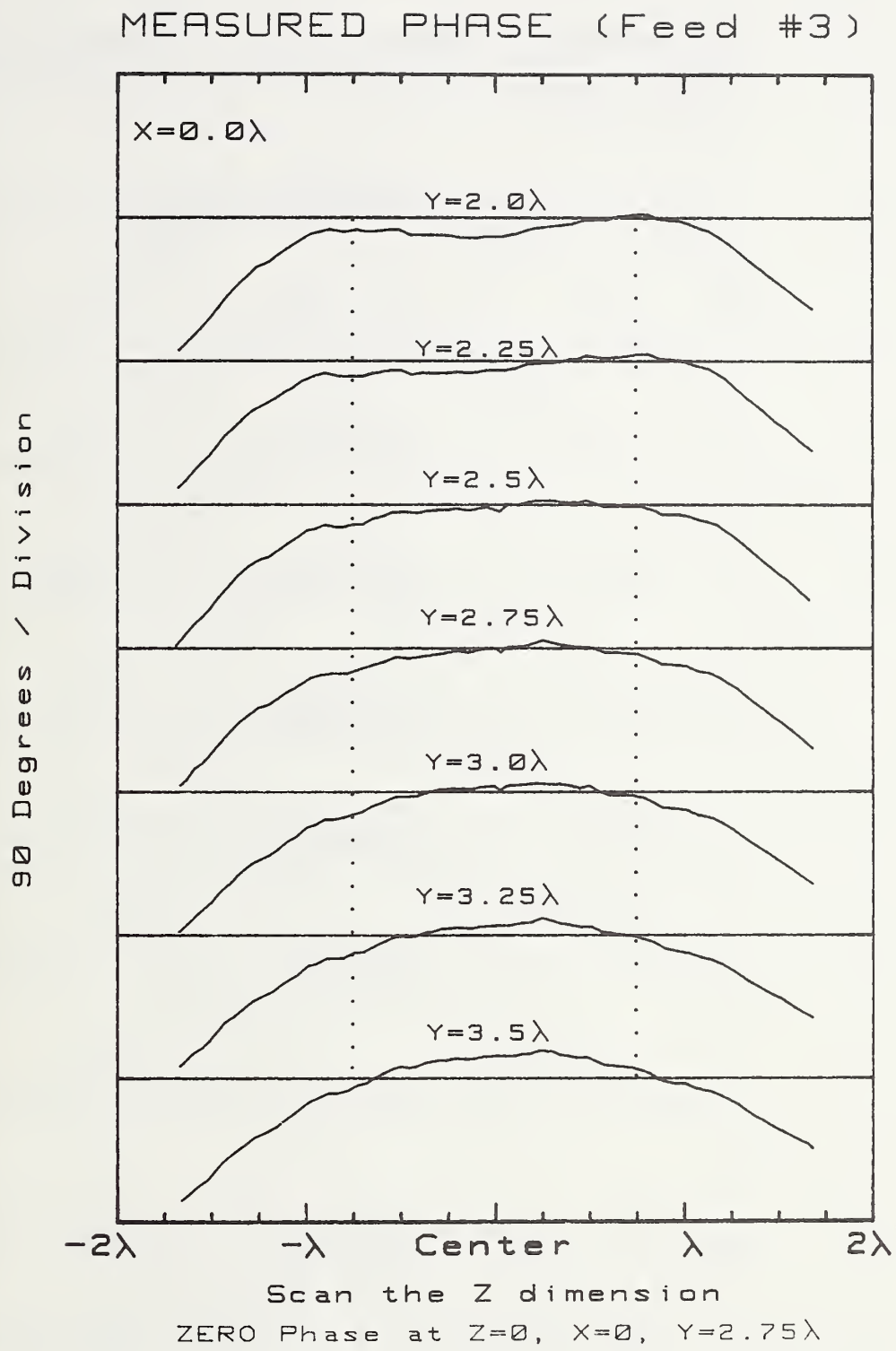


Figure 51. Measured phase of $E_z$ at λ/4 spacings throughout the more distant test volume.

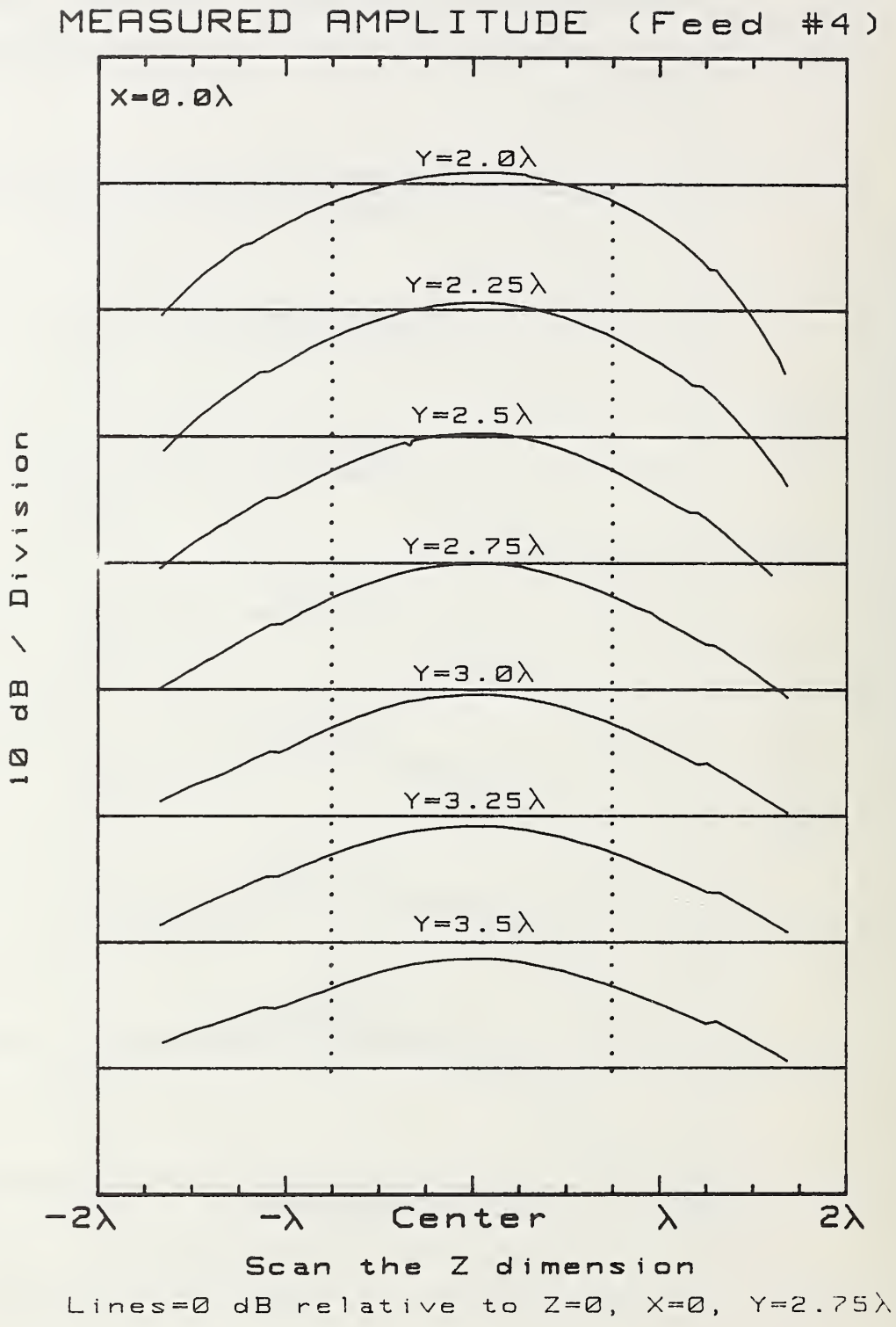


Figure 52. Measured amplitude of $E_z$ at λ/4 spacings throughout the test volume. Mutual coupling effects are included in the feed.

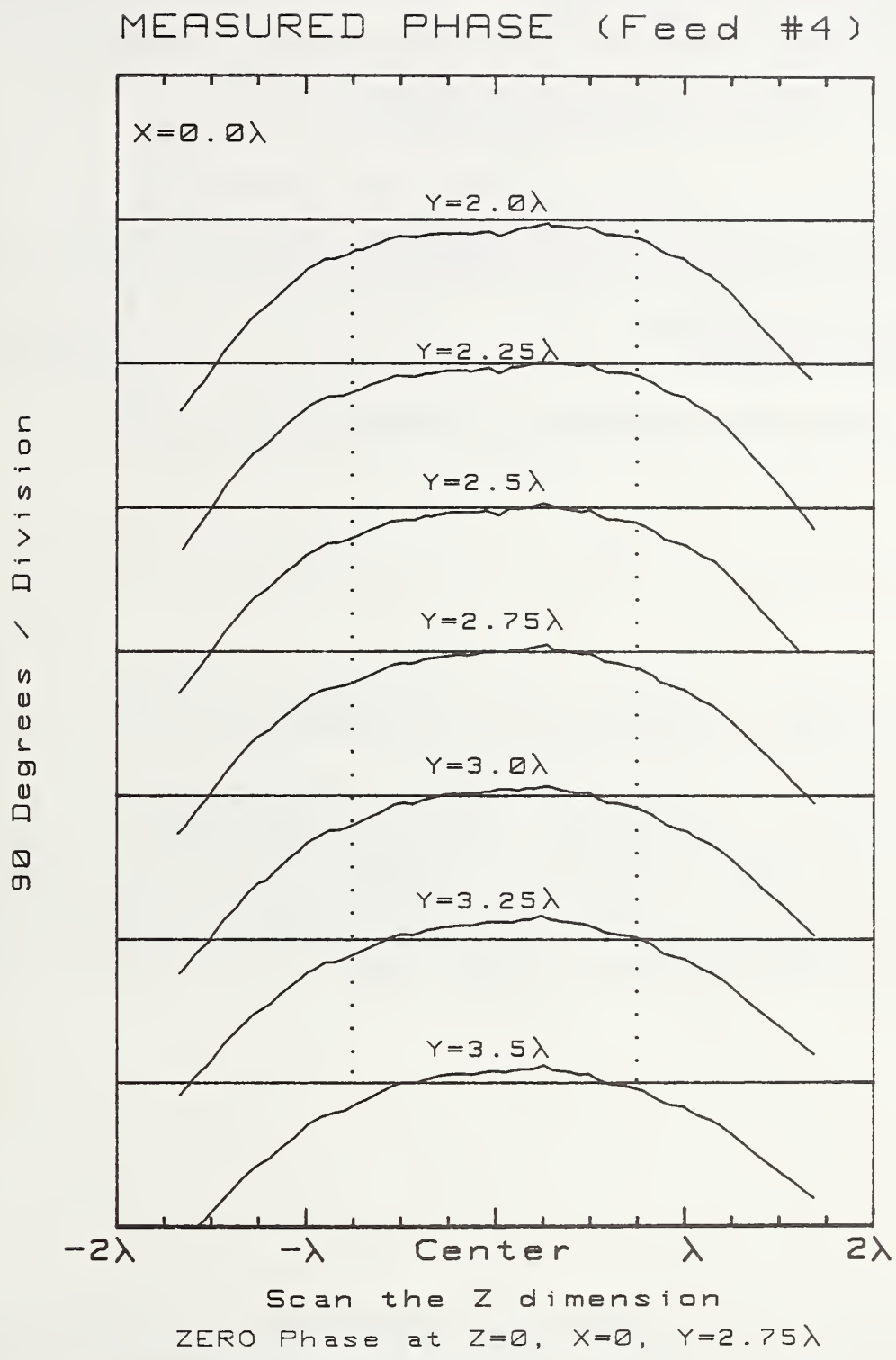


Figure 53. Measured phase of $E_z$ at λ/4 spacings throughout the test volume. Mutual coupling effects are included in the feed.

NBS-114A (REV. 2-8C)

| U.S. DEPT. OF COMM. BIBLIOGRAPHIC DATA SHEET (See instructions) | 1. PUBLICATION OR REPORT NO. NBS TN-1082 | 2. Performing Organ. Report No. | 3. Publication Date July 1985 |
|---|---|---|---|

4. TITLE AND SUBTITLE

A Near-Field Array of Yagi-Uda Antennas for Electromagnetic Susceptibility Testing

5. AUTHOR(S)

David A. Hill and Galen H. Koepke

6. PERFORMING ORGANIZATION (If joint or other than NBS, see instructions)

NATIONAL BUREAU OF STANDARDS
DEPARTMENT OF COMMERCE
WASHINGTON, D.C. 20234

7. Contract/Grant No.

8. Type of Report & Period Covered

9. SPONSORING ORGANIZATION NAME AND COMPLETE ADDRESS (Street, City, State, ZIP)

10. SUPPLEMENTARY NOTES

☐ Document describes a computer program; SF-185, FIPS Software Summary, is attached.

11. ABSTRACT (A 200-word or less factual summary of most significant information. If document includes a significant bibliography or literature survey, mention it here)

In electromagnetic susceptibility testing of electronic equipment, the ideal incident field is a plane wave. To approximate this condition, a seven-element array of Yagi-Uda antennas has been constructed and tested at a frequency of 500 MHz. The element weightings are determined by a near-field synthesis technique which optimizes the uniformity of the field throughout a rectangular test volume in the near field of the array. The amplitude and phase of the electric field have been measured throughout the test volume with a short dipole probe, and the agreement with the theory is excellent.

12. KEY WORDS (Six to twelve entries; alphabetical order; capitalize only proper names; and separate key words by semicolons)

antenna array; array synthesis; dipole antenna; electromagnetic susceptibility testing; mutual coupling; near field; plane wave; Yagi-Uda antenna.

13. AVAILABILITY

☒ Unlimited

☐ For Official Distribution. Do Not Release to NTIS

☒ Order From Superintendent of Documents, U.S. Government Printing Office, Washington, D.C. 20402.

☐ Order From National Technical Information Service (NTIS), Springfield, VA. 22161

14. NO. OF PRINTED PAGES 82

15. Price

USCOMM-DC 6043-P80

☆ U. S. GOVERNMENT PRINTING OFFICE: 1985—579-804/25293 REGION NO. 8

# NBS Technical Publications

## Periodical

**Journal of Research**—The Journal of Research of the National Bureau of Standards reports NBS research and development in those disciplines of the physical and engineering sciences in which the Bureau is active. These include physics, chemistry, engineering, mathematics, and computer sciences. Papers cover a broad range of subjects, with major emphasis on measurement methodology and the basic technology underlying standardization. Also included from time to time are survey articles on topics closely related to the Bureau's technical and scientific programs. Issued six times a year.

## Nonperiodicals

**Monographs**—Major contributions to the technical literature on various subjects related to the Bureau's scientific and technical activities.

**Handbooks**—Recommended codes of engineering and industrial practice (including safety codes) developed in cooperation with interested industries, professional organizations, and regulatory bodies.

**Special Publications**—Include proceedings of conferences sponsored by NBS, NBS annual reports, and other special publications appropriate to this grouping such as wall charts, pocket cards, and bibliographies.

**Applied Mathematics Series**—Mathematical tables, manuals, and studies of special interest to physicists, engineers, chemists, biologists, mathematicians, computer programmers, and others engaged in scientific and technical work.

**National Standard Reference Data Series**—Provides quantitative data on the physical and chemical properties of materials, compiled from the world's literature and critically evaluated. Developed under a worldwide program coordinated by NBS under the authority of the National Standard Data Act (Public Law 90-396).
NOTE: The Journal of Physical and Chemical Reference Data (JPCRD) is published quarterly for NBS by the American Chemical Society (ACS) and the American Institute of Physics (AIP). Subscriptions, reprints, and supplements are available from ACS, 1155 Sixteenth St., NW, Washington, DC 20056.

**Building Science Series**—Disseminates technical information developed at the Bureau on building materials, components, systems, and whole structures. The series presents research results, test methods, and performance criteria related to the structural and environmental functions and the durability and safety characteristics of building elements and systems.

**Technical Notes**—Studies or reports which are complete in themselves but restrictive in their treatment of a subject. Analogous to monographs but not so comprehensive in scope or definitive in treatment of the subject area. Often serve as a vehicle for final reports of work performed at NBS under the sponsorship of other government agencies.

**Voluntary Product Standards**—Developed under procedures published by the Department of Commerce in Part 10, Title 15, of the Code of Federal Regulations. The standards establish nationally recognized requirements for products, and provide all concerned interests with a basis for common understanding of the characteristics of the products. NBS administers this program as a supplement to the activities of the private sector standardizing organizations.

**Consumer Information Series**—Practical information, based on NBS research and experience, covering areas of interest to the consumer. Easily understandable language and illustrations provide useful background knowledge for shopping in today's technological marketplace.
*Order the* **above** *NBS publications from: Superintendent of Documents, Government Printing Office, Washington, DC 20402.*
*Order the* **following** *NBS publications—FIPS and NBSIR's—from the National Technical Information Service, Springfield, VA 22161.*

**Federal Information Processing Standards Publications (FIPS PUB)**—Publications in this series collectively constitute the Federal Information Processing Standards Register. The Register serves as the official source of information in the Federal Government regarding standards issued by NBS pursuant to the Federal Property and Administrative Services Act of 1949 as amended, Public Law 89-306 (79 Stat. 1127), and as implemented by Executive Order 11717 (38 FR 12315, dated May 11, 1973) and Part 6 of Title 15 CFR (Code of Federal Regulations).

**NBS Interagency Reports (NBSIR)**—A special series of interim or final reports on work performed by NBS for outside sponsors (both government and non-government). In general, initial distribution is handled by the sponsor; public distribution is by the National Technical Information Service, Springfield, VA 22161, in paper copy or microfiche form.

**U.S. Department of Commerce**
National Bureau of Standards
Gaithersburg, MD 20899

Official Business
Penalty for Private Use $300


POSTAGE AND FEES PAID
U.S. DEPARTMENT OF COMMERCE
COM-215

SPECIAL FOURTH-CLASS RATE
BOOK